DOT/FAA/AR-12/1

Federal Aviation Administration
William J. Hughes Technical Center
Aviation Research Division
Atlantic City International Airport
New Jersey 08405

Teardown Evaluation of a Decommissioned Boeing 737-200 Carbon Fiber-Reinforced Plastic Composite Right-Hand Horizontal Stabilizer

December 2013

Final Report

This document is available to the U.S. public through the National Technical Information Services (NTIS), Springfield, Virginia 22161.

This document is also available from the Federal Aviation Administration William J. Hughes Technical Center at actlibrary.tc.faa.gov.

U.S. Department of Transportation
Federal Aviation Administration

NOTICE

This document is disseminated under the sponsorship of the U.S. Department of Transportation in the interest of information exchange. The U.S. Government assumes no liability for the contents or use thereof. The U.S. Government does not endorse products or manufacturers. Trade or manufacturers' names appear herein solely because they are considered essential to the objective of this report. The findings and conclusions in this report are those of the author(s) and do not necessarily represent the views of the funding agency. This document does not constitute FAA policy. Consult the FAA sponsoring organization listed on the Technical Documentation page as to its use.

This report is available at the Federal Aviation Administration William J. Hughes Technical Center's Full-Text Technical Reports page: actlibrary.tc.faa.gov in Adobe Acrobat portable document format (PDF).

Technical Report Documentation Page

1. Report No.	2. Government Accession No.	3. Recipient's Catalog No.
DOT/FAA/AR-12/1		

4. Title and Subtitle	5. Report Date
TEARDOWN EVALUATION OF A DECOMMISSIONED BOEING 737-200 CARBON FIBER-REINFORCED PLASTIC COMPOSITE RIGHT-HAND HORIZONTAL STABILIZER	December 2013
	6. Performing Organization Code
7. Author(s)	8. Performing Organization Report No.
John S. Tomblin, Lamia Salah, Dan Hoffman, and Matthew Miller	
9. Performing Organization Name and Address	10. Work Unit No. (TRAIS)
National Institute for Aviation Research Wichita State University 1845 Fairmount St. Wichita, KS 67260	11. Contract or Grant No.
12. Sponsoring Agency Name and Address	13. Type of Report and Period Covered
U.S. Department of Transportation Federal Aviation Administration Northwest Mountain Region-Transport Airplane Directorate 1601 Lind Avenue, SW Renton, WA 98057	Final Report
	14. Sponsoring Agency Code AIR-100

15. Supplementary Notes

The Federal Aviation Administration William J. Hughes Technical Center Aviation Research Division Technical Monitor was Curtis Davies.

16. Abstract

The use of fiber-reinforced composites in aircraft structural components has significantly increased in the last few decades due to their improved specific strength and stiffness and superior corrosion resistance and fatigue performance with respect to their metal counterparts. Furthermore, current economic conditions require the use of most military and commercial aircraft beyond their original design service objectives; therefore, it is necessary to understand in-service-induced deterioration to ensure the airworthiness and structural integrity of these airframes. Most aging aircraft studies conducted thus far have focused on metallic structures; however, as more composite components are being certified and used on aircraft structural components, it is crucial to address this aging concern for composite components as well.

This report summarizes the findings of the aging study conducted on a Boeing 737 carbon fiber-reinforced plastics composite stabilizer after 18 years of service. The B-737-200 stabilizer was developed by The Boeing Company as part of the National Aeronautics and Space Administration Aircraft Energy Efficiency (ACEE) program initiated in July 1977. Five B-737 horizontal stabilizer shipsets were manufactured and certified in August 1982.

This report provides highlights of the ACEE program, a summary of the B-737 horizontal stabilizer teardown activities, and outcomes of the aging aircraft study. Nondestructive inspection (NDI) methods were conducted on the structure, prior to disassembly. The current state-of-the-art inspection methods were used to evaluate their accuracy in detecting flaws in the structure. Inspection methods prior to teardown included thermography, RapidscanTM, laser UT, and Boeing NDI. NDI inspections conducted after teardown included TTU (through transmission) and PE (pulse echo) ultrasonics. Results indicate that the composite structure maintained its structural integrity over its service life and did not show significant degradation or detrimental signs of aging.

17. Key Words	18. Distribution Statement
B-737-200 aircraft, Carbon fiber-reinforced plastics, NASA ACEE program	This document is available to the U.S. public through the National Technical Information Service (NTIS), Springfield, Virginia 22161. This document is also available from the Federal Aviation Administration William J. Hughes Technical Center at actlibrary.tc.faa.gov.

19. Security Classif. (of this report)	20. Security Classif. (of this page)	21. No. of Pages	22. Price
Unclassified	Unclassified	100	

Form DOT F 1700.7 (8-72) Reproduction of completed page authorized

ACKNOWLEDGEMENTS

The authors would like to thank Jeff Kollgaard and Karl Nelson from The Boeing Company for their guidance and invaluable contributions to the program. The authors also thank Abhijit Sonambekar, John Fitzpatrick, and Matthew Opliger from the National Institute for Aviation Research; and Joe Dimambro and Dennis Roach from Sandia National Laboratories.

TABLE OF CONTENTS

		Page
EXECUTIVE SUMMARY		xiii
1.	INTRODUCTION	1
1.1	Overview of the NASA ACEE Comprehensive Program	2
1.2	Overview of the ACEE Composites Program	8
2.	THE B-737 COMPOSITE HORIZONTAL STABILIZE	16
2.1	The B-737 Horizontal Stabilizer Description	17
2.2	Material Selection	21
2.3	Corrosion Protection Scheme	22
2.4	Lightning Protection Scheme	23
2.5	Component Manufacturing	23
2.6	Maintenance Planning Program	25
2.7	The B-737 Horizontal Stabilizer Certification	26
2.8	The B-737 Composite Horizontal Stabilizer Fleet Status	28
3.	THE B-737 HORIZONTAL STABILIZER TEARDOWN RESULTS	29
3.1	Visual Inspection and Nondestructive Inspection Prior to Teardown	29
3.1.1	Rapidscan™ Inspections	29
3.1.2	Boeing NDI	31
3.2	Disassembly	34
3.3	Visual Inspection Findings	38
3.4	Visual Inspection and Destructive Evaluation of Disbonded Areas	41
3.5	Nondestructive Inspection After Teardown	43
3.6	Thermal Analysis	46
3.7	Moisture Content Evaluation	68
3.8	Void Content Evaluation	71
3.9	Microscopic Image Analysis	73
3.10	Mechanical Tests	75
4.	CONCLUSIONS	83
5.	REFERENCES	84

LIST OF FIGURES

Figure		Page
1	Pratt & Whitney EEE Configuration and Pratt & Whitney EEE Ten-Stage, High-Pressure Compressor Rotor Assembly	4
2	Advanced Design Investigated by the EET Project	6
3	Conventional vs. Supercritical Airfoil Flow Fields and Pressure Distributions	6
4	Effect of FMC System on Damping for the B-52 Model and Airplane	7
5	Effect of ALDCS on C-5A Model Wing, Spanwise Distribution of Bending Moment	7
6	Potential Fuel Savings With the Implementation of EET	8
7	Composite Secondary Components Douglas DC-10 Upper Aft Rudder, Boeing B-727 Elevators, and Lockheed L-1011 Inboard Aileron	10
8	Composite Medium Primary Components Lockheed L-1011 Vertical Fin, Douglas DC-10 Vertical Stabilizer, and Boeing B-737 Horizontal Stabilizer	11
9	Structural Arrangement of L-1011 CFRP Inboard Aileron	11
10	Structural Arrangement of DC-10 CFRP Upper Aft Rudder	12
11	Structural Arrangement of B-727 CFRP Elevator	12
12	The L-1011 Composite Vertical Fin	13
13	The L-1011 Composite Vertical Fin Structural Arrangement	14
14	The DC-10 Composite Vertical Stabilizer Structural Arrangement	15
15	The DC-10 Composite Vertical Stabilizer CFRP Cover	15
16	The DC-10 Composite Vertical Stabilizer Substructure	16
17	The B-737 Horizontal Stabilizer General Arrangement	17
18	Stabilizer Box Concepts Evaluated During Design Phase	18
19	Composite Stabilizer Structural Arrangement	19

20	Metal Stabilizer Structural Arrangement	19
21	Stabilizer Skin and Rib Details	20
22	Corrosion Protection Scheme	22
23	Lightning Protection Scheme	23
24	Stabilizer Upper Skin Stacking Sequence	24
25	Rapidscan Analysis of the B-737 RH Stabilizer	30
26	Pulse Echo Amplitude Scan of the B-737 RH Stabilizer Performed at 3.5 MHz	32
27	Pulse Echo Amplitude Scan of the B-737 LH Stabilizer Performed at 3.5 MHz	33
28	The B-737 CFRP RH Horizontal Stabilizer Prior to Disassembly, Upper Skin Side	34
29	The B-737 CFRP RH Horizontal Stabilizer Prior to Disassembly, Lower Skin Side	35
30	Upper Skin Disassembly	35
31	The B-737 RH Composite Stabilizer Upper Skin After Disassembly	36
32	The B-737 RH Composite Stabilizer Lower Skin After Disassembly	36
33	The B-737 RH Composite Stabilizer Structural Box	37
34	The B-737 RH Composite Stabilizer Spars: Front Spar and Rear Spar	38
35	Corroded Fasteners Due to Sealant Deterioration (Rear Spar, Center Lug)	38
36	Corroded Fasteners Due to Sealant Deterioration (Rear Spar, Bottom Lug)	39
37	Degradation of Tedlar	39
38	Phenolic Shims Used to Fill Gaps Between Upper Skin and Rib Stations 2, 4, and 7	40
39	Liquid Shims Used to Fill Gaps Between Upper Skin and Stabilizer Ribs	41
40	Upper Skin Delaminations at Stringer 3, 4, and 7 Runouts	42
41	Lower Skin Disbonds Confirmed After Teardown	43
42	1970s Ultrasonic Inspection Sensitivity vs. Today's Equipment Capability	44

43	The NIAR PE Scans of a B-737 RH Horizontal Stabilizer	45
44	Specimen Nomenclature	46
45	The DMA Analysis of Coupon Extracted from B-737 Upper Skin	47
46	The DMA Results for As-Extracted Coupons From the Upper Skin of the B-737 Horizontal Stabilizer (Boeing Method)	48
47	The DMA Results for As-Extracted Coupons From the Upper Skin of the B-737 Horizontal Stabilizer (ASTM E 1640)	48
48	The DMA Results for Dried Coupons From the Upper Skin of the B-737 Horizontal Stabilizer (ASTM Standard)	51
49	The DMA Data for As-Extracted Coupon From Upper Skin Rib 7	53
50	The DMA Data for Dried Coupon From Upper Skin Rib 2 Stringer 4	53
51	The DMA Results for As-Extracted Coupons From the Lower Skin of B-737 Horizontal Stabilizer	54
52	The DMA Results for As-Extracted Coupons From the Lower Skin of B-737 Horizontal Stabilizer	54
53	The DMA Results for Dried Coupons From Lower Skin of B-737 Horizontal Stabilizer	57
54	The DMA Data for As-Extracted Coupon From Lower Skin Rib 4 Stringer 6	58
55	The DMA Data for Dried Coupon From Lower Skin Rib 4 Stringer 5	59
56	The DSC Data for As-Extracted Coupons From Upper Skin Rib 5 Stringer 8	62
57	The DSC Data for As-Extracted Coupon From Lower Skin Rib 1 Stringer 4	64
58	The DSC Data for As-Extracted Coupon From Front Spar at Stabilizer Station 111	66
59	The DSC Data for As-Extracted Coupon From Rear Spar at Stabilizer Station 111	67
60	Moisture Loss as a Function of Time for Coupons Extracted From Lower Skin	68
61	Moisture Distribution in Lower Skin	68
62	Moisture Loss as a Function of Time for Coupons Extracted From Upper Skin	69

63	Moisture Distribution in Upper Skin	69
64	Moisture Loss as a Function of Time for Coupons Extracted From Front Spar	70
65	Moisture Loss as a Function of Time for Coupons Extracted From Rear Spar	70
66	Moisture Distribution in Spars	71
67	Void Content Summary	72
68	Cross Section of Stringer Web and Flange Intersection for Stringer 2 and Stringer 3 at Rib Station 2 Showing Porosity at Magnification 50X, Microcracks, and Cracks Emanating From the Voids and Porous Areas	73
69	Cross Section of Upper Skin Stringer 2 at Rib Station 2 Web Showing Porosity at Magnification 50X	74
70	Cross Section of Stringer Web and Flange Intersection for Upper Skin Stringer 2 at Rib Station 1 and Lower Skin Stringer 2 at Rib Station 3 Showing Macrocracks at Magnification 50X	74
71	Cross Section of Stringer Web and Flange Intersection for Stringer 3 at Rib Station 7 and Stringer 1 at Rib Station 5 Showing a Sound Structure at Magnification 50X	74
72	Compression Test Fixture and Test Specimens	75
73	Upper Skin Compression Strength Test Data of As-Extracted Coupons	76
74	Upper Skin Compression Ultimate Strain Test Data of As-Extracted Coupons	77
75	Lower Skin Compression Strength Test Data of As-Extracted Coupons	77
76	Lower Skin Compression Ultimate Strain Test Data of As-Extracted Coupons	78
77	Tabbing Fixture for Tension Coupons	78
78	Tension Test Setup and Coupon Configuration	79
79	Upper Skin Tension Strength Data of As-Extracted Coupons	80
80	Upper Skin Tension Ultimate Strain Test Data of As-Extracted Coupons	80
81	Lower Skin Tension Strength Data of As-Extracted Coupons	81
82	Lower Skin Tension Ultimate Strain Test Data of As-Extracted Coupons	81

83 Crippling Test Setup for Three-Stringer Element 82

84 Post-test Three-Stringer Element 82

85 Crippling Element Load vs. Strain Data 83

LIST OF TABLES

Table		Page
1	Comparison of Metallic vs. Composite Fin	14
2	Comparison of Metallic vs. Composite Horizontal Stabilizer	21
3	Maintenance Planning Schedule	25
4	The B-737 Composite Stabilizer Fleet Status as of March 2011	28
5	ASTM vs. Boeing Test Parameters	47
6	The DMA Test Data for Upper Skin Coupons Using Boeing Test Parameters	49
7	The DMA Test Data for Upper Skin Coupons Using ASTM Test Parameters	50
8	The DMA Test Data for Upper Skin Coupons Using ASTM Test Parameters	51
9	The DMA Test Data for Lower Skin Coupons Using Boeing Parameters	55
10	The DMA Test Data for Lower Skin Coupons Using ASTM Test Parameters	55
11	The DMA Test Data for Lower Skin Coupons Using ASTM Test Parameters	57
12	The DMA Test Data for Front Spar Coupons	59
13	The DMA Test Data for Rear Spar Coupons	60
14	The DMA Test Data for Cytec T300/5208 Material	61
15	The DSC Test Data for Cytec T300/5208 Material	62
16	The DSC Test Data for As-Extracted Coupons From Upper Skin	63
17	The DSC Test Data for Dried Coupons From Upper Skin	63
18	The DSC Test Data for As-Extracted Coupons From Lower Skin	65
19	The DSC Test Data for Dried Coupons From Lower Skin	65
20	The DSC Test Data for As-Extracted Coupons From Front Spar	66
21	The DSC Test Data for As-Extracted Coupons From Rear Spar	67

ACRONYMS

ACEE	Aircraft Energy Efficiency
ALDCS	Active Lift Distribution Control System
ATP	Advanced Turboprop
CFRP	Carbon fiber-reinforced plastics
CPAS	Composite Primary Aircraft Structures
DMA	Dynamic mechanical analysis
DOC	Direct operating costs
DSC	Differential scanning calorimetry
ECI	Engine Component Improvement
EEE	Energy Efficient Engine
EET	Energy Efficient Transport
FAA	Federal Aviation Administration
FMC	Flutter mode control
GE	General Electric
LFC	Laminar Flow Control
LH	Left hand
MEK	Methyl ethyl ketone
NASA	National Aeronautics and Space Administration
NDI	Nondestructive inspection
NIAR	National Institute for Aviation Research
OEM	Original equipment manufacturer
PE	Pulse echo
RECAST	Long-Range Planning Study for Composites
RH	Right hand
RTA	Room temperature ambient
SFC	Specific fuel consumption
T_g	Glass transition temperature
TMA	Thermomechanical analysis
USAF	U.S. Air Force
UT	Ultrasonics

EXECUTIVE SUMMARY

The use of carbon fiber-reinforced plastic (CFRP) composites in aircraft structural components has significantly increased in the last few decades due to their improved specific strength and stiffness, and superior corrosion resistance and fatigue performance with respect to their metal counterparts. Furthermore, current economic conditions require the use of most military and commercial aircraft beyond their original design service objectives. Therefore, it is necessary to understand the in-service-induced deterioration of aging composite aircraft to ensure the airworthiness and structural integrity of these airframes. Most aging aircraft studies conducted thus far have focused on metallic structures; however, as more composite materials are being used in aircraft structures, it is crucial to address this aging concern for composite components as well.

This report summarizes the findings of the aging study conducted on a Boeing B-737 CFRP composite stabilizer after 18 years of service. The B-737-200 stabilizer was developed by The Boeing Company as part of the National Aeronautics and Space Administration Aircraft Energy Efficiency (ACEE) program initiated in July 1977. Certification was completed in August 1982, and all five shipsets were deployed in 1984. This report provides highlights of the ACEE program, a summary of the B-737 horizontal stabilizer teardown activities, and findings of the aging aircraft study. Nondestructive inspection (NDI) methods were conducted on the structure, prior to disassembly. The current state-of-the-art inspection methods were used to evaluate their accuracy in detecting flaws in the structure. Inspection methods prior to teardown included thermography, Rapidscan™, laser UT, and Boeing NDI. NDI inspections conducted after teardown included TTU (Through transmission) and PE (Pulse echo) ultrasonics. Results indicate that the composite structure maintained its structural integrity over its service life and did not show significant degradation or detrimental signs of aging.

1. INTRODUCTION.

As more commercial and military airplanes are required to maintain operational capability beyond their original design service objectives, it has become necessary to answer questions regarding their continued airworthiness and structural integrity. Most research conducted on aging structures thus far has focused on metallic components. However, with the increasing use of composite materials in primary and secondary structures, it has become necessary to address the long-term structural health of aging composite components as well.

Advanced composite materials offer great advantages over metals, including improved specific strength and stiffness and the ability to be tailored to design requirements in various directions. These features offer the potential of significant weight savings, which are closely related to fuel savings. Manufacturing cost advantages can accrue due to reduced part count and, therefore, lower assembly costs. These materials also improve airline profitability in terms of lower operating and maintenance costs. However, for composite materials to be used in aircraft structures, it is necessary that components fabricated from them demonstrate equivalent levels of safety, damage tolerance, and durability with respect to their aluminum counterparts. This report examines the structural integrity of a composite Boeing B-737-200 right-hand (RH) horizontal stabilizer after 18 years of service and presents data that can be used to quantify the aging and durability of composite structures.

The B-737-200 horizontal stabilizer, which is the subject of the current investigation, was the oldest commercial medium-size primary structure made of composite materials. The structure was built as part of the National Aeronautics and Space Administration (NASA) Aircraft Energy Efficiency (ACEE) program using carbon fiber-reinforced plastics (CFRP) composites fully certified by the Federal Aviation Administration (FAA). The structure entered service in August 1984, was in service for 18 years, and was retired in 2002 after completing 48,000 flights and 52,000 hours of service.

To characterize the structural health of the horizontal stabilizer after 18 years of service, the National Institute for Aviation Research (NIAR) at Wichita State University acquired the aged structure and conducted several nondestructive and destructive tests to evaluate its structural integrity. The data generated can be used to understand aging mechanisms on composite parts currently in service and to reveal the main differences between damage mechanisms and damage accumulation in metallic versus composite components. This data can aid in future inspection and maintenance plans for composite structures to ensure their continued airworthiness and safety.

Nondestructive inspection (NDI) methods were conducted on the structure prior to disassembly. The objective here was to use current state-of-the-art inspection methods and evaluate their accuracy in detecting flaws in the structure. All inspections prior to teardown were conducted at the Sandia National Laboratories and at The Boeing Company. The inspection methods used included thermography, Rapidscan™, laser ultrasonic (UT) testing, and Boeing pulse echo (PE). NDI inspections conducted after teardown included through-transmission ultrasonics and PE ultrasonics. Destructive evaluation included thermal analysis, image analysis, as well as physical

and mechanical tests according to appropriate ASTM standards and/or standards used to generate the baseline data, as summarized in a NASA report [1].

Thermal analysis was conducted using both dynamic mechanical analysis (DMA) and differential scanning calorimetry (DSC) to determine the aged material's glass transition temperature (T_g) as well as its degree of cure. Image analysis was conducted to characterize the state of the structure at the microscopic level and to detect possible flaws induced during manufacture or service. Physical tests were conducted to establish moisture and porosity levels in the composite structure and compare them to the design values. Mechanical tests were performed using the same standards applied to generate the allowable values. Strength and stiffness values of coupons and elements extracted from the aged structure were compared to those obtained during the design phase used to generate material allowables.

The main goal of this investigation was to assess the overall structural health of the composite stabilizer after 18 years of service by identifying possible changes in the material properties due to environmental effects and/or flight service, obtaining data to help understand aging mechanisms in composite structures, and gaining confidence in the long-term durability and safety of composite materials.

1.1 OVERVIEW OF THE NASA ACEE COMPREHENSIVE PROGRAM.

The B-737-200 RH CFRP horizontal stabilizer used for this investigation was built as part of the NASA ACEE program, which was initiated in late 1975, as the result of escalating fuel prices. Between 1973 and 1976, fuel costs increased from 12 to 31 cents per gallon for U.S. local carriers and from 12 to 42 cents per gallon for U.S. international carriers. As a result, fuel direct operating costs (DOC) increased from 20% in the early 1970s to nearly 45% in 1976 [2-5]. Numerous articles in the literature have been written regarding the energy crisis and the impact on airline operations, as well as on advanced aeronautical technologies and their potential for energy conservation [6-14].

For years, NASA had been working on projects that would result in aircraft energy efficiency, but in January 1975, subsequent to the oil energy crisis and the escalation of jet fuel prices, the U.S. Senate asked NASA to develop a comprehensive program to develop fuel-efficient aeronautical technology. NASA responded by establishing a task force comprised of engineers and scientists from the Department of Defense, FAA, NASA, and the Department of Transportation [6 and 7]. The task force obtained recommendations from engine manufacturers, major aircraft manufacturers, and other NASA research centers, and defined a preliminary plan for fuel-efficient technology. An advisory board was also formed, which was comprised of representatives from industry, airlines, other government agencies, and universities. The preliminary energy efficiency plan was first presented to the advisory board in May 1975, revised in June 1975, and finally presented and endorsed in September 1975.

The ACEE program was implemented in six major projects: Engine Component Improvement (ECI), Energy Efficient Engine (EEE), Advanced Turboprop (ATP), Composite Primary Aircraft Structures (CPAS), Energy Efficient Transport (EET), and Laminar Flow Control (LFC). The

first three were conducted at the NASA Lewis Research Center (currently known as Glenn Research Center, hereafter referred to as NASA Lewis/Glenn) [6], and the other three were conducted at the NASA Langley Research Center (hereafter referred to as NASA Langley) [15].

The key element around which engine development was centered (and to a larger extent, the focal point of the ACEE program) was the reduction/minimization of specific fuel consumption (SFC), i.e., the ratio of fuel flow rate (pounds per hour) to a given engine thrust (pounds). The lower the SFC, the more efficient the engine, i.e, less fuel is required for a given engine thrust. During the performance improvement investigation, 58 General Electric (GE) and 95 Pratt & Whitney proposed concepts were evaluated by representatives from various manufacturing companies and airlines, including NASA, GE, Pratt & Whitney, Boeing, McDonnell Douglas, United, American, TWA, Pan Am, and Eastern. Several areas of performance improvement were selected, including advanced aerodynamics, reduced clearances, improved cooling techniques, compressor bleed reduction, and nacelle drag reduction.

As part of the ECI project, NASA Lewis/Glenn was tasked with developing new components to reduce fuel consumption and improve performance, identifying the sources and causes of performance losses in existing engines, and providing recommendations to minimize these losses for existing as well as future turbofan engines [6].

The goal of engine diagnostics, the second portion of the ECI project, was to identify the causes of engine performance deterioration by conducting ground tests and gathering in-flight data for both new and existing GE CF6 and Pratt & Whitney JT9D engines used to power the DC-10 and the B-747 airframes. For both engines considered, examination of the data collected and the hardware used revealed that engine performance losses occur in the initial flights and can be attributed to an increase in clearance due to friction between blades and stationary seals. Long-term performance loss is due to increased blade-tip clearance in all engine components, thermal warpage and distortion in the turbines and airfoil, and seal erosion in the fan and low-pressure compressor. The project revealed that aerodynamic loads on the nacelle were the main cause of increased clearance in the engine's cold sections, and that aerodynamic loads on the nacelle and thermal expansion mismatch were the main cause of increased clearance in the engine's hot sections. By 1982, most of the ECI concepts were being implemented in engine components, thus improving their efficiency and providing conceptual design modifications for the next generation of engines to ensure fuel efficiency.

The goal of the EEE project, also managed by NASA Lewis/Glenn, was to design, test, and evaluate, under controlled conditions, new turbofan engine concepts with the following objectives: SFC reduction by at least 12%, performance deterioration rate reduction by at least 50%, DOC improvement by at least 5%, and compliance with future FAA regulations and Environmental Protection Agency exhaust emission standards [6]. Both GE and Pratt & Whitney designed and built flight propulsion systems, including engine components, nacelles, exhaust gas mixer engine control systems, and engine accessories with estimated SFC improvements with respect to baseline engines between 14% and 15%. The Pratt & Whitney EEE design is illustrated in figure 1.

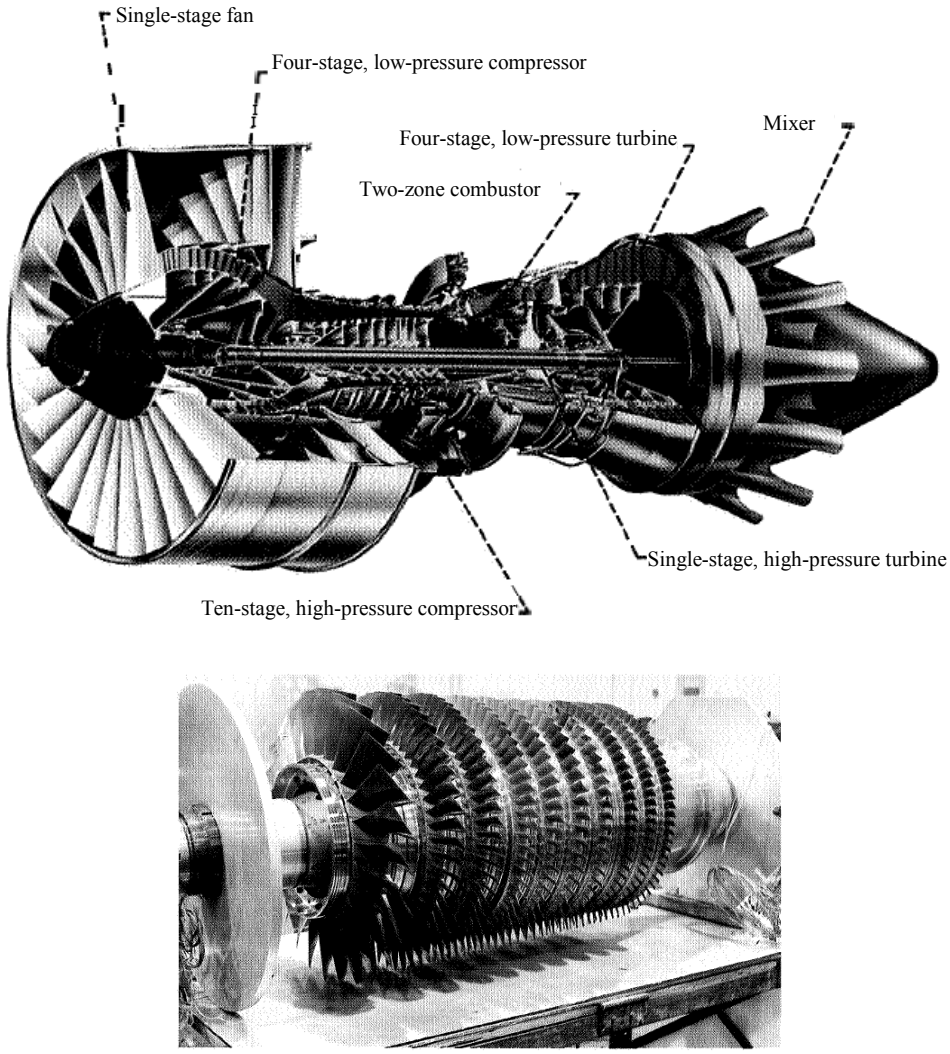

Figure 1. Pratt & Whitney EEE Configuration (top) and Pratt & Whitney EEE Ten-Stage, High-Pressure Compressor Rotor Assembly (bottom) [6]

The objective of the ATP project, also managed by NASA Lewis/Glenn, was to develop efficient, reliable, and acceptable operation of a turboprop aircraft at cruise speeds up to Mach 0.8 and altitudes up to 35,000 feet [6]. The goal was to achieve up to 20% fuel savings with respect to existing turbofan engines. From 1955 to 1975, all efforts were focused on developing jet technology; therefore, the ATP project had to overcome a 20-year gap in high-speed propeller research. It was clear to propeller fan designers that several aspects of technology development and integration needed to be solved and demonstrated before successful implementation of propeller fan designs could be implemented into existing airframes. Challenges remained in the areas of propeller acoustics, structure, installation-related losses, cabin noise and vibration levels, and gearbox capability.

The purpose of the CPAS project, managed by NASA Langley, was to promote the use of advanced materials in existing airframe components to reduce the weight of these components and thereby reduce airframe fuel consumption. For years, NASA and several aircraft companies

studied the use of composite materials in airframe structures, with major advancements occurring in the early 1970s. In 1972, under the Long-Range Planning Study for Composites (RECAST) project, representatives from government agencies, academia, and industry established a long-term goal—to study the possibility of using composites in NASA and U.S. Air Force (USAF) research. The results of the RECAST project revealed a lack of confidence in the materials and cost [16]. By 1976 and the start of the ACEE program, composite research and application was identified as one of the six major projects to be implemented under the program.

Composite materials were a key element in the ACEE program because of the potential weight savings they offer, due to their higher strength and stiffness but also because of the potential production and cost reduction by reducing part count [2]. The main objective of the CPAS project was to provide both military and commercial aircraft manufacturers the technology and the confidence they would require to commit to building composite parts. As of July 1976, numerous secondary structure components were used in commercial service on 43 airframes or 139 aircraft components (L-1011 fairings, B-737 spoilers, DC-10 aft pylon skins, and DC-10 upper aft rudders) [2]. However, these components account for only a small percentage of the airframe's total weight. Significant weight savings of up to 25% could be achieved by using composite materials extensively on primary structural components, yielding an increased fuel efficiency of up to 15% [6 and 16]. The CPAS project initially focused on redesigning and certifying small aircraft secondary components, with the intent of implementing composite technology in more complex primary components through the 1990s.

Another important aspect of the ACEE program was to identify and implement new aerodynamic technologies that would lead to more efficient airframes. The EET project, also conducted at NASA Langley, focused on developing technologies in advanced aerodynamics and active controls. Those advanced aerodynamic development areas included the use of supercritical wings, lower swept wings, and the addition of winglets to reduce induced drag and increase the overall wing and aircraft efficiency, as shown in figure 2 [6 and 17-19].

Near the speed of sound, supercritical airfoils, unlike conventional airfoils, provide pressure distributions that prevent the boundary layer separation that is associated with increased drag, as shown in figure 3. A higher cruising speed can be achieved using supercritical aerodynamics, with a corresponding fuel consumption reduction of up to 15% due to the decrease in induced drag [6]. A thicker airfoil, which provides a greater wing depth for a lighter more efficient wing construction, may be used. Another major source of induced drag is the trailing vortex that forms at the tip of the wing as a result of the pressure gradient between the top and bottom surfaces. Winglets can reduce the induced drag, thus improving the lift-to-drag ratio and increasing the overall airframe efficiency.

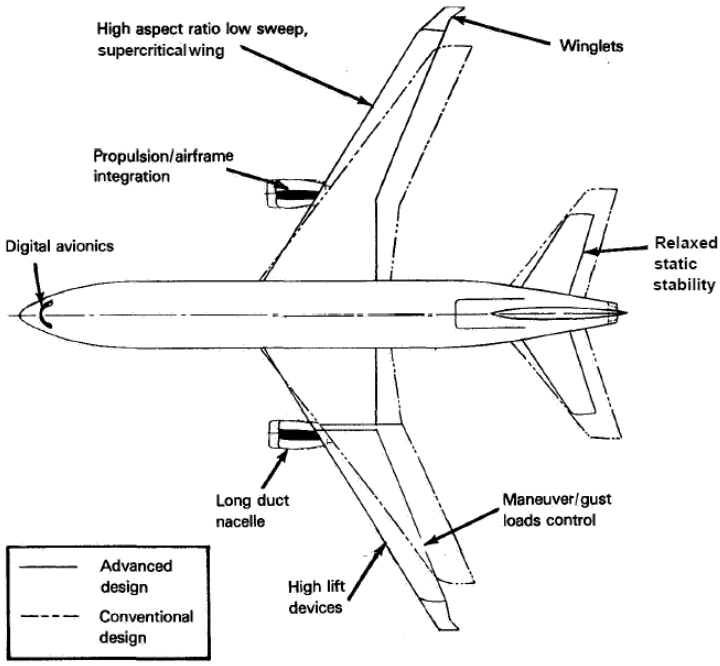

Figure 2. Advanced Design Investigated by the EET Project [6]

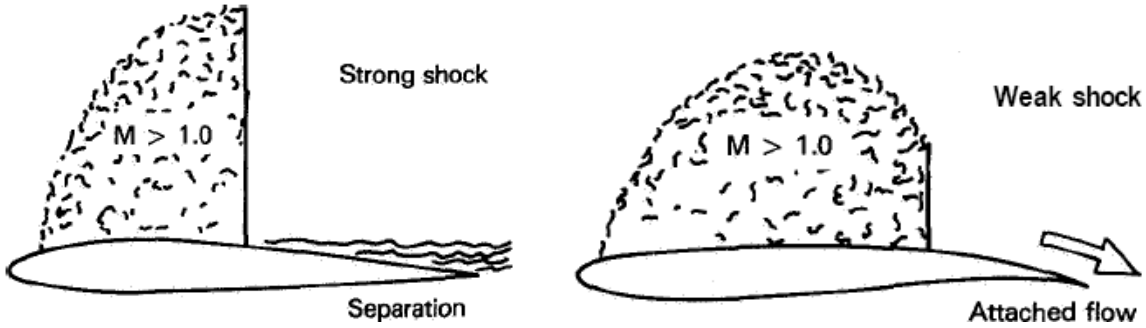

Figure 3. Conventional (left) vs. Supercritical (right) Airfoil Flow Fields and Pressure Distributions

Extensive research was conducted to demonstrate the increased efficiency associated with the use of active control systems [20-22]. This was identified as another major component in aircraft energy efficiency. Several wind tunnel models of existing aircraft were used to study and validate active control systems: a flutter suppression system and an active lift distribution control system (ALDCS) [20]. Wind tunnel and flight tests on the B-52 model and airplane demonstrated that the flutter mode control (FMC) system delayed or prevented the onset of flutter, with zero damping corresponding to the onset of flutter, as shown in figure 4. Similarly, wind tunnel [20] and flight tests showed that the ALDCS system reduced the wing inboard stresses induced during gusts and maneuvers, thereby reducing wing fatigue damage and extending the life of the part, as shown in figure 5.

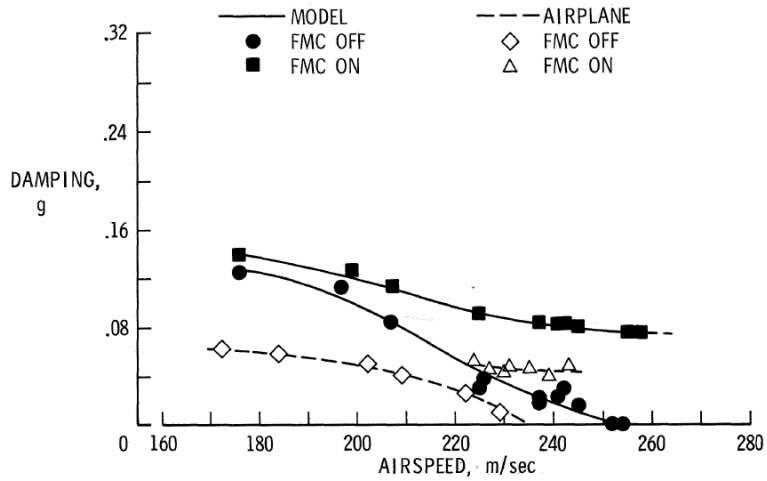

Figure 4. Effect of FMC System on Damping for the B-52 Model and Airplane [20]

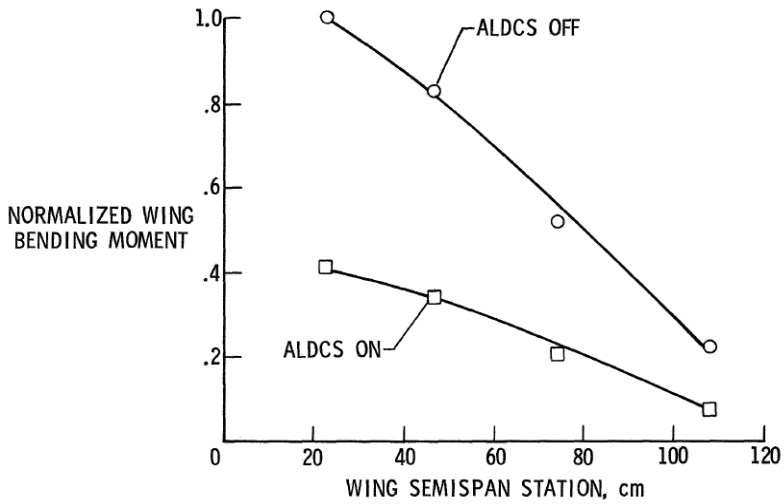

Figure 5. Effect of ALDCS on C-5A Model Wing, Spanwise Distribution of Bending Moment [20]

The LFC project, also managed by NASA Langley, focused on the design and implementation of the laminar boundary layer stabilization system. One of the main challenges of modern civil air transport, which operates at constantly faster speeds, is to maintain a thin smooth layer of air between the surfaces of the aircraft and the free airstream, a condition referred to as laminar flow. When the flow changes from laminar to turbulent, drag is increased, thus reducing fuel efficiency. LFC provides a potential 20% to 40% fuel savings; however, implementation of the concept requires major structural changes, including the development of slotted porous surfaces that allow suction of the turbulent boundary layer. Pumping systems are also required to permit this suction. Laminar flow research predates World War II; however, it was not until the 1960s that Northrop Grumman conducted an LFC demonstration, under a USAF contract using the X-21 aircraft. More than 200 t est flights incorporating the LFC system showed good performance reliably and repeatedly, and laminar flow was achieved over most of the USAF X-21 intended laminar wing area [23]. Under the ACEE program, Boeing, Douglas Aircraft

Company, and Lockheed Corporation were tasked with designing and testing suction system approaches. This included wind tunnel tests of slotted wings, laboratory tests of wings that incorporate suction systems, and construction and evaluation of feasibility coupons. The cost of production hardware remains one of the main challenges in implementing LFC systems.

Major accomplishments have been achieved with the ACEE program, including the introduction of lighter materials in aircraft secondary and medium primary components, the use of practical active controls to improve aerodynamic efficiency, and the use of improved engine components to promote fuel efficiency. The ACEE technology base provided benefits to both the commercial and military sectors and laid a foundation for future research in fuel-efficient transport. With the progressive implementation of fuel-efficient technology in new aircraft designs over a 25-year span (from 1975 to 2000), up to 40% potential fuel savings could be achieved, as illustrated in figure 6. Parallel to the ACEE composites project, and during the same time frame, NASA initiated the Composites Advanced Space Transportation Systems project to develop composite polyimide structures with an operational capability up to 600°F for space vehicle applications [24].

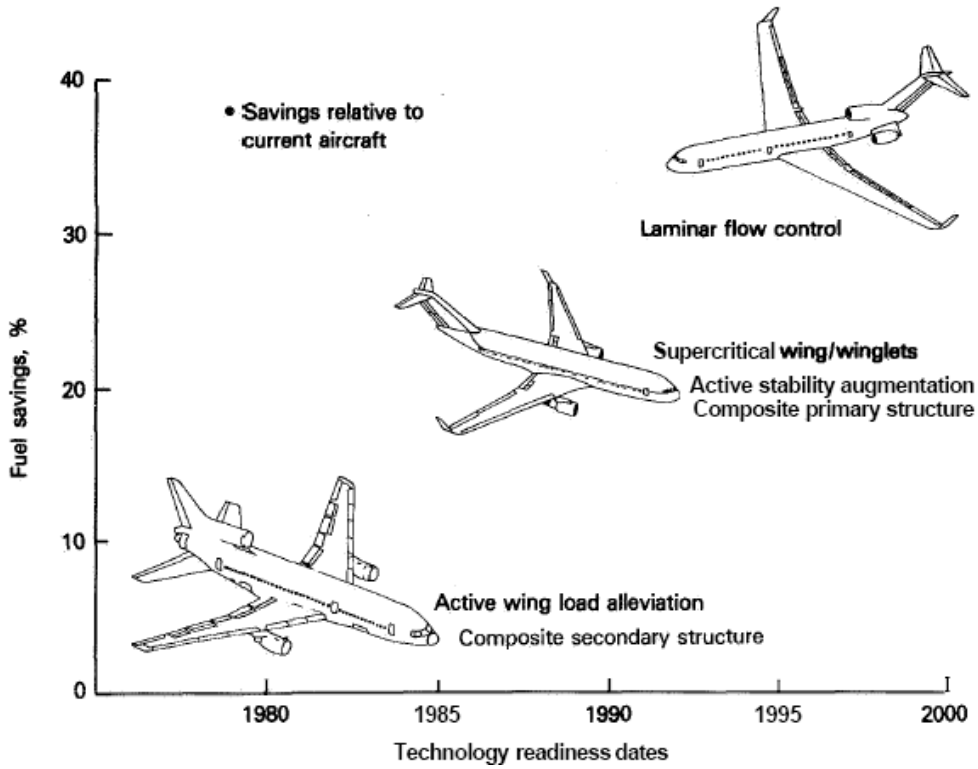

Figure 6. Potential Fuel Savings With the Implementation of EET [6]

1.2 OVERVIEW OF THE ACEE COMPOSITES PROGRAM.

The NASA ACEE composites program achieved significant developments between 1976 and 1986 in the areas of composite materials and structures. During this time, the development and implementation of composite technology in aircraft components became a national effort

involving scientists from industry, government, and academia. The composites program focused on using advanced materials in existing aircraft structural components, thus offering greater potential for weight savings and, ultimately, operating costs of commercial aircraft. More extensive implementation of composite technology in aircraft structural components would require overcoming a few obstacles, such as uncertainties related to production costs, development costs, long-term durability and performance, and maintenance requirements. In addition, composite expertise needed to be transferred from research groups to production designers, analysts, and manufacturing personnel. A systematic building-block approach was adopted whereby composite structure development would start with lightly loaded secondary components, followed by medium primary components, and conclude with wing and fuselage design. Although considered highly successful, the program was terminated before the implementation of composite materials in wing or fuselage primary structures.

Under the ACEE composites program, Boeing, McDonnell-Douglas, and Lockheed contracted to develop the following secondary and medium primary components (see figures 7 and 8):

- The upper aft rudder of the DC-10
- The inboard ailerons of the L-1011
- The elevators of the B-727
- The vertical stabilizers of the L-1011 and DC-10
- The horizontal stabilizer of the B-737-200

All these components yielded weight savings of at least 21.6% compared to the original aluminum alloy components [15]. The common element in these parts was the material system, the same Narmco T300/5208 graphite epoxy 350°F cure system used for all ACEE composite components.

The structural details of the L-1011 advanced composite aileron assembly are shown in figure 9. The aileron covers are of a sandwich construction using three-ply facesheets and a syntactic epoxy core. The front spar is a ten-ply CFRP channel, and the rear spar is a constant thickness aluminum 7075-T6. Ribs are channeled with various thicknesses that consist of three main ribs, five intermediate ribs, and two closeout ribs. The three main ribs are reinforced at the caps by adding five unidirectional plies. Five shipsets of ailerons were manufactured and entered into service in 1982.

(a)

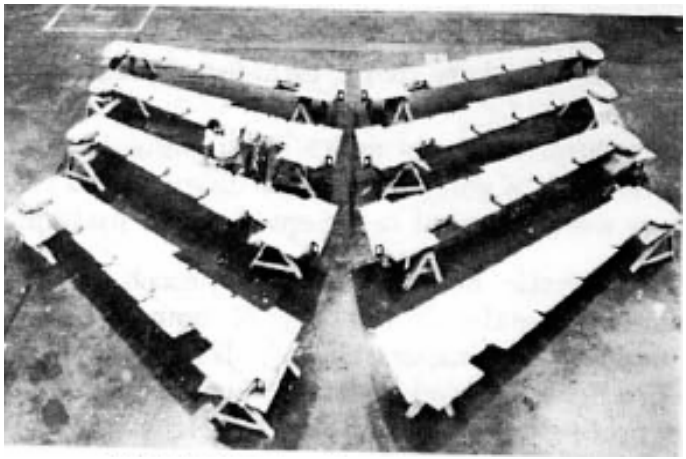

(b)

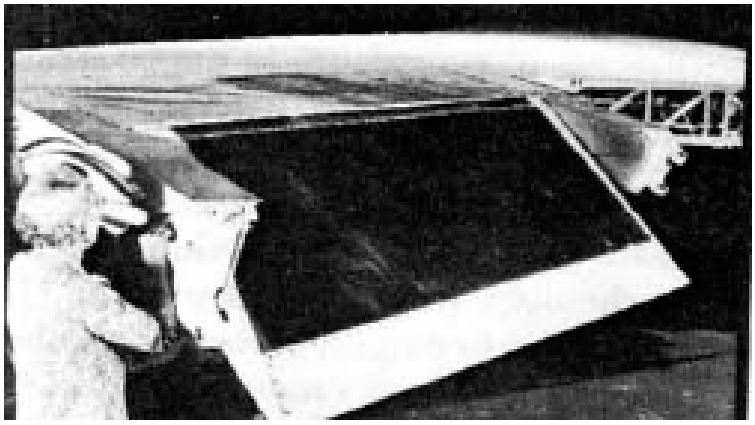

(c)

Figure 7. Composite Secondary Components (a) Douglas DC-10 Upper Aft Rudder, (b) Boeing B-727 Elevators, and (c) Lockheed L-1011 Inboard Aileron [15]

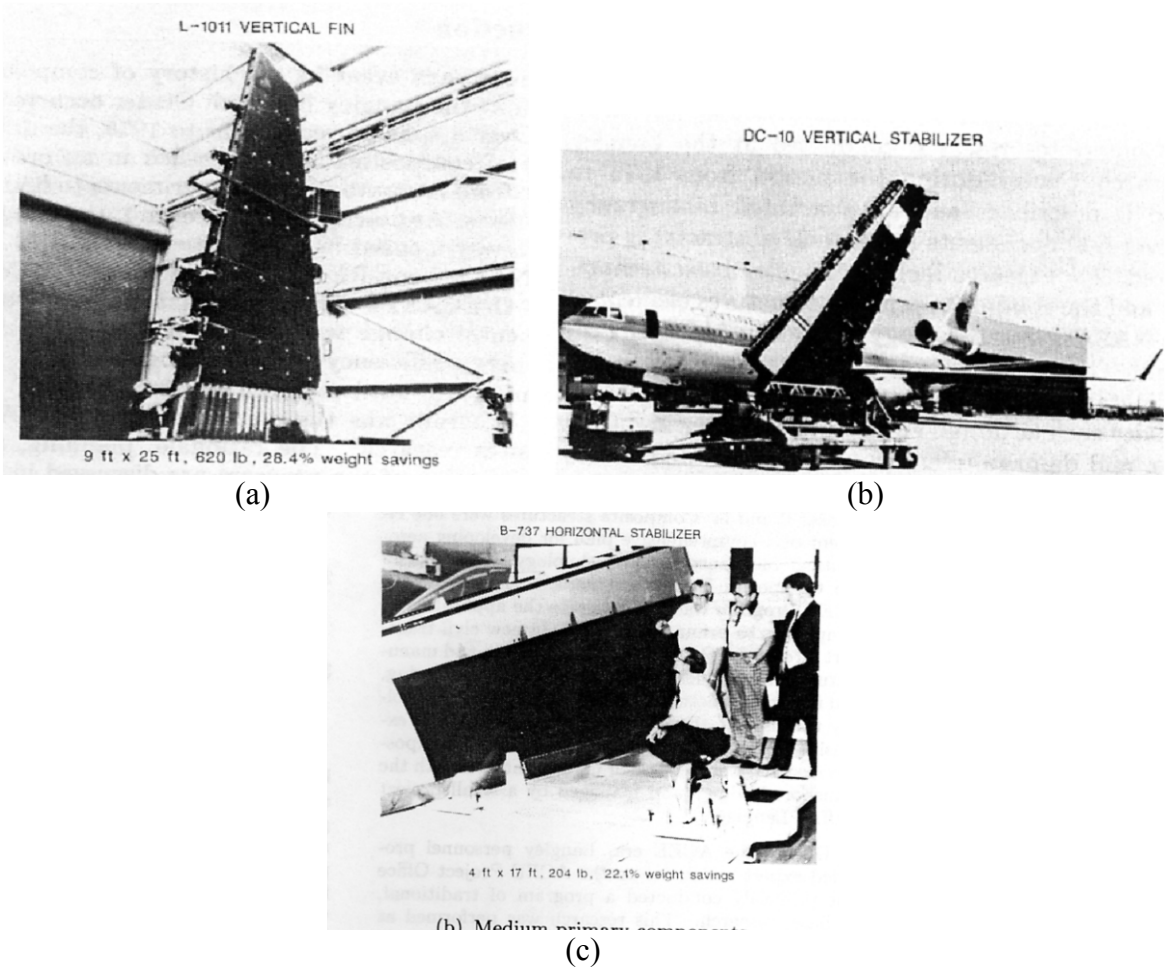

Figure 8. Composite Medium Primary Components (a) Lockheed L-1011 Vertical Fin, (b) Douglas DC-10 Vertical Stabilizer, and (c) Boeing B-737 Horizontal Stabilizer [15]

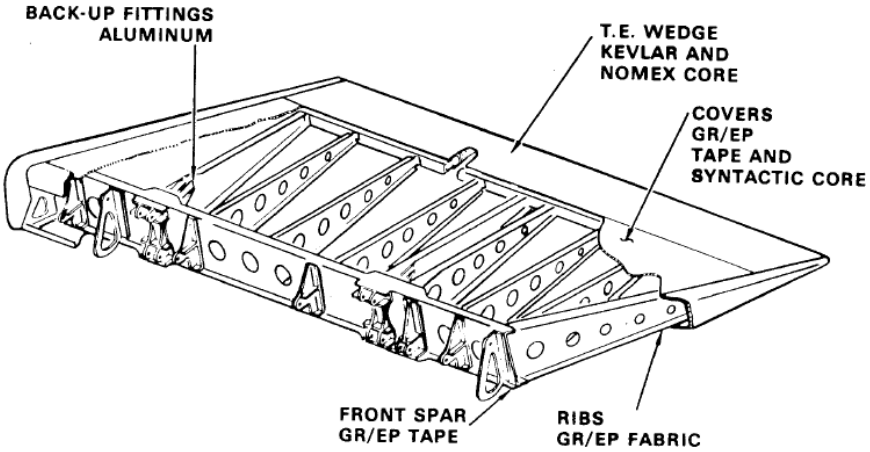

Figure 9. Structural Arrangement of L-1011 CFRP Inboard Aileron [25]

The structural details of the DC-10 CFRP aft rudder are shown in figure 10. The rudder consists of left-hand (LH) and RH skins, front and rear spars, and 33 ribs, all of which are of CFRP tape and fabric. Twenty rudders were manufactured and entered into service in 1976 [26].

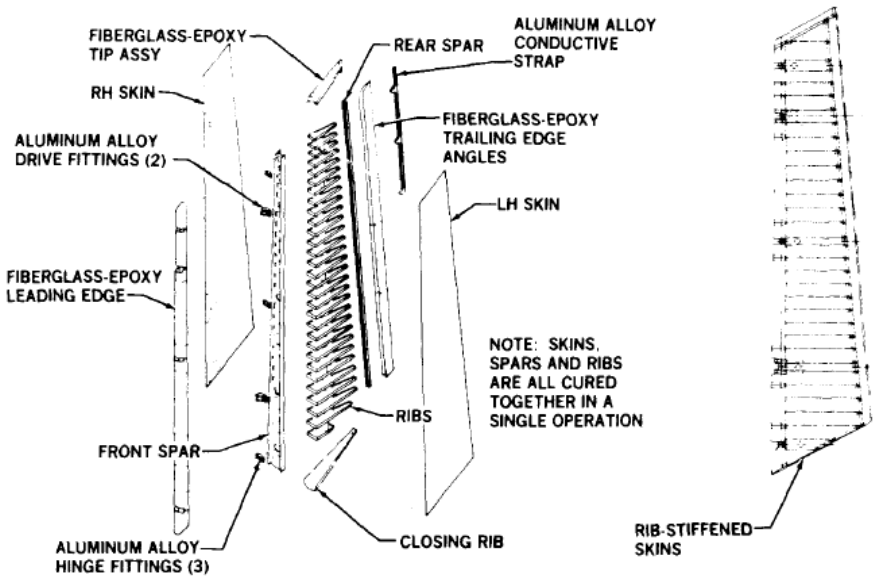

Figure 10. Structural Arrangement of DC-10 CFRP Upper Aft Rudder [26]

Figure 11 shows the structural details of the B-727 CRFP aft elevator, which consists of skin sandwich panels and ribs, and solid laminate spars [27]. Five shipsets were manufactured and entered into service in March 1980.

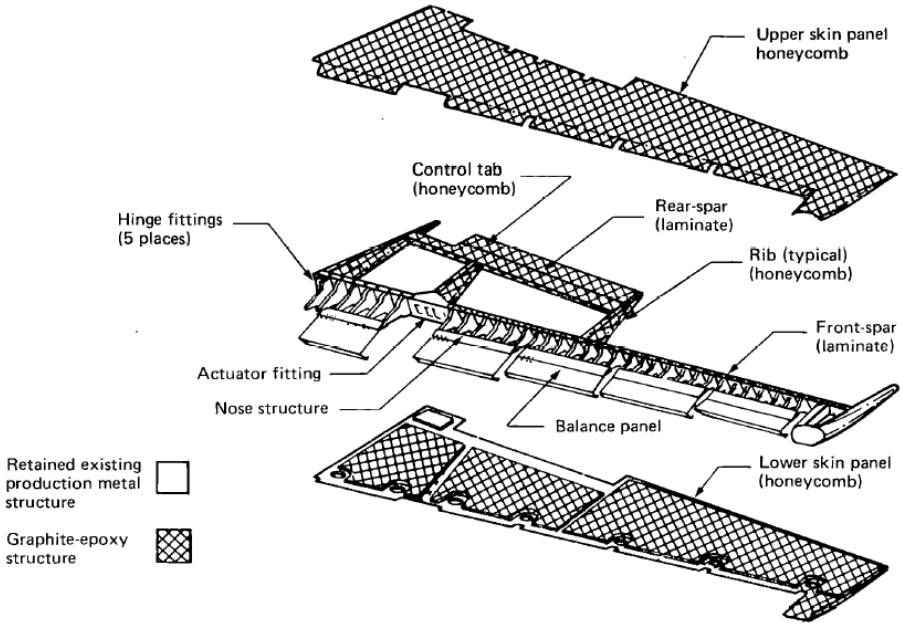

Figure 11. Structural Arrangement of B-727 CFRP Elevator [27]

The composite L-1011 vertical fin was designed so that it would have the equivalent bending and torsional stiffness as the metallic fin so as not to affect the aero elastic response. Details of the fin construction are shown in figures 12 and 13. The fin box consists of 2 covers, 2 spars, 1 stub spar with 11 ribs: 3 solid laminate ribs, 2 actuator ribs, and 6 truss ribs, resulting in a 25.2% weight savings with respect to the metallic configuration, as described in table 1. The covers are stiffened laminates with cocured hat sections. The two main spars consist of an individual component cocured with rib-attach angles, stiffeners, caps, and webs [28]. The stub spar is an aluminum assembly. The truss rib caps are CFRP C channels, and the truss members are aluminum extrusions.

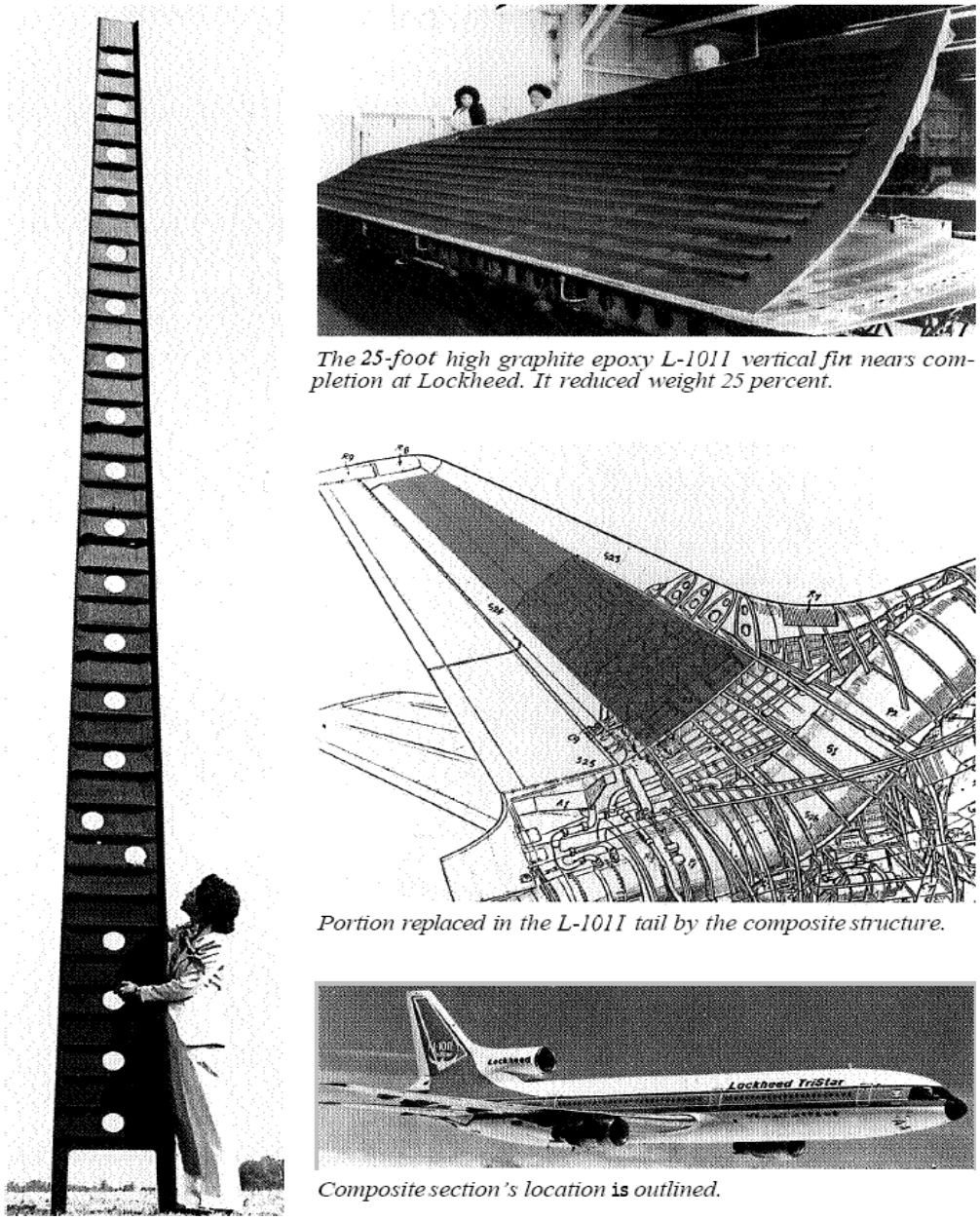

The 25-foot high graphite epoxy L-1011 vertical fin nears completion at Lockheed. It reduced weight 25 percent.

Portion replaced in the L-1011 tail by the composite structure.

Composite section's location is outlined.

Figure 12. The L-1011 Composite Vertical Fin [28]

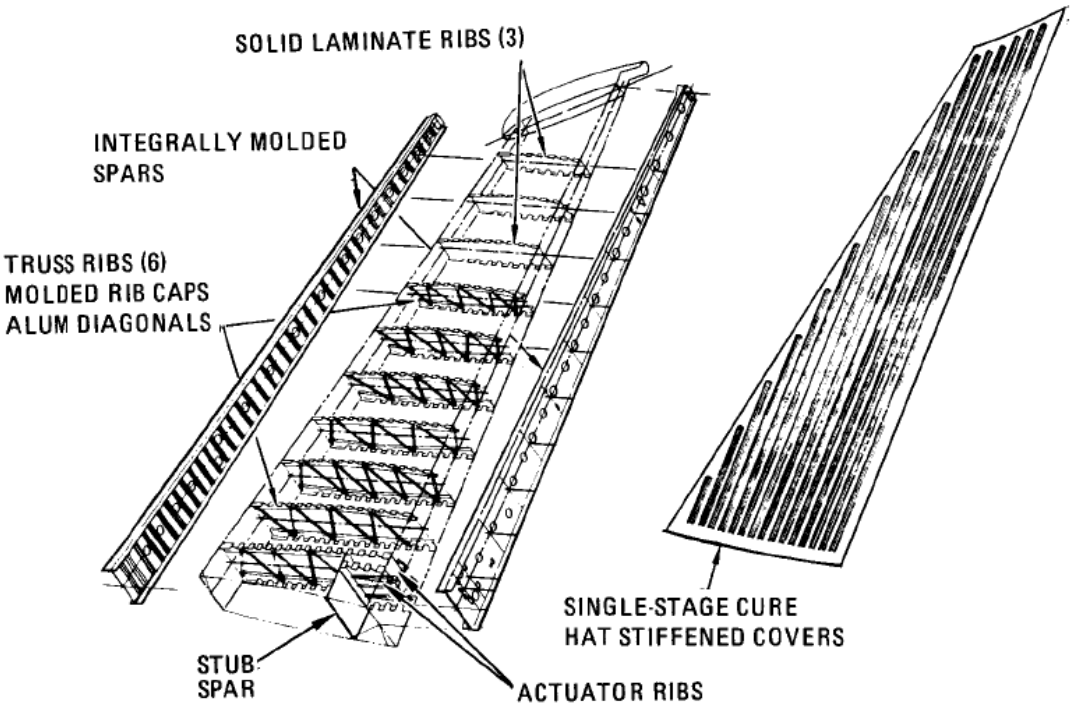

Figure 13. The L-1011 Composite Vertical Fin Structural Arrangement [28]

Table 1. Comparison of Metallic vs. Composite Fin [28]

	Metal Box	Composite Box
Weight (lb)	858	642
Percent Composite Material	-	76
Weight Saved (lb)	-	216
No. of Ribs	17	11
No. of Parts	716	201
No. of Fasteners	40,371	6911

The first static test article failed prematurely at 98% of the ultimate load design at the spar cap. Analysis shows that the failure was the result of high out-of-place secondary loads, which induced interlaminar tension and bending loads to the spar caps. To provide more resistance to out-of-plane loads, the existing spar caps were reinforced with formed aluminum angles from root to tip; the co-cured CFRP tees attaching the front spar to the ribs were also reinforced with aluminum angles mechanically attached to the webs, and aluminum doublers were bonded and fastened to the covers/skins to provide additional support in the run-out bays.

After reinforcing the failure sites, static and fatigue tests were successfully completed on a second test article according to FAA certification requirements, but no flight tests were ever performed.

The composite DC-10 vertical stabilizer construction is illustrated in figures 14, 15, and 16. The structure consists of two, one-piece skin panels and four spars and ribs. The ribs and spars were adhesively bonded using B-stage (partially cured) prepreg epoxy angles. The honeycomb skin panels were bolted to the spar-rib substructure. The first test article failed during initial baseline limit load tests at the rear spar web, in the location of the spar access cutouts. High-stress concentrations were induced by oversized holes and, consequently, resulted in the inadequate fit of the fasteners attaching the covers to the spar web cutouts. Design modifications were incorporated in subsequent units and included a cover redesign for all cutouts and secondarily bonded ply reinforcements to selected rib and spar webs to increase their margins of safety [29 and 30]. The second test article was successfully tested and demonstrated fatigue capability (one lifetime without damage and one fatigue lifetime with damage), limit lo ad capability (with damage), and ultimate residual strength capability after damage repair. The stabilizer received FAA certification in 1986 and was entered into commercial service in January 1987.

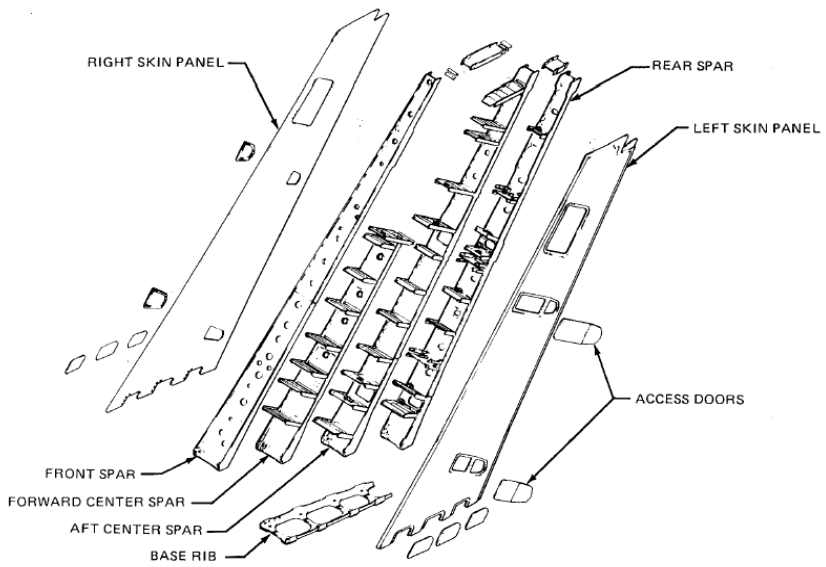

Figure 14. The DC-10 Composite Vertical Stabilizer Structural Arrangement [29 and 30]

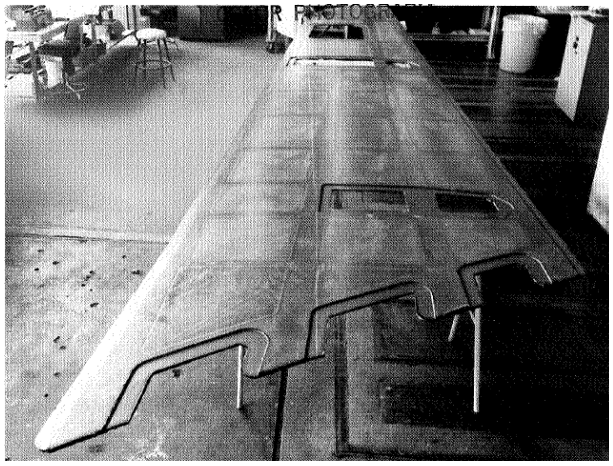

Figure 15. The DC-10 Composite Vertical Stabilizer CFRP Cover [6]

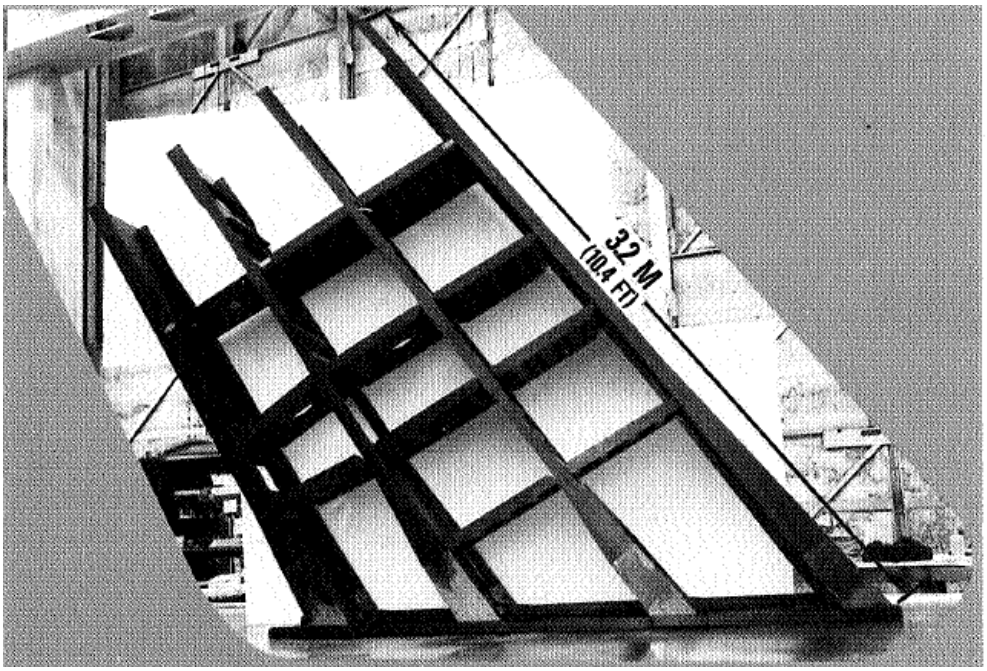

Figure 16. The DC-10 Composite Vertical Stabilizer Substructure [6]

The last test article that was designed and constructed was the B-737 composite horizontal stabilizer. This test article is the subject of this study and is described in detail in section 2.

2. THE B-737 COMPOSITE HORIZONTAL STABILIZER.

As part of the NASA ACEE composites program, Boeing redesigned and manufactured five shipsets of the B-737-200 horizontal stabilizer using CFRP composites. The original equipment manufacturer (OEM) adopted a f ail-safe, damage-tolerant approach to certify the structure, whereby the structure's capability to sustain ultimate loads was validated with analysis supported by appropriate test substantiation [31]. This complies with Title 14 Code of Federal Regulations (CFR) Part 25 [32].

The objectives of the B-737-200 composite horizontal stabilizer program included achieving a minimum 20% weight reduction with respect to the metal structure, fabricating at least 40% by weight of its components using composite materials, demonstrating cost-effectiveness of the structure, obtaining FAA certification for the structure, and closely monitoring its performance in service.

Analysis was conducted to establish the most critical environment in which the stabilizer would be operating. It was found that a combined moisture level of 1.1% ±0.1 with temperature extremes of 180° and -75°F would simulate the worst environmental conditions to which the structure would be exposed [1]. Laminate, element, and subcomponent data were generated at these extreme conditions to obtain allowable values. Subsequent statistical reduction factors were implemented and provided high-confidence design values to use in the substantiating analysis.

Certification was completed in August 1982, and all five shipsets were deployed in 1984. The OEM closely monitored the performance of the stabilizers for 7 years. Outstanding performance was demonstrated with no in-service incidents attributed to the composite structure.

2.1 THE B-737 HORIZONTAL STABILIZER DESCRIPTION.

The B-737 horizontal stabilizer, shown in figure 17, consists of a structural box, an aluminum leading edge, a stabilizer tip, a fixed fiberglass honeycomb trailing edge and ribs, an elevator, and body gap covers. Each stabilizer is secured to a metal center structure with three lugs at the rear spar and two lugs at the front spar. The structural box was redesigned using CFRP composites so that maximum commonality was achieved with the existing metal configuration and that both structures are interchangeable in terms of geometry and aerodynamic shape. No modifications to the interface with the center section were made to meet the interchangeability requirements. The bending and torsional stiffness of the composite stabilizer as well as its aerodynamic shape and planform were made comparable to the metal stabilizer to meet control effectiveness and flutter requirements [1]. Furthermore, the composite stabilizer was designed to be damage tolerant, and its strength, durability, inspectability, and serviceability equivalent to that of the metal structure.

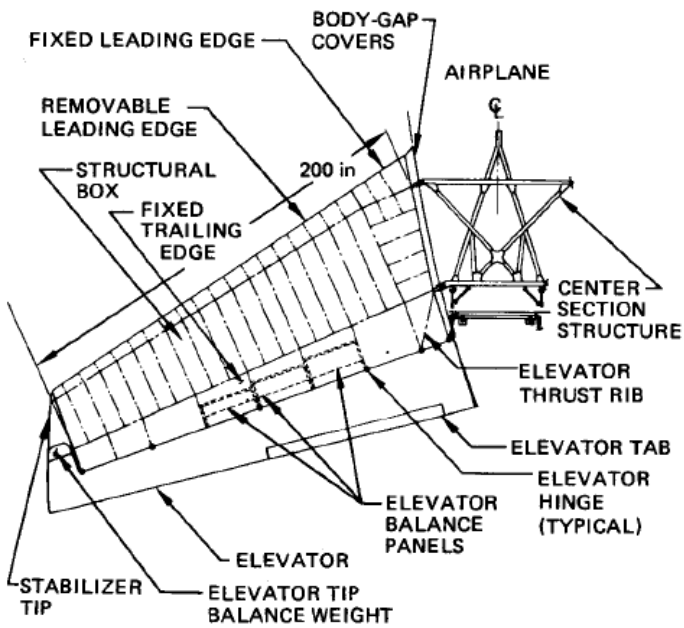

Figure 17. The B-737 Horizontal Stabilizer General Arrangement [1]

Several composite structural box arrangements were evaluated during the design phase of the composite stabilizer, i.e., a multiple-rib concept, a honeycomb concept, and a stiffened skin concept. The multiple-rib concept involved the fabrication of numerous parts and the use of many fasteners. The honeycomb concept increased in complexity as multiple reinforcements and doublers were required in various areas to be compatible with the side-of-body attachments and to react the trailing edge and elevator loads. The stiffened skin concept, as shown in figures 18 and 19, was chosen due to its structural efficiency and minimal program cost [1]. The complexity of the stiffened skin concept was concentrated on the skin panel fabrication. The

remaining substructure was simplified, using a minimal number of parts and, thus, a reduced number of fasteners.

The structural details of the composite stiffened skin and existing metal stabilizer designs are shown in figures 19 and 20, respectively. The structural arrangement of the stabilizer consists of a single co-cured skin I-stiffener combination, 191 inches long and 50.5 inches wide at the inboard end with stringers spaced 3.85 inches apart. Details of the stiffened skin are shown in figure 19. The skin I-stiffeners were manufactured as two C-channels placed back to back using debulked mandrels that were subsequently positioned onto the skin for cocuring. Mechanical fasteners were used to attach the stabilizer skins to the spars and ribs. Titanium Hi-Lok® fasteners with corrosion-resistant steel collars and washers were used to assemble the lower skin. Inconel Monogram blind fasteners, commonly referred to as "Big Foot" fasteners, were used to assemble the upper skin.

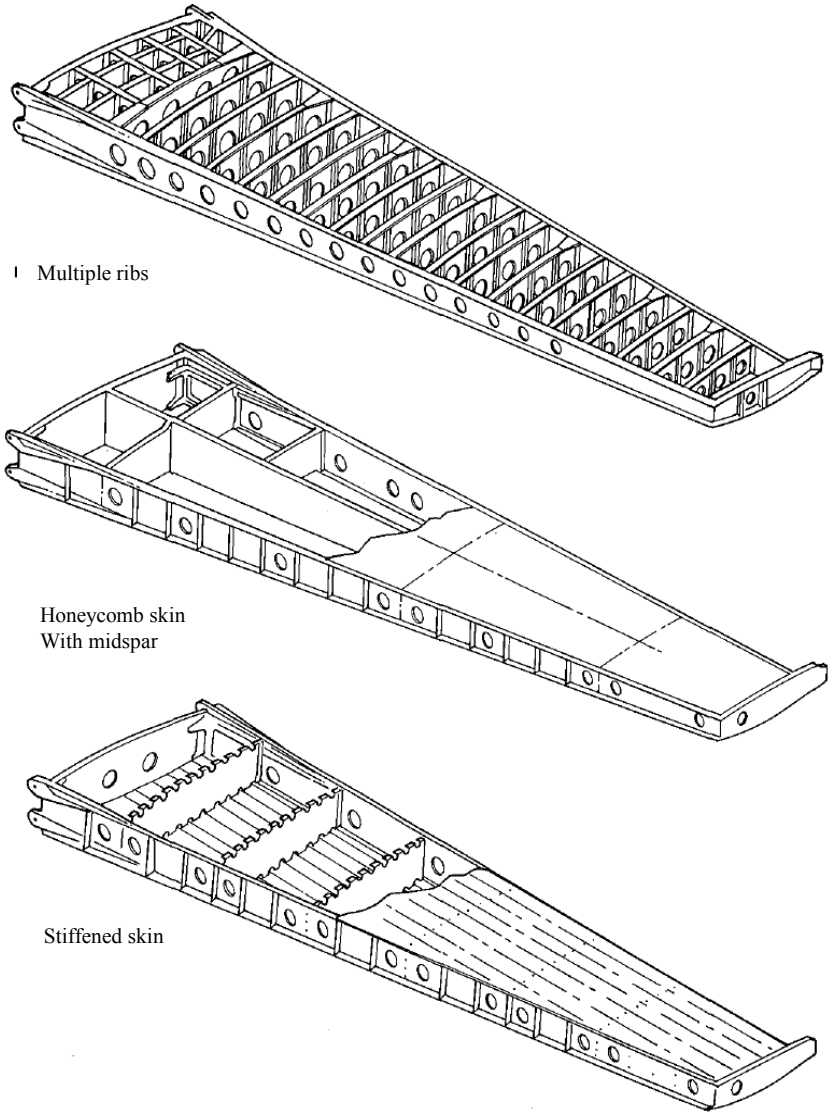

Figure 18. Stabilizer Box Concepts Evaluated During Design Phase [1]

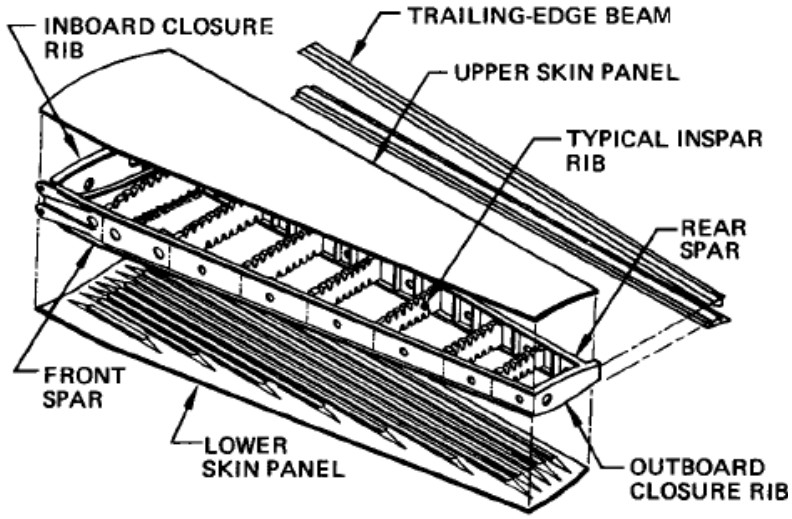

Figure 19. Composite Stabilizer Structural Arrangement [1]

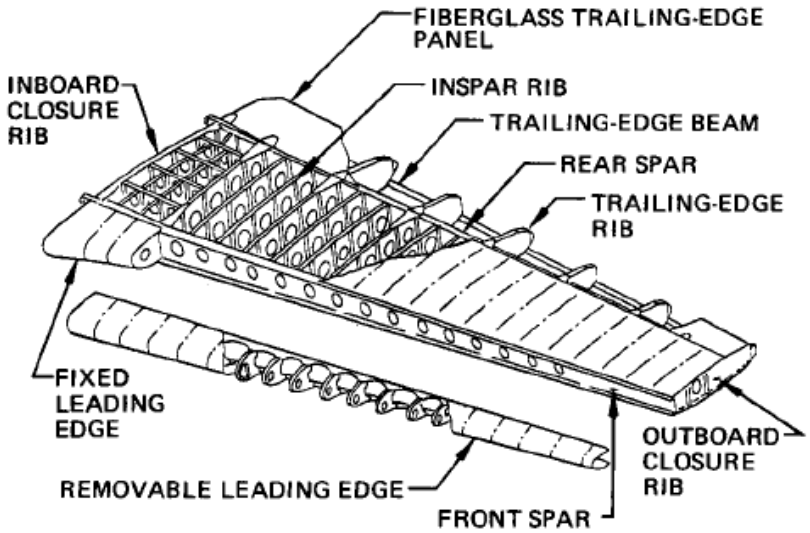

Figure 20. Metal Stabilizer Structural Arrangement [1]

Honeycomb inspar ribs were used because of the concept's simplicity in terms of tooling, fabrication, and cost. They were fastened to the skins using CFRP shear ties. The stabilizer box contained seven inspar ribs, an outboard closure rib, and an inboard closure rib. The inboard closure rib closed the inboard section of the stabilizer and was used to react the torsional shear loads in the skin panels and to redistribute the load into the spars, which in turn was reacted by the stabilizer center section. The inboard closure rib was a laminate construction. The outboard closure rib closes the outboard section of the stabilizer and is a laminate construction with aluminum caps that form an I-section. The sandwich inspar ribs have a channel cross section with cutouts along the upper and lower attach angles to provide clearance for the skin I-stiffeners. The sandwich ribs were protected from moisture ingression using paint applied on the tool side and a Tedlar™ film applied on the bag side. Details of the honeycomb rib cross sections are shown in figure 21.

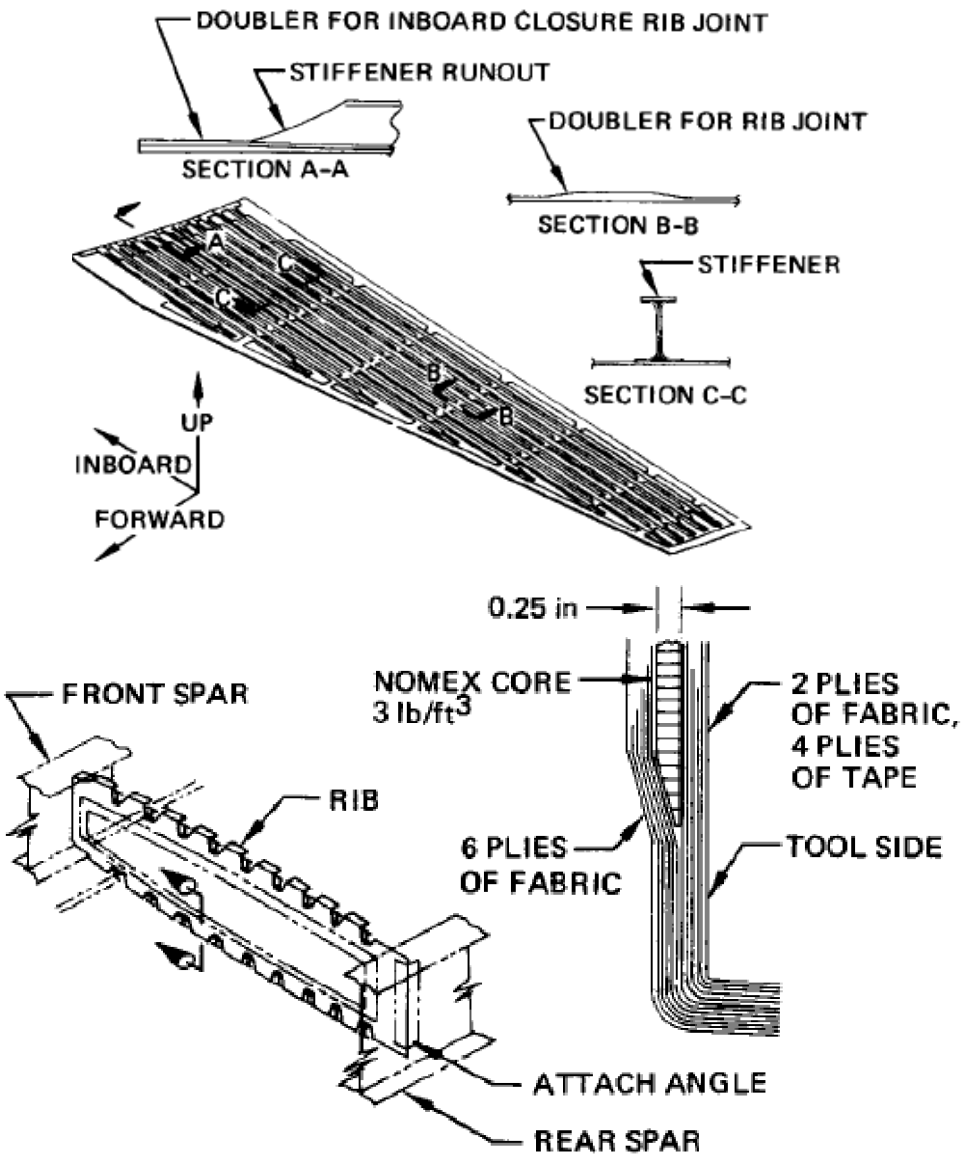

Figure 21. Stabilizer Skin and Rib Details [1]

The spars were I-beams consisting of two precured C-channels and two precured caps bonded together using film adhesive. The rear spar is 191 inches long and 15.25 inches deep at the inboard end. The front spar is 200.5 inches long and 12.25 inches deep at the inboard end. The rear spar has a third lug to meet fail-safe requirements. The front spar does not have an additional lug, as load paths are maintained in the case of either lug failure. Both spars were reinforced with steel straps at the lugs that were used to attach the composite stabilizer to the fuselage center section.

The composite design yielded 21.5% weight savings with respect to the metal configuration, with a final weight of approximately 412.6 pounds, as summarized in table 2.

Table 2. Comparison of Metallic vs. Composite Horizontal Stabilizer [33]

Item	Baseline aluminum stabilizer structure, Kg (lb)/airplane		Advanced composite stabilizer structure, Kg (lb)/airplane		Weight difference, Kg (lb)/airplane		Weight Difference %
Front spar	31.3	(69.0)	21.2	(46.8)	-10.1	(-22.2)	-32.2
Rear spar	71.1	(156.8)	51.6	(113.7)	-19.5	(-43.1)	-27.5
Skins							
Upper	36.2	(79.8)	39.0	(86.0)	2.8	(+6.2)	7.8
Lower	36.2	(79.8)	40.2	(88.7)	4.0	(+8.9)	11.2
Ribs	60.9	(134.2)	34.1	(75.2)	-26.8	(-59.0)	-44.0
Corrosion protection	-	-	1.0	(2.2)	1.0	(+2.2)	-
Lightning Protection	-	-	0.0	(0.0) *	-		-
Access doors	0.7	(1.6)	0.0	(0.0) **	-0.7	(-1.6)	-100
Gap cover support	1.9	(4.2)	0.0	(0.0)	-1.9	(-4.2)	-100
Total stabilizer inspar Structure per airplane	238.3	(525.4)	187.1	(412.6)	-51.2	(-112.8)	-21.5
Stabilizer TE/elevator interface thermal expansion provision	-	-	15.5	-	15.5	-	-

* 1.0 lb included in skin panel weight.
** Gap cover support structure integral design of inboard closure rib installation

2.2 MATERIAL SELECTION.

Various materials were evaluated, and manufacturing producibility was assessed by fabricating test panels from each candidate material to determine factors such as drape, tack, work time, and layup difficulty. In addition, all materials were expected to comply with specific requirements and specifications on prepreg and cured laminate physical properties. Additional factors, such as available industrial database, demonstrated resin durability in various environments, supplier production experience, capacity and control, and ability to produce all material forms, were also considered.

The material systems evaluated included Narmco T300/5208 and T300/5235, Fiberite T300/934 and T300/976, Hercules AS/3501-5A, and Hexcel T300/F263 and T300/F288. Narmco T300/5208 was the material of choice because it satisfied most of the evaluation criteria, was widely used in the industry, and had good environmental properties [1]. The predominant material form was fabric with selected use of tape. The structural details used hand-layup procedures throughout.

2.3 CORROSION PROTECTION SCHEME.

The corrosion protection system used on the composite stabilizer was aimed at isolating the graphite-epoxy areas from the aluminum structure. This was done to avoid galvanic corrosion of the aluminum, as shown in figure 22. Corrosion protection was achieved by (1) co-curing a fiberglass isolation ply onto the CFRP structure in areas where the CFRP structure interfaced the aluminum surface or (2) painting the surface with primer and epoxy enamel. In addition to protecting all graphite-epoxy surfaces from galvanic corrosion, all aluminum surfaces were anodized or Alodine® treated, primed, and enameled. During assembly, wet polysulfide sealant was used between the graphite-epoxy and the aluminum parts. All fasteners through the aluminum surface were installed with wet polysulfide sealant.

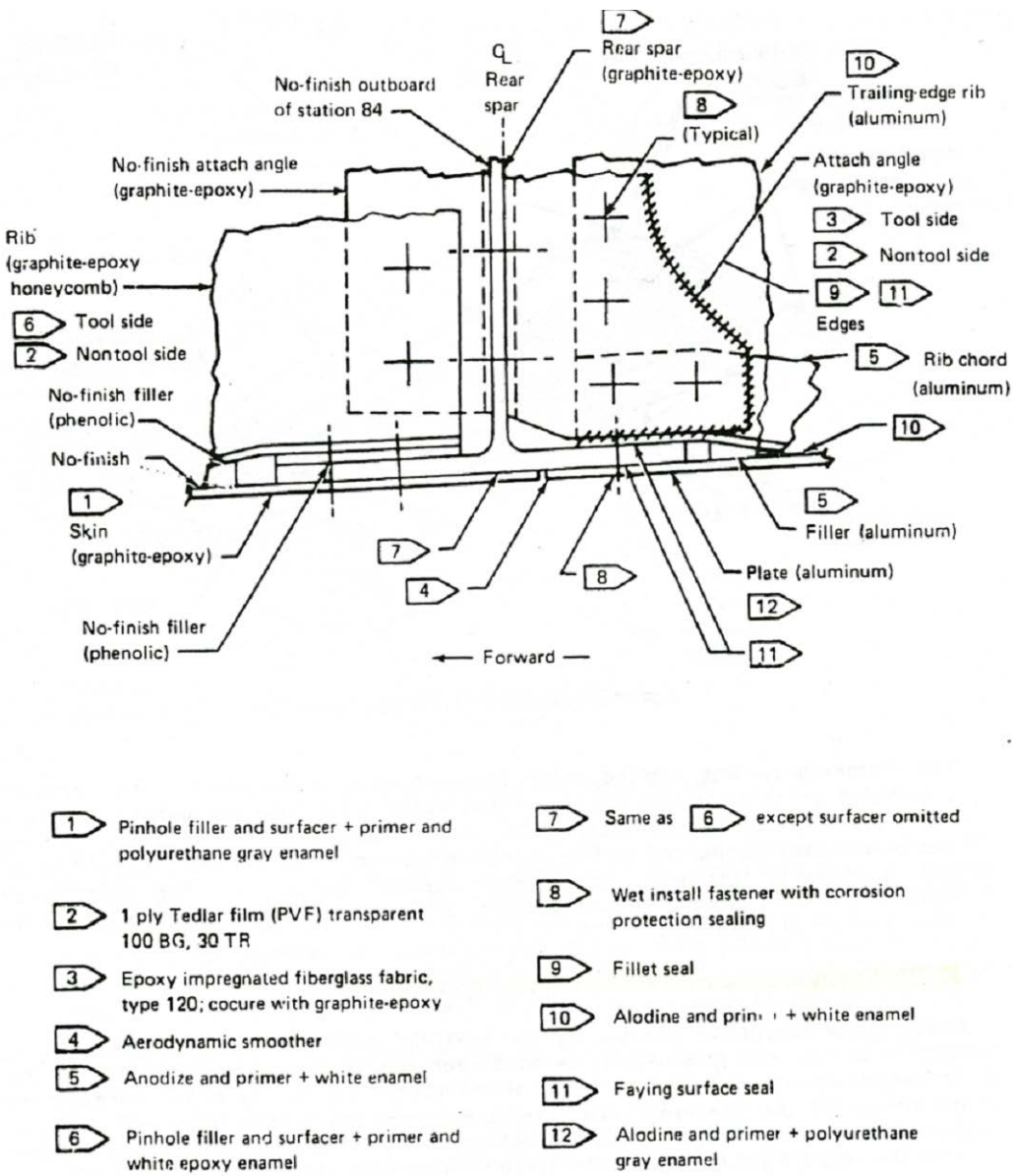

Figure 22. Corrosion Protection Scheme [1]

2.4 LIGHTNING PROTECTION SCHEME.

The lightning protection system developed for the advanced composite stabilizer provided an electrical path around the entire perimeter of the structural box by using bonding straps connecting the aluminum leading edge, the aluminum rib cap of the outboard closure rib, and the aluminum elevator spar. All components were electrically grounded to the fuselage by using the spar lugs and the leading- and trailing-edge ribs.

An aluminum flame spray coating was applied to the composite stabilizer's critical strike zone. This was determined to be the outboard 18 inches on the upper and lower skins, as shown in figure 23. The area under the flame spray coating was insulated using a layer of fiberglass that was co-cured to the skin panels. The flame spray coating was applied to the outboard sections of the skin after fabrication. It was then electrically connected to the metal cap of the outboard closure rib using four mechanical fasteners. The conductive surface was then Alodine coated, primed, and painted.

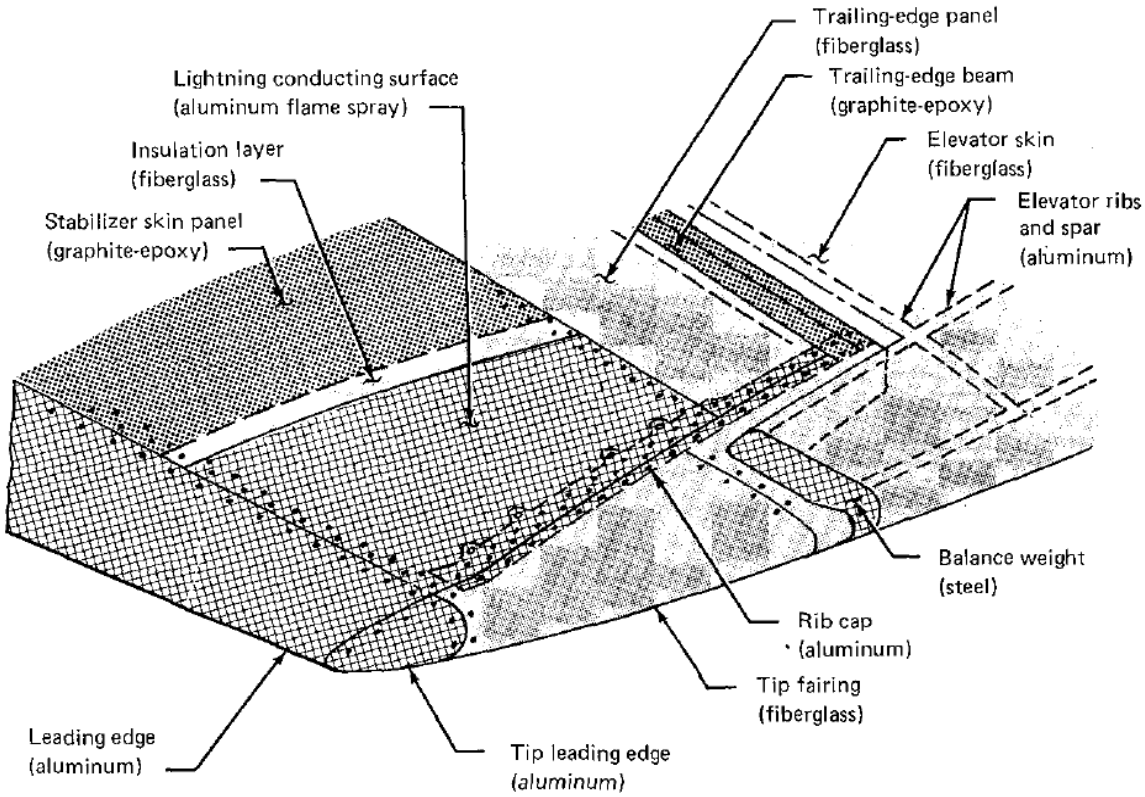

Figure 23. Lightning Protection Scheme [1]

2.5 COMPONENT MANUFACTURING.

The advanced composite stabilizer components were manufactured at Boeing's Fabrication Division in Auburn, Washington. The stabilizer component assembly was conducted at the Boeing facility in Wichita, Kansas. The upper skin layup schedule is shown in figure 24.

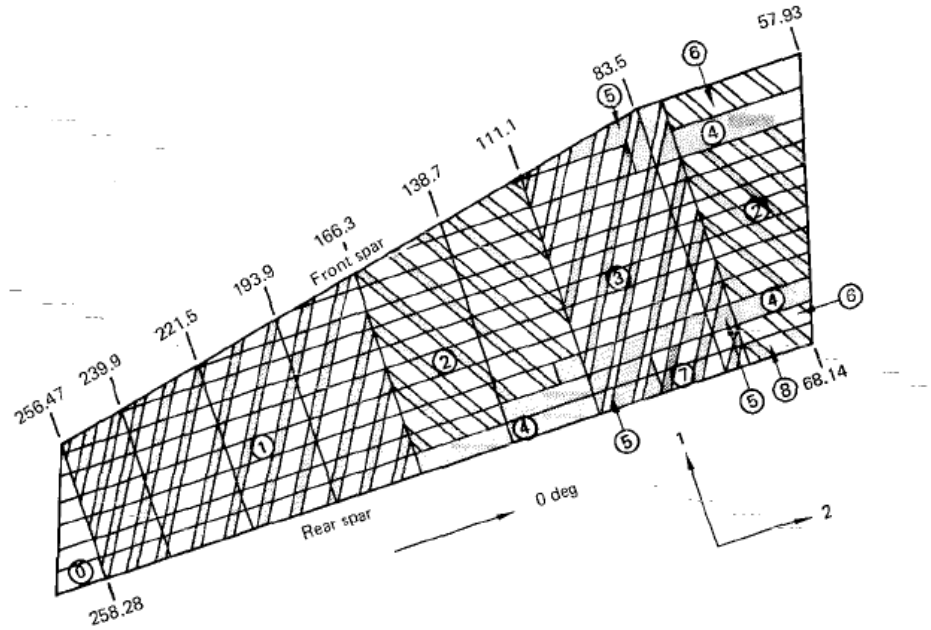

○ Zone
▷ Number of plies in each zone

Zone / Layup	0	1	2	3	4	5	6	7	8
±45 fabric		4	5	5	7	7	9	9	10
0/90 fabric		2	2	2	3	3	3	3	4
90 tape				2		2		2	
Thickness mm(in)	1.27 (0.05)	1.14 (0.045)	1.35 (0.053)	1.70 (0.067)	1.91 (0.075)	2.29 (0.090)	2.03 (0.080)	2.67 (0.105)	2.67 (0.105)
E_1, MPa (lbf/in^2)	18 614 (2.7×10^6)	39 985 (5.8×10^6)	37 572 (5.45×10^6)	56 600 (8.21×10^6)	38 262 (5.55×10^6)	52 394 (7.6×10^6)	35 849 (5.2×10^6)	48 327 (7.01×10^6)	37 572 (5.45×10^6)
E_2, MPa (lbf/in^2)	18 614 (2.7×10^6)	39 985 (5.8×10^6)	37 572 (5.45×10^6)	33 229 (4.82×10^6)	38 262 (5.55×10^6)	34 884 (5.06×10^6)	35 849 (5.2×10^6)	33 298 (4.83×10^6)	37 572 (5.45×10^6)
G, MPa (lbf/in^2)	5 515 (0.8×10^6)	21 371 (3.1×10^6)	22 406 (3.25×10^6)	19 165 (2.78×10^6)	22 406 (3.25×10^6)	19 786 (2.87×10^6)	23 440 (3.4×10^6)	21 027 (3.05×10^6)	22 406 (3.25×10^6)
ν	0.15	0.40	0.43	0.42	0.43	0.42	0.47	0.46	0.43

Figure 24. Stabilizer Upper Skin Stacking Sequence [1]

Although some manufacturing problems were encountered, they caused minimal delays in the production schedule. Delaminations on the upper skin panel of shipset one, at the stringer cap, were detected after cure completion. These were caused by buckling and movement of the caul strips during cure. Therefore, the caul strips were shortened, and the tape used to hold the strips in place was extended to the mandrels. No delaminations were found after these changes were made.

A bonding failure occurred on the rear spar and trailing edge of the LH shipset 3. A close examination of the fractured surfaces revealed traces of silicon, the same compound found in the Frekote® release agent. It was determined that the sources of contamination were either the cleaning cloths or the methyl ethyl ketone (MEK) fluid. Furthermore, MEK and Frekote are similar in appearance and were stored in identical containers. Appropriate changes in bonding procedures were implemented to ensure that such problems did not reoccur. A resin-starved

surface appearance was observed on stabilizer rib and skin panels, and fabrication was suspended for shipsets 2 through 5 until the problem was resolved. The 3K-PW fabric was replaced with 95-grade tape on the tool side of these components.

Spanwise warpage was detected during the LH rear spar assembly. The causes of warpage were identified as the temperature differential between the upper spar cap and lower spar cap, interface friction between the tool and the part, and cool-down rates. Process changes were implemented and corrected for the observed warpage. Fiberglass plies were used on the upper spar cap as an insulation blanket. This allowed a more uniform temperature distribution in the caps during autoclave cure. A Teflon® slip sheet was placed between the part and the tool to allow for tool expansion and contraction without stress buildup during the cure, and a cool down rate of 1°C/min (rather than the allowable 3°C/min) was used.

2.6 MAINTENANCE PLANNING PROGRAM.

A maintenance program was developed by the OEM to assist the operators in defining inspection procedures and schedules to ensure the airworthiness and safety of the horizontal stabilizers [34]. The proposed maintenance plan was accepted by the FAA and is presented in table 3. In addition, the OEM agreed to perform an early structural inspection, as described in the table, for the first two horizontal stabilizer shipsets to reach 7000 flights. Both inspections required 17- and 24-hour downtimes, respectively, which is very consistent with the downtime required to inspect the metal stabilizers [34]. No structural problem or in-service deterioration was reported.

Table 3. Maintenance Planning Schedule [34]

Check	Inspection Interval (Flight Hour)	Description
Preflight-Transit		Walk Around
A	75	Visual Inspection of exterior surface, from ground level
B	300	Visual Inspection of external surfaces
C	1200	External Visual Inspection Exposed Rear Spar Area Exposed Hinge Fittings and thermal linkage
	2400	Front and Rear Spar to center section attachment lugs Inboard Edge of Rear Spar Web Trailing Edge Cavities
Structural	14000	External Visual Inspection NDT Inspection upper and lower skin from the rear spar forward to stringer 3 between the side-of-body and the rib at stabilizer station 111.1 Front and rear spar attachment lugs, pins, bushings and fittings Internal trailing-edge structure Internal structure, spars, stiffeners, closure ribs; access by removing gap covers, access hole covers, removable leading edge, removable lower trailing edge panels and removable tip

2.7 THE B-737 HORIZONTAL STABILIZER CERTIFICATION.

Certification requirements for commercial transport airframes are defined in the FAA regulations (14 CFR Part 25) [32]. FAA advisory circular (AC) 20-107 [35] sets forth recommendations for compliance with provisions of the regulations. Compliance items of prime importance to composite structures include requirements pertaining to material and process specifications, material properties, proof of structure static strength, proof of structure fatigue and damage tolerance requirements, and additional requirements pertaining to lightning protection, structure protection, and structure repair and maintenance.

The certification approach adopted by the OEM was based on analytical substantiation supported by appropriate test evidence. The structure's ultimate load-carrying capability was demonstrated by analytically produced positive margins of safety. Supporting test evidence included material lamina, laminate data, structural detail, and subcomponent testing generated at the extreme environmental conditions to which the structure would be subjected.

A comprehensive ancillary test program was carried out to support the data generation necessary to certify the structure. A building-block approach was followed where coupons, elements, large panels, and test boxes were tested [1 and 36]. Coupons and elements were used to generate mechanical properties; identify interlaminar properties, stress concentration effects, and environmental factors; characterize impact damage properties; and demonstrate material durability. Large panels and test boxes were used to validate design concepts, verify analysis methods, and correlate test and analytical data.

As part of the comprehensive ancillary test program, structural repair procedures and techniques were developed and substantiated. The OEM used the data generated to establish a structural repair manual for the advanced stabilizer.

Material specifications and a comprehensive process control plan were developed by the OEM to ensure that material properties were reliably reproduced in the full-scale test article. These same specifications were approved by the FAA during the certification of the B-727 CFRP elevator.

To demonstrate the static strength of the stabilizer, the OEM conducted full-scale static tests on ultimate loads on the structure, at ambient temperature, and accounted for environmental effects analytically by calculating moisture and thermal strains under the worst environmental conditions to which the structure would be subjected. A detailed finite element analysis was developed for the stabilizer under the most critical load cases considered. Ultimate strains were obtained by combining the mechanical load strains and the thermal and moisture analysis strains. Margins of safety were obtained by comparing the calculated ultimate strains with the allowable strains for the different environments. The analytical predictions were validated by element tests conducted at the design temperature and moisture extremes [31].

Damage tolerance substantiation was achieved by subcomponent and full-scale tests that validated the no-growth philosophy which implied that any visible damage that was not critical would not grow under spectrum loading. The no-growth philosophy was adopted because the

stabilizer had low operating strains due to stiffness design requirements. The other damage tolerance requirement was the ability of the structure to withstand reasonable loads expected at the completion of a flight where damage from discrete sources, such as uncontained engine failure, hailstones, and bird impact, occurred.

The full-scale test article that was used for static, durability, and damage tolerance substantiation was structurally complete with elevator, balance panels, leading edge, trailing edge, closure rib, and associated hardware. The full-scale test article was supported horizontally by a steel test fixture. The stabilizer was attached to a metal production center section. A dummy RH stabilizer was attached to the center section and used for symmetrical loading [37]. Stabilizer airloads were applied to the upper and lower skins using pads bonded to the skin panels. Rosette and axial gages were used to monitor strain distribution during the full-scale tests. Deflections were measured using electronic deflection indicators at 18 different locations.

The full-scale tests conducted on the structure included a limit load strain survey at four static loading conditions: one-half lifetime of fatigue with no damage, one lifetime of fatigue with small damage, ultimate load at four static load conditions, and residual strength fail-safe tests with large damage. The static load cases considered included maximum torsion, maximum positive bending, maximum negative bending and surface pressure, and maximum negative bending and ultimate damage tolerance [37]. Fail-safe load cases that were considered included the lower front spar pin removed, lower rear spar pin removed, upper front spar pin removed, and upper rear spar pin removed. The stabilizer sustained limit load for all fail-safe load cases considered, except for the one in which the upper rear spar pin was removed. During this load case, a shear failure of the rear spar web between stations 68 and 96 occurred at 61% of the design ultimate load. The rear spar web was subsequently reinforced with a steel strap.

At the successful completion of all ground tests, the composite stabilizer was subjected to lightning strike tests. Ground vibration and flight tests were conducted using a production B-737 aircraft with a CFRP stabilizer. The purpose of the ground vibration tests was to establish the damping characteristics, natural frequencies, and modes of the CFRP stabilizer, the elevator, and the tab. These damping characteristics were compared with those used in the flutter analysis. A portable vibration shaker was used to excite the structure at different locations and directions. Accelerometers placed in the RH and LH stabilizers, elevators, and tabs were used to measure control system dynamic characteristics. The measured natural frequencies of the CFRP structure were in close agreement with those of the metal stabilizer. Flight tests were conducted to demonstrate flutter clearance as well as stability and control performance [37]. The results demonstrated equivalent flutter and handling characteristics to the metal stabilizer. All 14 CFR Part 25 certification requirements [32] and composite guidelines specified in AC 20-107A [35] were met, and FAA certification was obtained in August 1982.

The ACEE composite stabilizer program achieved all of its objectives and laid the groundwork for the design of larger primary structures using composite materials. The composite stabilizer achieved a weight reduction greater than 20% (compared to the aluminum stabilizer). Parts and assemblies were manufactured on production-type tooling; quality assurance and repair methods were developed and substantiated, analytical methods were developed and substantiated using

supporting test evidence; and FAA certification was obtained. All five shipsets were entered into service in 1984.

2.8 THE B-737 COMPOSITE HORIZONTAL STABILIZER FLEET STATUS.

The status of all five composite stabilizer shipsets as of March 2011 is summarized in table 4, which shows that three shipsets were removed from service after accumulating 19,300, 55,000, and 48,000 flights, respectively. Shipset 1 was sold and is being operated by a foreign carrier. It has been reported that shipset 2 is for sale by an aircraft commercial part supplier.

Table 4. The B-737 Composite Stabilizer Fleet Status as of March 2011

Shipset/Production Line No.	Entry Into Service	Carrier	Status as of March 2011
1/1003	2 May 1984	A & E	Sold to foreign carrier (60,000 hours, 45,000 flights)
2/1012	21 March 1984	A	Reported for sale by a commercial part supplier (62,000 hours, 47,000 flights)
3/1025	11 May 1984	B	Aircraft damaged beyond repair 1990; partial teardown completed in 1991 (17,300 hours, 19,300 flights)
4/1036	17 July 1984	B & C	Stabilizers removed from service in 2002 (approximately 39,000 hours, 55,000 flights); partial teardown of RH unit at Boeing
5/1042	14 August 1984	B & C	Stabilizers removed from service in 2002 (approximately 52,000 hours, 48,000 flights); teardown at LH unit at Boeing; teardown of RH unit at NIAR WSU

Shipset 3 became available for a teardown in 1990 after an aircraft crashed on a landing approach that led to no fatalities and minimal damage to the LH stabilizer. The OEM acquired the stabilizer shipset and conducted a partial teardown on the structure. An inspection of areas that were not damaged during the crash revealed no structural damage or delaminations; no corrosion on the aluminum/CFRP interfaces; and no evidence of visual degradation, cracking, deterioration, or fretting [34].

Shipsets 4 and 5 were removed from service after skin/stringer delaminations were discovered at the inboard end of the upper skin. A design oversight omitted a “No Step” designation in this area. Airline personnel routinely stood on the horizontal stabilizer’s upper skin while servicing the vertical stabilizer. The repeated flexing of the upper surface eventually resulted in the delaminations. When the damage was initially discovered, the OEM ordered inspections on the other three aircraft remaining in service. All three had similar delaminations. As a result, a “No Step” zone was added in this area, shipsets 4 and 5 were retired from service, and shipsets 1 and 2 were repaired and returned to service.

3. THE B-737 HORIZONTAL STABILIZER TEARDOWN RESULTS.

The objective of the horizontal stabilizer teardown was to evaluate the aging effects on the performance of the composite structure after 18 years of service or 48,000 flights, which is the equivalent of about two-thirds of its design service lifetime. The main goal was to evaluate the structural health of the aged composite structure. To accomplish this, the research was divided into several nondestructive and destructive subtasks. The goal of the nondestructive inspections was to characterize the state of the structure after 18 years of service and to investigate the existence and extent of flaws introduced during manufacture or service using current methods used in the field as well as more sophisticated methods, including thermography, laser UT testing, Rapidscan™, etc. The objective of the destructive inspection and evaluation was to confirm the existence of flaws using NDI to conduct mechanical tests, thermal analysis, physical tests, and image analysis, and to compare the data to that generated during the design phase, whenever possible.

3.1 VISUAL INSPECTION AND NONDESTRUCTIVE INSPECTION PRIOR TO TEARDOWN.

The general visual inspection conducted on the outside of the structure prior to teardown revealed numerous cracked and peeled paint areas on the upper and lower skins. In numerous fastened areas, the paint was cracked and loose. Surface blemishes were also observed and were most probably caused by excessive paint/surfacer, aging, and exposure to weather.

3.1.1 Rapidscan™ Inspections.

Nondestructive inspection scans were taken at the Sandia National Laboratories, by NDT Solutions Ltd., using their pulse echo UT Rapidscan equipment. The results of the scans are shown in figure 25. The upper skin scans showed excessive porosity and confirmed the disbonds of upper skin stringer 7. The areas circled in red show excessive porosity from the Rapidscan PE inspection but were identified as disbonds after teardown. Rapidscan inspections also showed a very porous circular field repair between rib stations 2 and 3 at stringers 5 and 8. Because of the excessive porosity in the repair and a bug in the software at the time of the inspection, no useful signal could be obtained.

As shown in figure 25, the lower skin scans showed less porosity compared to the upper skin scans, but a few areas were identified as disbonds: at the inboard section of the lower skin at stringer 1 runout; at the outboard section of the skin at rib 6 at stringers 2 and 3; and between ribs 5 and 6 at stringer 3. The main findings of the NDI inspection were the excessive porosity levels found in the upper skin but also the stringer disbonds in both the upper and lower skins.

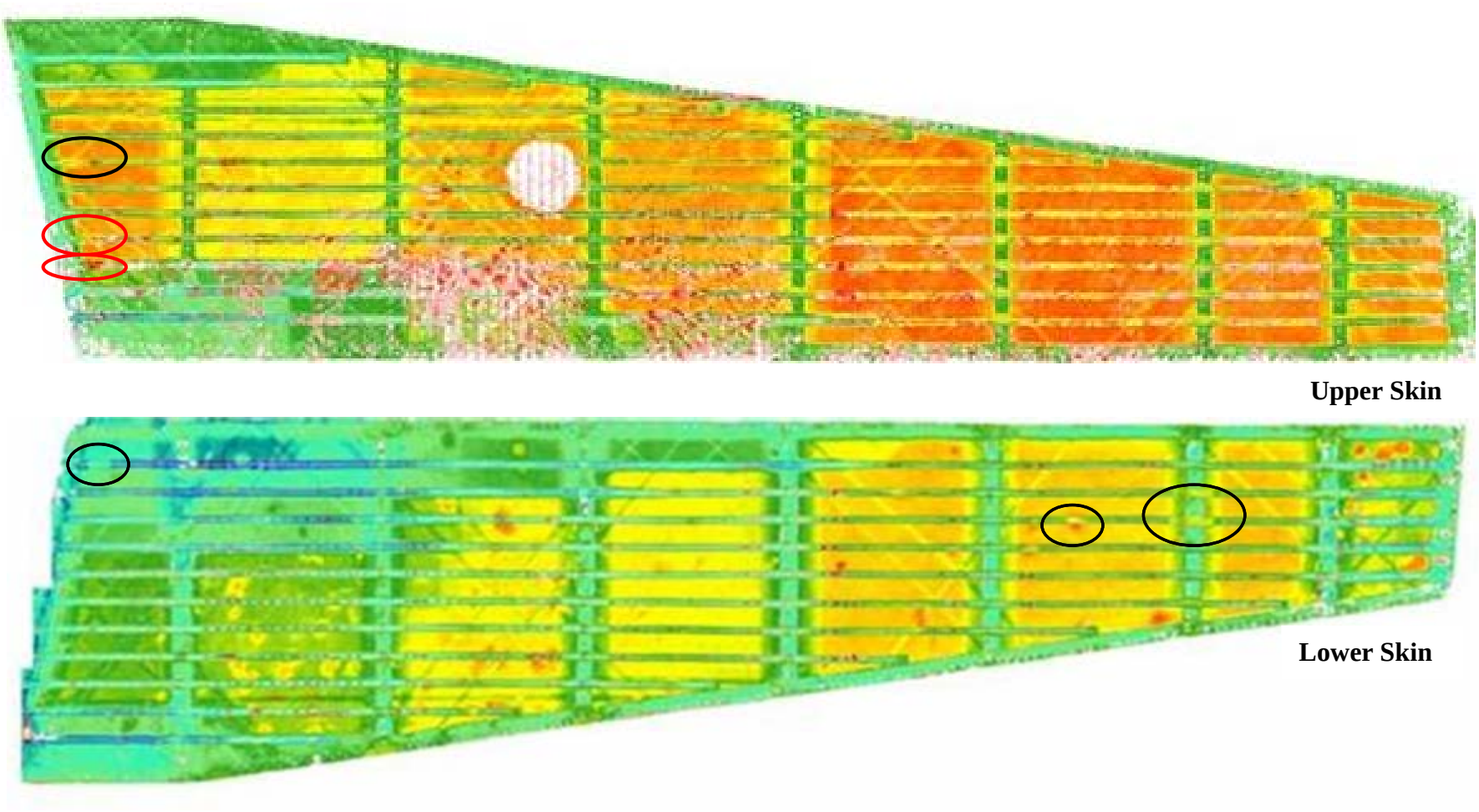

Figure 25. Rapidscan Analysis (Pulse Echo Time of Flight Data) of the B-737 RH Stabilizer (courtesy of Sandia National Laboratories and NDT Solutions Ltd., UK)

3.1.2 Boeing NDI.

Boeing performed a nondestructive evaluation on the RH stabilizer using pulse echo at a frequency of 3.5 MHz, as shown in figure 26. The PE scans show a very porous upper skin compared to the lower skin. The upper skin scan also shows a very porous repair between rib stations 2 and 3 at stringers 5 and 8. The PE scans of the LH stabilizer, shown in figure 27 for illustration purposes only (disassembled by the OEM), also show significant porosity in both skins.

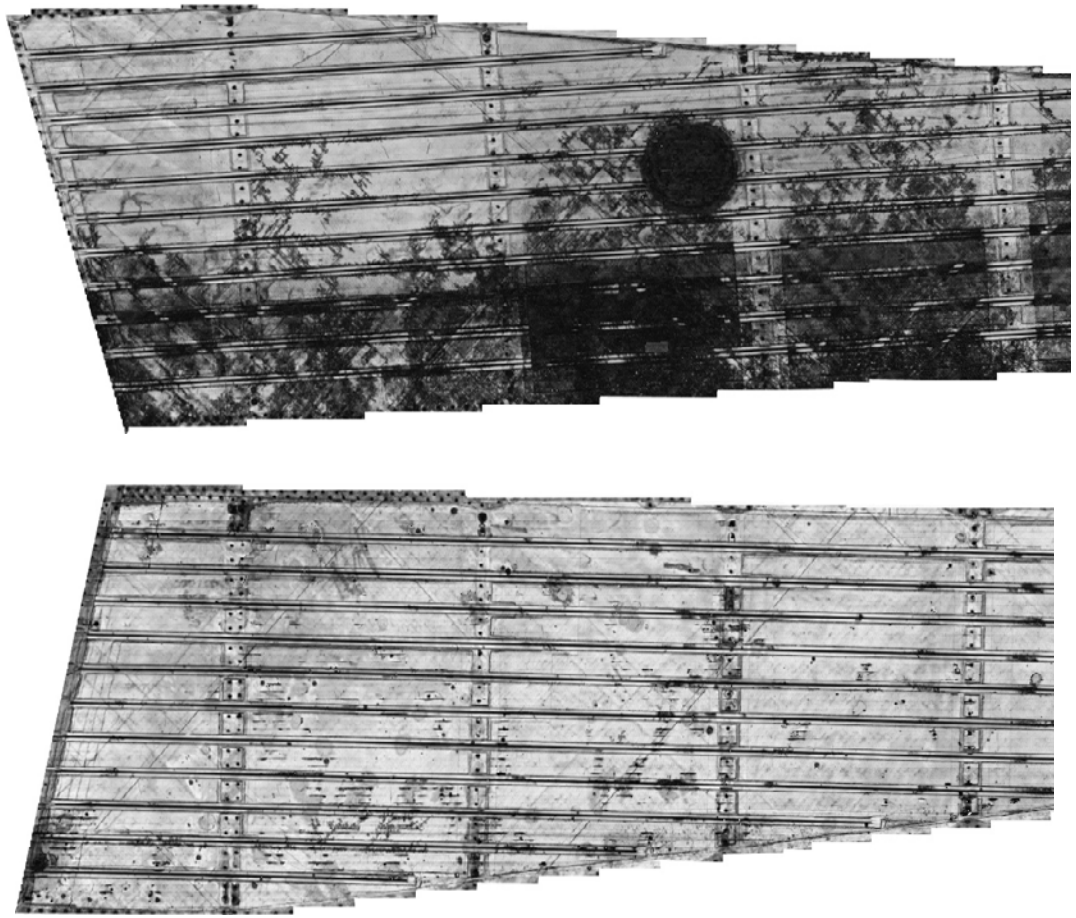

Upper Skin

Lower Skin

Figure 26. Pulse Echo Amplitude Scan of the B-737 RH Stabilizer Performed at 3.5 MHz (courtesy of The Boeing Company)

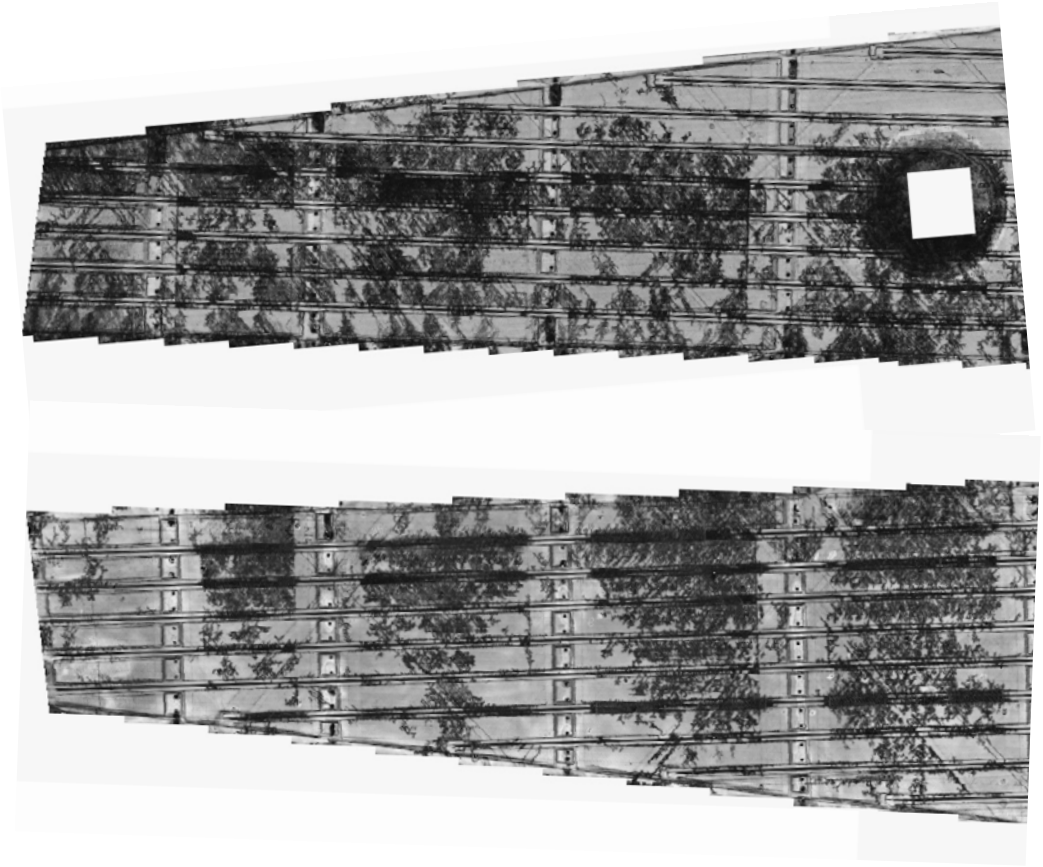

Upper Skin

Lower Skin

Figure 27. Pulse Echo Amplitude Scan of the B-737 LH Stabilizer Performed at 3.5 MHz (courtesy of The Boeing Company)

3.2 DISASSEMBLY.

The RH B-737-200 horizontal stabilizer, as received and prior to disassembly, is shown in figures 28 and 29. Stabilizer disassembly was conducted in the following sequence: first the upper skin, followed by the lower skin, and finally, the stabilizer box itself. The upper skin was demated by drilling out the "Big Foot" blind fasteners using a combination of carbide and cobalt drill bits, illustrated in figure 30. Once the fastener heads were drilled out, the fastener shanks were accessible and could be easily driven out of the structure. All Big Foot blind fasteners attaching the upper skin to the spars and the ribs were carefully drilled out so as not to introduce additional damage to the structure. The dismantled upper skin is shown in figure 31. The RH upper skin appears to be flat with no evidence of curvature or residual strain. Furthermore, both skins appear to be in extremely good condition, with no e vidence of detrimental aging or deterioration. Once the upper skin was demated, the lower skin was accessed for disassembly at the titanium Hi-Lok® attachment points to the spars and ribs. Figure 32 shows the lower skin after disassembly. Next, the stabilizer box components, spars, and ribs were disassembled. Figure 33 shows the stabilizer after skin disassembly. The stabilizer front and rear spars are shown in figure 34.

The main observation following disassembly of the structure was that the stabilizer, to the naked eye, appeared to be in very good condition, with no e vidence of deterioration, corrosion, or pitting that is typically observed for a metallic structure with a similar service history. The various components are shown in figures 31 to 34.

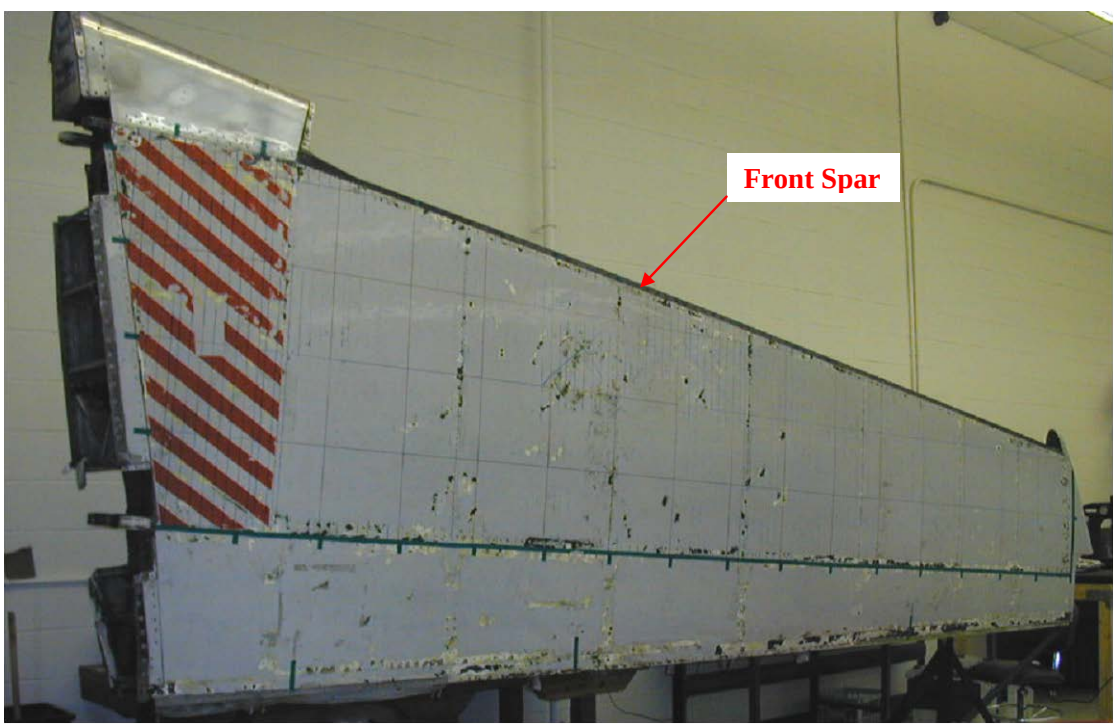

Figure 28. The B-737 CFRP RH Horizontal Stabilizer Prior to Disassembly, Upper Skin Side

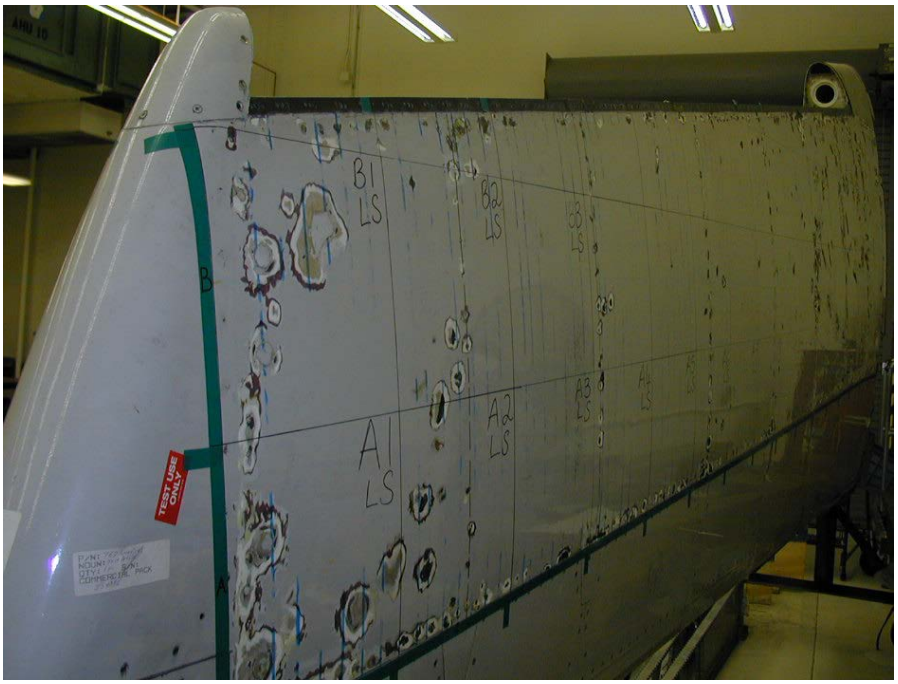

Figure 29. The B-737 CFRP RH Horizontal Stabilizer Prior to Disassembly, Lower Skin Side

Figure 30. Upper Skin Disassembly

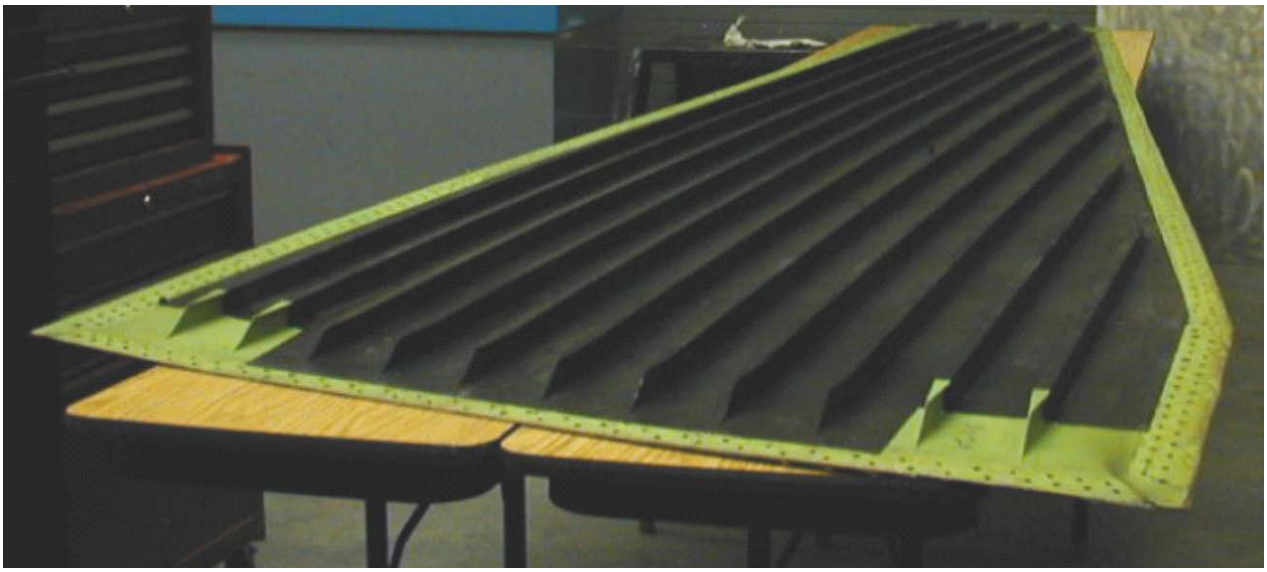

Figure 31. The B-737 RH Composite Stabilizer Upper Skin After Disassembly

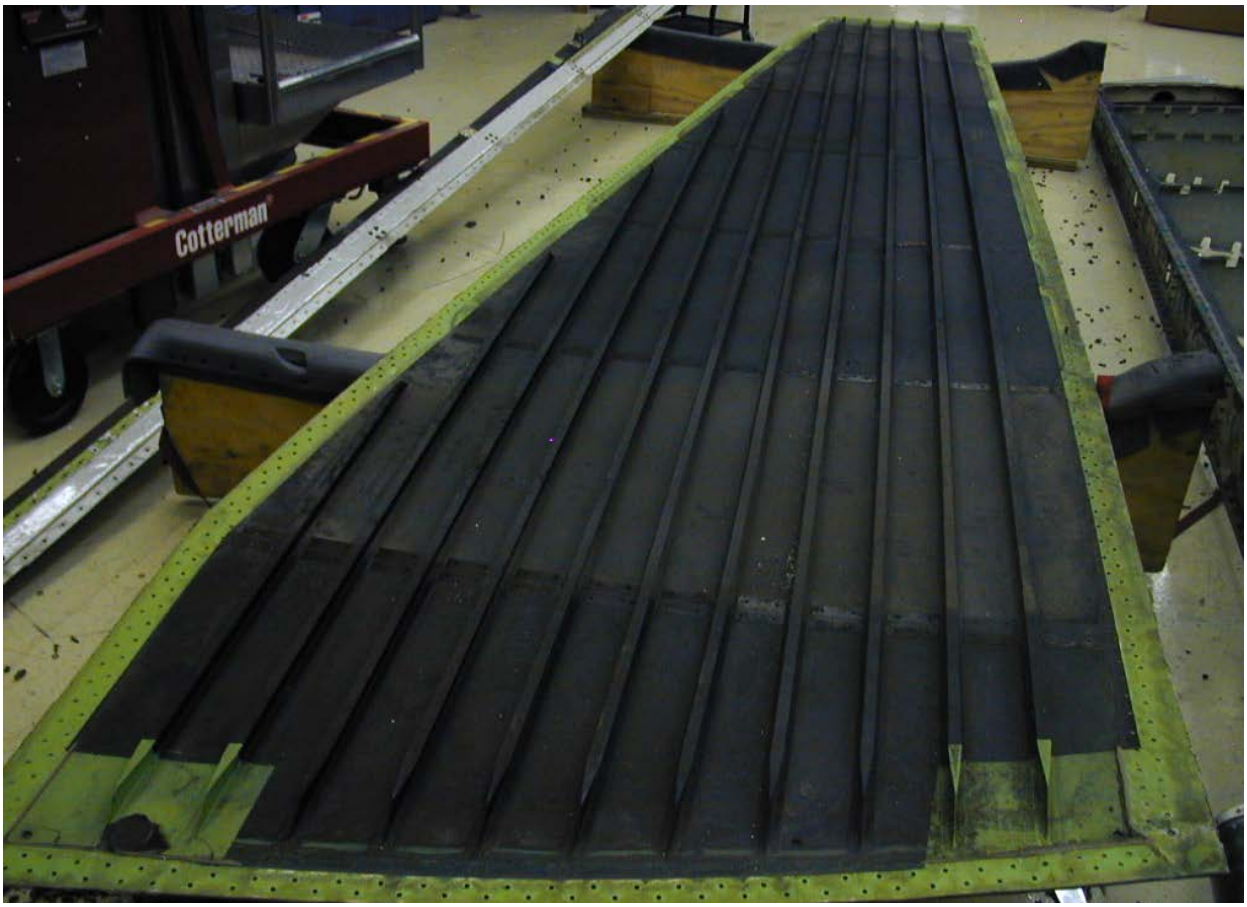

Figure 32. The B-737 RH Composite Stabilizer Lower Skin After Disassembly

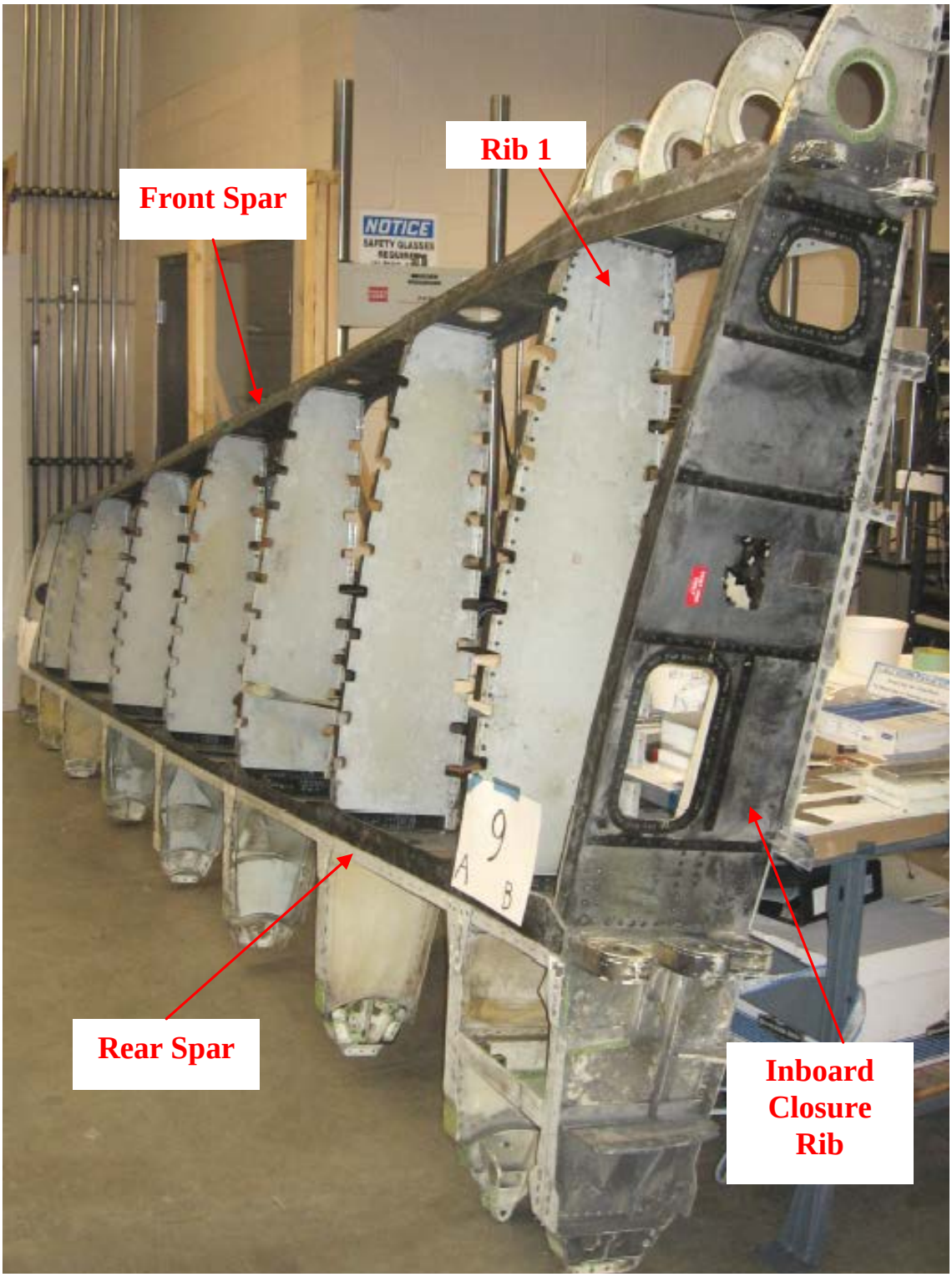

Figure 33. The B-737 RH Composite Stabilizer Structural Box

Figure 34. The B-737 RH Composite Stabilizer Spars: Front Spar (top) and Rear Spar (bottom)

3.3 VISUAL INSPECTION FINDINGS.

As shown in figures 31 to 34, the B-737 RH horizontal stabilizer appeared to be in very good condition with no evidence of degradation or excessive deterioration. Fasteners seemed to be in very good condition, with a few exceptions, as shown in figures 35 and 36.

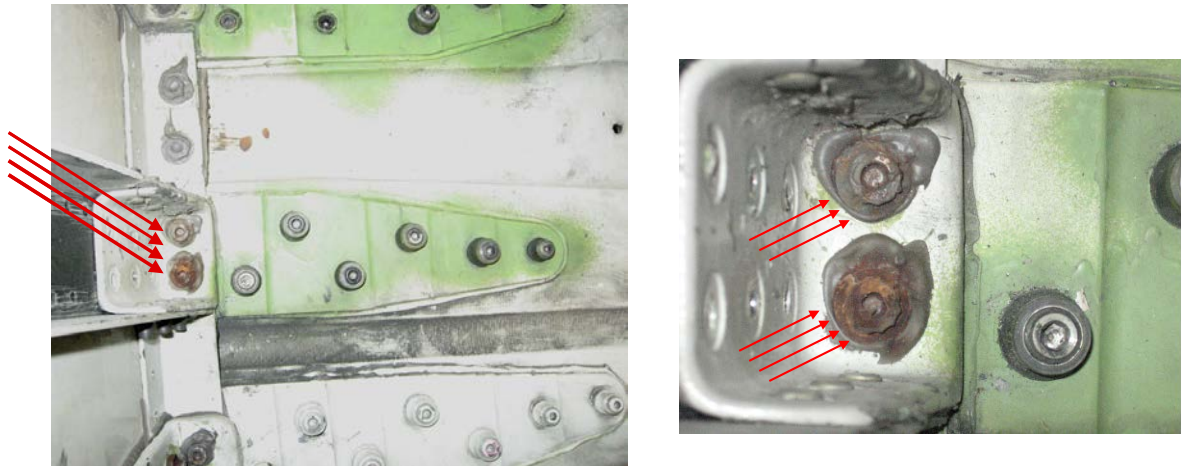

Figure 35. Corroded Fasteners Due to Sealant Deterioration (Rear Spar, Center Lug)

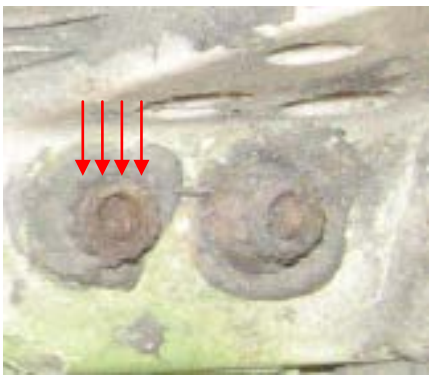

Figure 36. Corroded Fasteners Due to Sealant Deterioration (Rear Spar, Bottom Lug)

Visual inspection also showed evidence of Tedlar degradation due to environmental exposure, as shown in figure 37. Tedlar was used as a moisture-protective film and was co-cured to parts of the structure, mainly ribs and spars. Tedlar disbonding and deterioration was observed on both spars.

Figure 37. Degradation of Tedlar

After a careful inspection of the disassembled structure, the presence of both liquid and phenolic solid shims was found, as shown in figures 38 and 39. The shims seemed to be very effective in service and held up very well. The bonding of the liquid shim was effective, yet the release agent used on one side allowed separation at disassembly. There were no signs of the liquid shim breaking up, softening, or deteriorating.

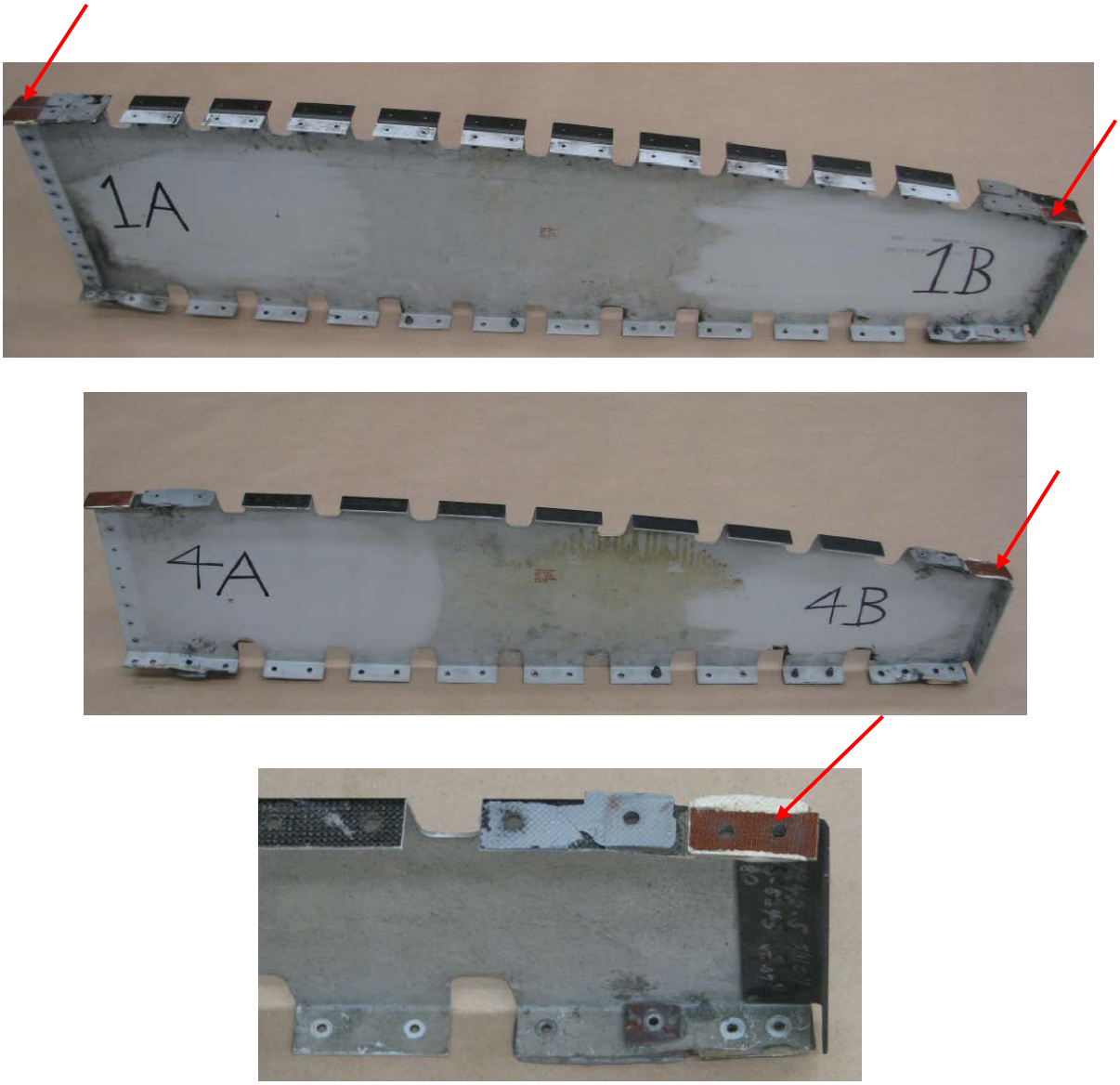

Figure 38. Phenolic Shims Used to Fill Gaps Between Upper Skin and Rib Stations 2, 4, and 7

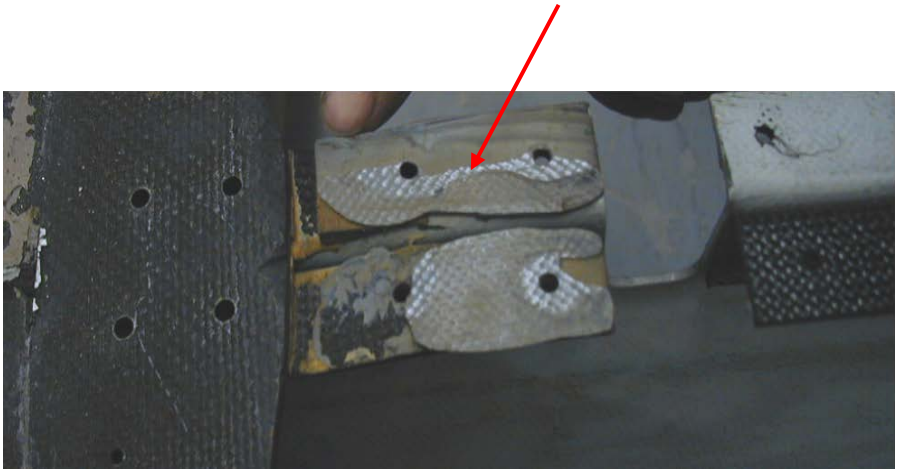

Figure 39. Liquid Shims Used to Fill Gaps Between Upper Skin and Stabilizer Ribs

The visual inspection/findings of the B-737 RH stabilizer teardown showed that the composite structure held up extremely well, with minor signs of degradation or deterioration due to environmental exposure. Tedlar and fastener-sealant degradation were the only signs of deterioration due to environmental exposure found on the structure. Disassembly also showed evidence of shimming to seal the gaps between the stabilizer's skins and ribs. All shims held up extremely well, with no evidence of softening or cracking. Furthermore, a visual inspection of the upper skin repair found between rib stations 2 and 3 confirmed that the repair was a surface repair only and did not extend to the stringers.

3.4 VISUAL INSPECTION AND DESTRUCTIVE EVALUATION OF DISBONDED AREAS.

Visual inspection showed the existence of disbonds at the upper skin runouts for stringers 3, 4, 6, and 7, as illustrated in figure 40. Inboard delaminations at the stringer runouts are believed to have been caused by technicians stepping on the inboard section of the stabilizer to conduct routine maintenance on the vertical stabilizer.

Similar to the delaminations found in the inboard section of the upper skin at stringer runouts, a delamination was detected in the inboard section of the lower skin runout at stringer 1 and was confirmed after disassembling the structure. Another disbond was found at the outboard section of the lower skin, at rib station 7 on stringers 2 and 3. Both disbonds found on the lower skin are illustrated in figure 41. The cause of the isolated lower-surface outboard stringer runout damage is unknown but might have been caused by foreign-object damage, such as deicing equipment, runway debris, or a blown tire. Bondlines are notoriously weak for out-of-plane loading, whether it is caused by a technician standing on the surface, a tool drop, or contact with a foreign object. The use of mechanical fasteners at the runout could have prevented the delamination.

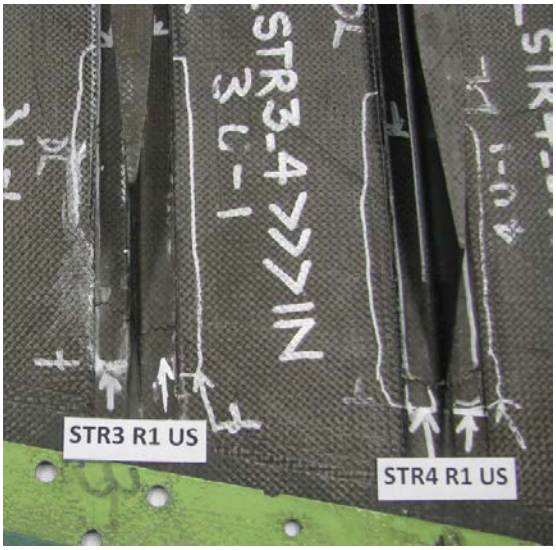

Figure 40. Upper Skin Delaminations at Stringer 3, 4, and 7 Runouts

Figure 41. Lower Skin Disbonds Confirmed After Teardown

3.5 NONDESTRUCTIVE INSPECTION AFTER TEARDOWN.

PE and through-transmission NDI methods were used to characterize the stabilizer's damage state after 18 years of service. PE results using today's equipment capabilities showed the improved accuracy/sensitivity of the current inspection methods compared to those used in the 1970s. To inspect the aged structure according to current inspection requirements, 5-MHz transducers were used. According to 1970s requirements, a 1-MHz transducer was used to obtain a scan, as shown in figure 42.

PE scans conducted confirmed the large amount of porosity in the upper skin, as previously identified in the Rapidscan inspection results. A summary of results is shown in figure 43. The field skin repair is also shown in that same figure, in the upper skin between rib stations 2 and 3 and stringers 5 and 8.

1970s Capability

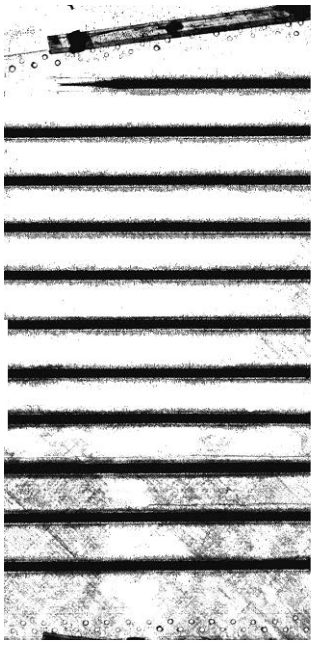

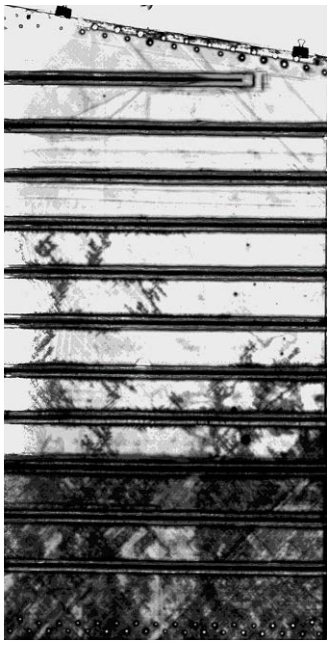

Current Capability

Figure 42. 1970s Ultrasonic Inspection Sensitivity vs. Today's Equipment Capability

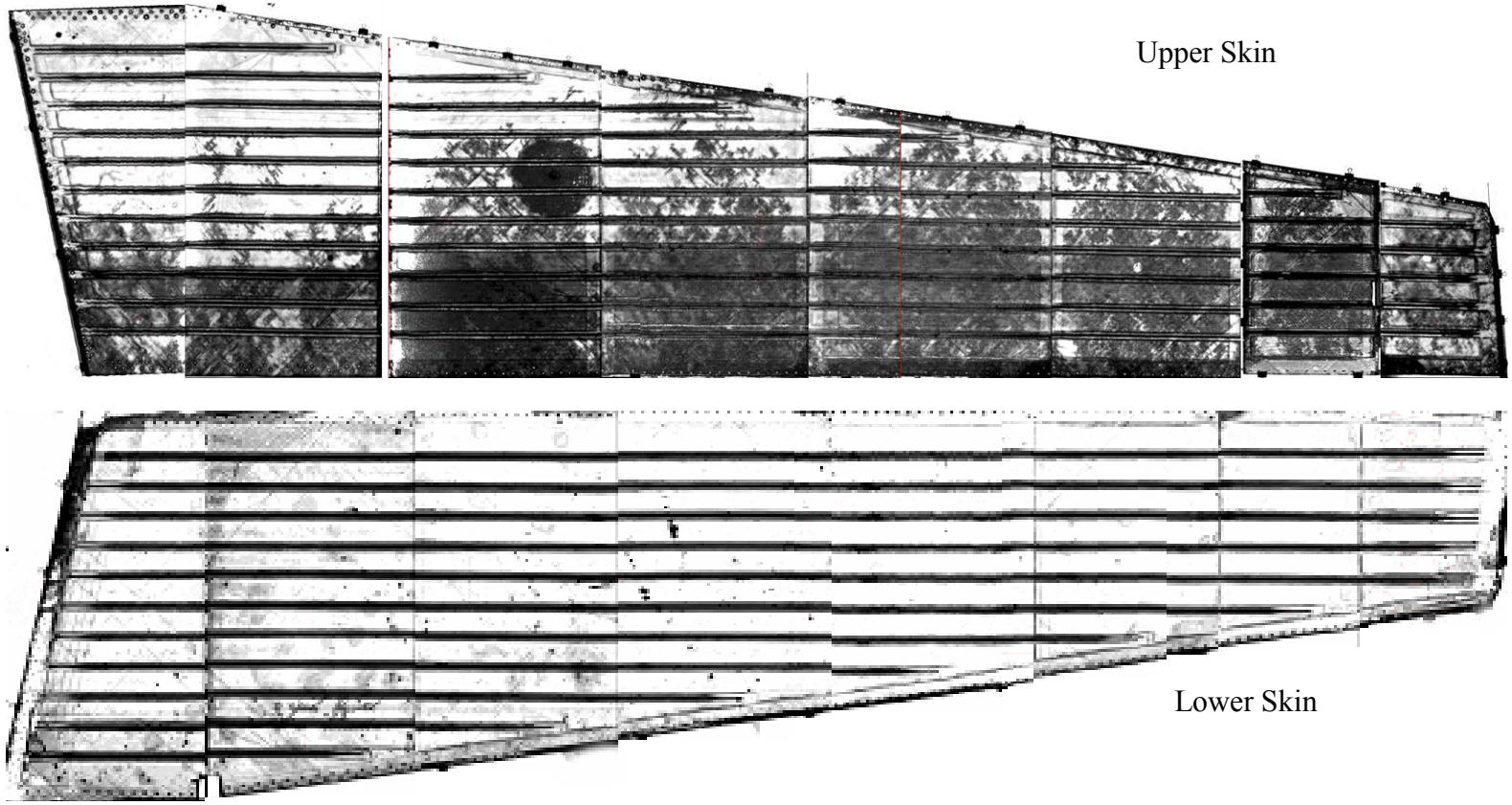

Figure 43. The NIAR PE Scans of a B-737 RH Horizontal Stabilizer

3.6 THERMAL ANALYSIS.

Thermal analysis was conducted on coupons extracted from both the upper and lower skins to evaluate any possible changes in the thermal properties of the material after 18 years of service. Specimen nomenclature is defined in figure 44. The first character typically describes either the skins or the spars, the second character describes the spanwise location (the stabilizer was subdivided into regions R1 through R8, where R1 describes the region between stations 57.93 and 83.5, R2 describes the region between stations 83.5 and 111.1, etc.); and the third character describes the chordwise locations using the stringers as references.

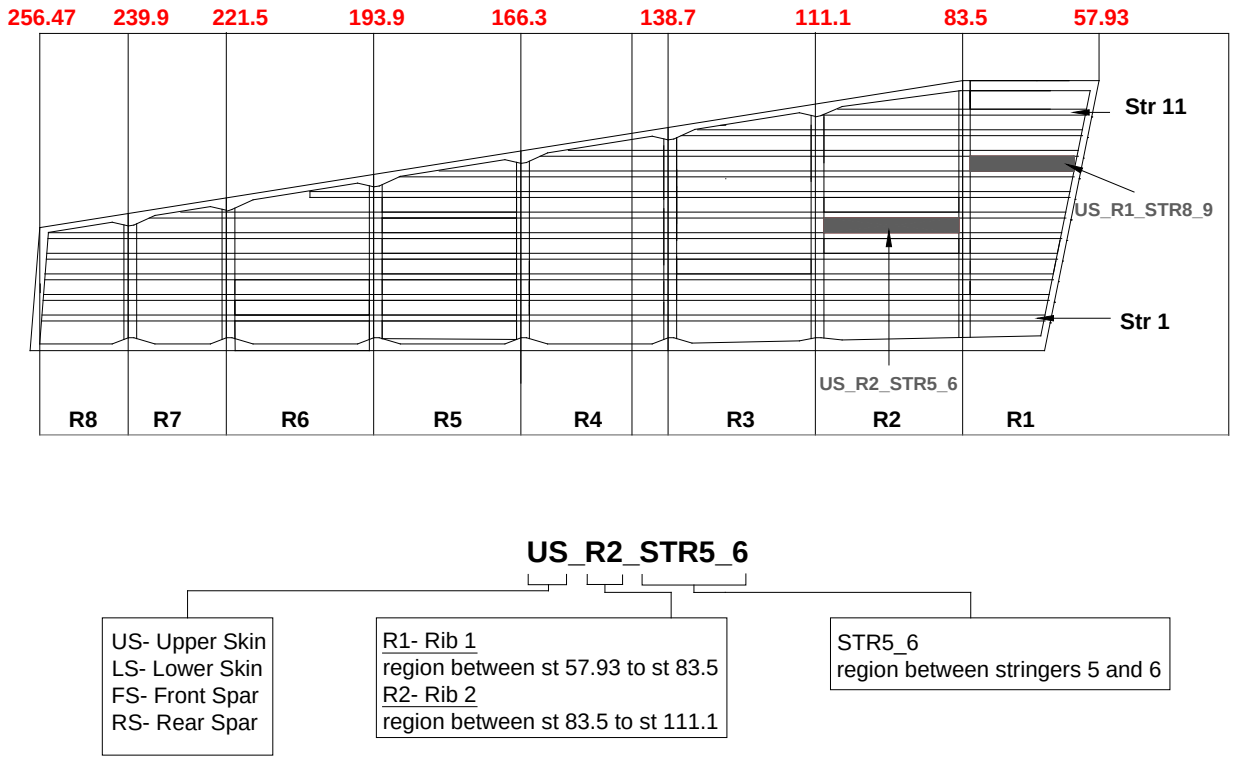

Figure 44. Specimen Nomenclature

The thermal tests conducted included dynamic mechanical analysis and differential scanning calorimetry. DMA tests measure the response of a material to periodic stress and provide information about the modulus and the damping of the material. DMA curves provide two values of T_g, a value based on the onset storage modulus or material fiber stiffness loss and a value based on material damping/maximum viscosity, which is the peak of tangent delta (tan delta), as shown in figure 45. Storage modulus is a characteristic of the material fiber stiffness, whereas damping is a characteristic of the material matrix. The T_g value, based on the onset of storage modulus, is always more conservative than the value obtained using the peak of tan delta.

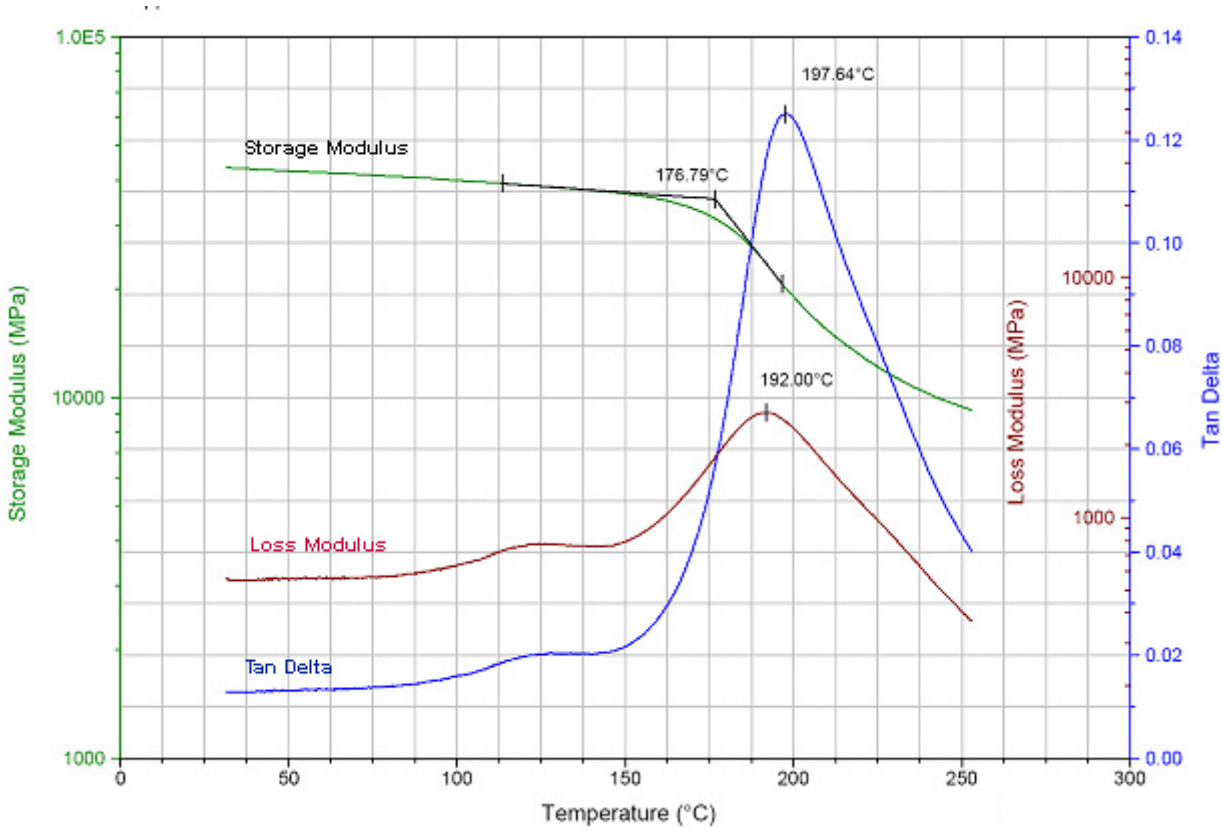

Figure 45. The DMA Analysis of Coupon Extracted From B-737 Upper Skin

DMA was conducted using the test parameters specified in ASTM E 1640 and according to the Boeing method. The parameters used in the two methods are compared in table 5. All values were compared against the baseline dry T_g obtained by Narmco using thermomechanical analysis (TMA). This test is sensitive to the methodology used, and thus, a T_g value from DMA cannot be directly compared to a T_g value from TMA.

Table 5. ASTM vs. Boeing Test Parameters

Test and Specimen Attributes	ASTM/NIAR Parameters	Boeing Parameters
Ramp rate	5°C/min	3°C/min
Range	100°-300°C	100°-300°C
Frequency	1 Hz	10 Hz
Specimen dimensions	1″ x 0.25″	1″ x 0.25″
Specimen thickness	Part thickness (paint sanded off)	Part thickness (paint sanded off)
Clamp type	20-mm 3-pt bend	20-mm 3-pt bend
Method	0.02% strain	Max force

DMA data were also generated for as-extracted and dried coupons to evaluate the effects of moisture on the T_g of the aged structure. Figures 46 and 47 summarize DMA data obtained for the stabilizer upper skin following the Boeing method and ASTM E 1640, respectively. The

DMA upper skin coupons tested according to ASTM E 1640 yielded average T_g values of 176.2°C (349.2°F) (onset of storage modulus) and 202°C (395.6°F) (peak of tan delta), respectively. Narmco's baseline value obtained from TMA is shown for reference only. The DMA coupons tested according to the Boeing method yielded average T_g values of 201.12°C (394.016°F) and 233.5°C (452.3°F), respectively. Detailed test data are summarized in tables 6 and 7, respectively.

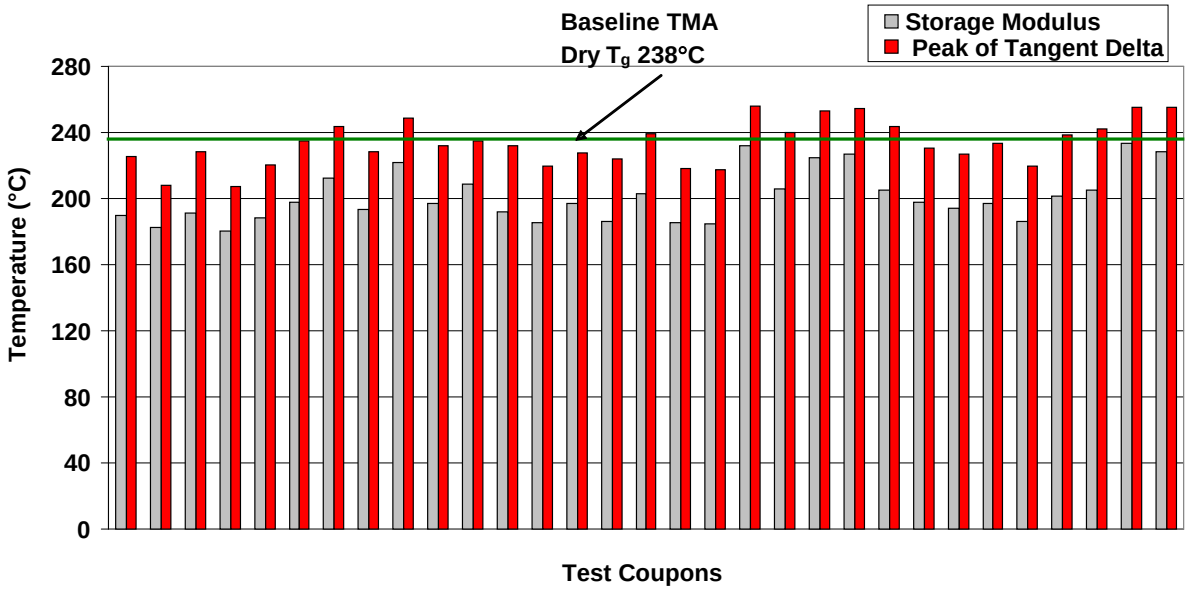

Figure 46. The DMA Results for As-Extracted Coupons From the Upper Skin of the B-737 Horizontal Stabilizer (Boeing Method)

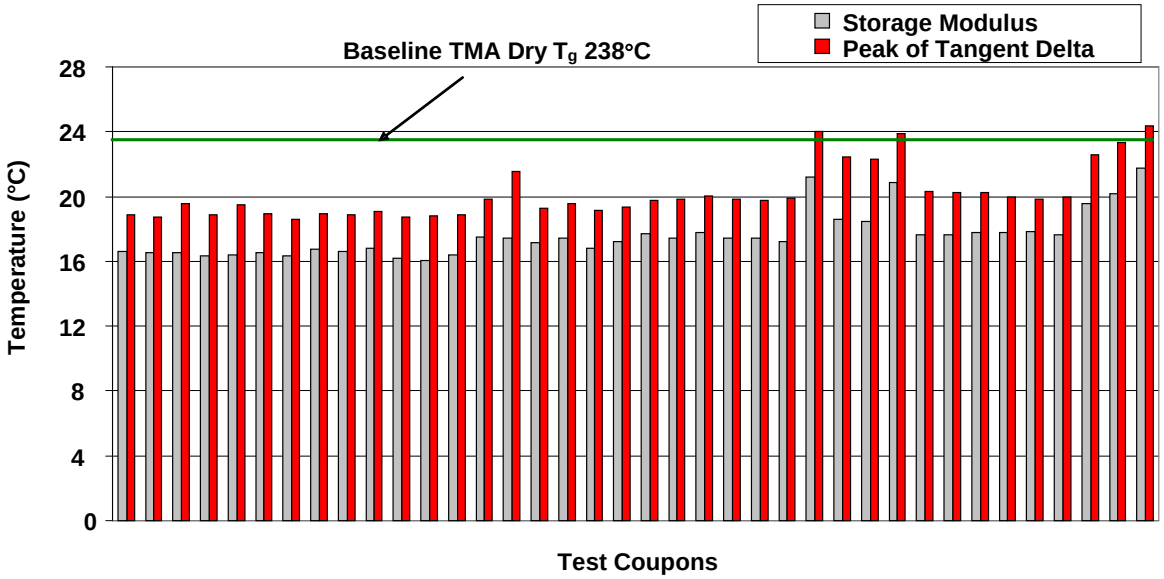

Figure 47. The DMA Results for As-Extracted Coupons From the Upper Skin of the B-737 Horizontal Stabilizer (ASTM E 1640)

Table 6. The DMA Test Data for Upper Skin Coupons Using Boeing Test Parameters

Coupon ID	Storage Modulus (ºC)	Loss Modulus (ºC)	Tan Delta (ºC)
Rib1 Str6	190.1	208.1	225.7
Rib1 Str10	182.7	195.0	208.3
Rib2 Str1	190.9	206.6	228.3
Rib2 Str11	180.2	195.1	207.5
Rib3 Str1	188.1	202.2	220.3
Rib3 Str4	197.7	219.4	235.3
Rib4 Str1	212.1	232.6	243.9
Rib4 Str6	193.4	212.7	228.1
Rib5 Str1	221.8	237.1	248.9
Rib5 Str5	197.0	216.9	232.0
Rib6 Str1	209.0	216.2	234.6
Rib8 Str2	192.2	213.0	231.7
Rib8 Str4	185.2	202.8	219.8
US_R1_STR8_9_T1	197.0	214.9	227.5
US_R1_STR9_10_T1	186.5	205.6	223.7
US_R2_STR4_5_T1	202.7	224.0	238.9
US_R2_STR5_6_T1	185.8	203.3	217.9
US_R2_STR5_6_T2	184.8	205.2	217.8
US_R3_STR3_4_T1	231.9	248.7	255.6
US_R6_STR0_1_T1	205.7	227.3	239.6
US_R6_STR0_1_T2	224.4	246.4	253.1
US_R6_STR1_2_T1	227.2	247.5	254.6
US_R1_STR9_10_C1	204.9	231.9	244.0
US_R1_STR9_10_C2	198.0	218.9	230.5
US_R1_STR9_10_C3	194.4	212.9	227.2
US_R2_STR4_5_C1	197.1	217.8	233.2
US_R2_STR4_5_C2	186.5	204.0	219.8
US_R2_STR4_5_C3	201.1	228.1	238.5
US_R6_STR0_1_C1	205.1	233.6	241.9
US_R6_STR0_1_C2	233.3	249.8	255.6
US_R6_STR0_1_C3	228.2	248.5	255.2
Average (ºC)	201.1	220.2	233.5
Standard deviation (ºC)	15.5	16.6	13.6

Table 7. The DMA Test Data for Upper Skin Coupons Using ASTM Test Parameters

Coupon ID	Storage Modulus (ºC)	Loss Modulus (ºC)	Tan Delta (ºC)
Rib1 Str6	166.0	180.5	188.4
Rib1 Str10	165.6	179.4	187.1
Rib2 Str1	165.2	183.2	195.5
Rib2 Str11	163.6	180.3	189.1
Rib3 Str1	164.1	183.1	194.6
Rib3 Str4	165.7	182.2	189.1
Rib4 Str1	163.4	177.6	185.9
Rib4 Str6	167.2	182.3	189.1
Rib5 Str1	165.9	180.7	188.7
Rib5 Str5	168.4	182.8	190.6
Rib6 Str1	162.0	178.3	187.1
Rib8 Str2	160.3	179.4	188.0
Rib8 Str4	164.1	182.0	188.8
Rib1 Str4	175.3	191.2	198.5
Rib2 Str1-2	174.2	192.4	215.3
Rib3 Str10	171.5	185.6	192.9
Rib4 Str6	174.1	188.7	195.5
Rib5 Str8	168.4	182.7	191.3
Rib6	172.1	188.1	193.6
Rib7	176.8	192.0	197.6
US_R1_STR8_9_T1	174.1	191.8	198.2
US_R1_STR9_10_T1	177.6	194.1	200.6
US_R2_STR4_5_T1	174.3	191.8	198.7
US_R2_STR5_6_T1	174.3	191.3	197.4
US_R2_STR5_6_T2	172.4	191.3	198.7
US_R3_STR3_4_T1	211.9	225.8	240.2
US_R6_STR0_1_T1	186.0	198.3	224.4
US_R6_STR0_1_T2	184.8	199.2	222.9
US_R6_STR1_2_T1	208.7	231.4	238.8
US_R1_STR9_10_C1	176.7	195.2	203.1
US_R1_STR9_10_C2	176.3	193.9	202.3
US_R1_STR9_10_C3	177.5	195.1	202.1
US_R2_STR4_5_C1	177.6	193.0	199.8
US_R2_STR4_5_C2	178.8	191.6	198.2
US_R2_STR4_5_C3	176.2	192.7	199.7
US_R6_STR0_1_C1	195.7	219.7	225.8
US_R6_STR0_1_C2	201.5	222.4	233.4
US_R6_STR0_1_C3	217.5	237.0	243.8
Average (ºC)	176.2	192.8	202.0
Standard deviation (ºC)	13.89	14.97	16.28

DMA results obtained using the Boeing method were consistently higher than DMA results generated using the ASTM standard. The Boeing method uses a slower temperature ramp-up rate than the ASTM standard, thus allowing the coupon to dry during the DMA test and yielding a higher T_g for a given coupon. The T_g values obtained were consistent with the values obtained for the LH stabilizer [38]. They are also consistent with the T_g values of a 350°F cure material system and are higher than the maximum temperature for which the structure was designed for.

To investigate the effects of moisture on the T_g, dried coupons were tested. The data are summarized in figure 48 and table 8. Drying the coupons increased the average storage modulus by 29°C and the average tan delta by 22°C. Sample DMA curves for as-extracted and dried coupons are shown in figures 49 and 50, respectively.

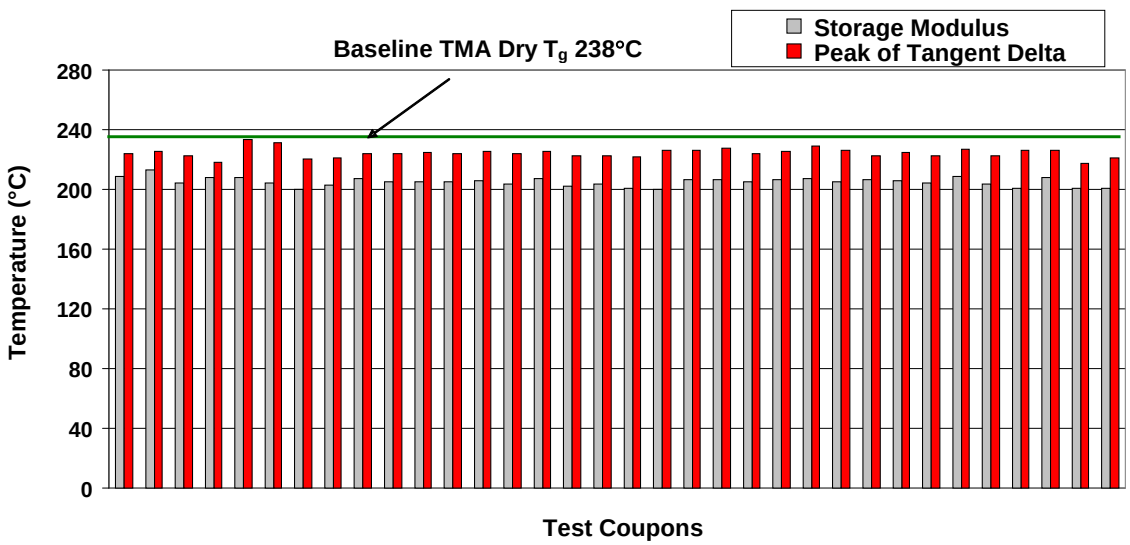

Figure 48. The DMA Results for Dried Coupons From the Upper Skin of the B-737 Horizontal Stabilizer (ASTM Standard)

Table 8. The DMA Test Data for Upper Skin Coupons (Dried) Using ASTM Test Parameters

Coupon ID	Storage Modulus (ºC)	Loss Modulus (ºC)	Tan Delta (ºC)
Rib1 Str8-1	208.68	218.36	223.95
Rib1 Str8-2	213.02	222.21	225.65
Rib1 Str11-1	204.55	215.99	222.26
Rib1 Str11-2	208.31	212.90	217.94
Rib2 Str4-1	208.32	224.20	233.18
Rib2 Str4-2	204.69	222.60	231.56
Rib2 Str5-1	200.20	214.07	220.62
Rib2 Str5-2	203.13	214.75	221.44
Rib2 Str11	206.95	217.16	223.65
Rib3 Str6	205.07	217.60	224.31

Table 8. The DMA Test Data for Upper Skin Coupons (Dried) Using ASTM Test Parameters (Continued)

Coupon ID	Storage Modulus (ºC)	Loss Modulus (ºC)	Tan Delta (ºC)
Rib3 Str7-1	205.34	217.89	224.80
Rib3 Str7-2	205.25	217.92	223.66
Rib3 Str8-1	205.68	217.60	225.30
Rib3 Str8-2	203.70	216.83	223.70
Rib4 Str4	207.20	219.31	225.77
Rib4 Str7-1	202.52	215.65	222.65
Rib4 Str7-2	203.50	216.61	222.60
Rib4 Str8-1	201.01	214.07	221.97
Rib4 Str8-2	199.89	214.46	226.10
Rib5 Str4-1	206.82	218.86	225.83
Rib5 Str4-2	206.19	222.14	227.92
Rib5 Str6-1	204.85	217.20	223.79
Rib5 Str6-2	206.25	220.69	225.69
Rib5 Str7	207.60	215.80	228.99
Rib6 Str4-1	205.07	219.50	226.29
Rib6 Str4-2	206.51	217.02	222.25
Rib6 Str5-1	206.17	218.85	224.90
Rib6 Str5-2	204.17	215.20	222.52
Rib6 Str6	208.98	220.81	226.77
Rib7 Str1-1	203.64	215.25	222.71
Rib7 Str1-2	200.95	217.30	226.10
Rib7 Str5	208.24	220.53	226.52
Rib7 Str6-1	200.77	206.33	217.36
Rib7 Str6-2	200.44	213.39	220.91
Average (ºC)	205.11	217.33	224.40
Standard deviation (ºC)	2.96	3.39	3.24

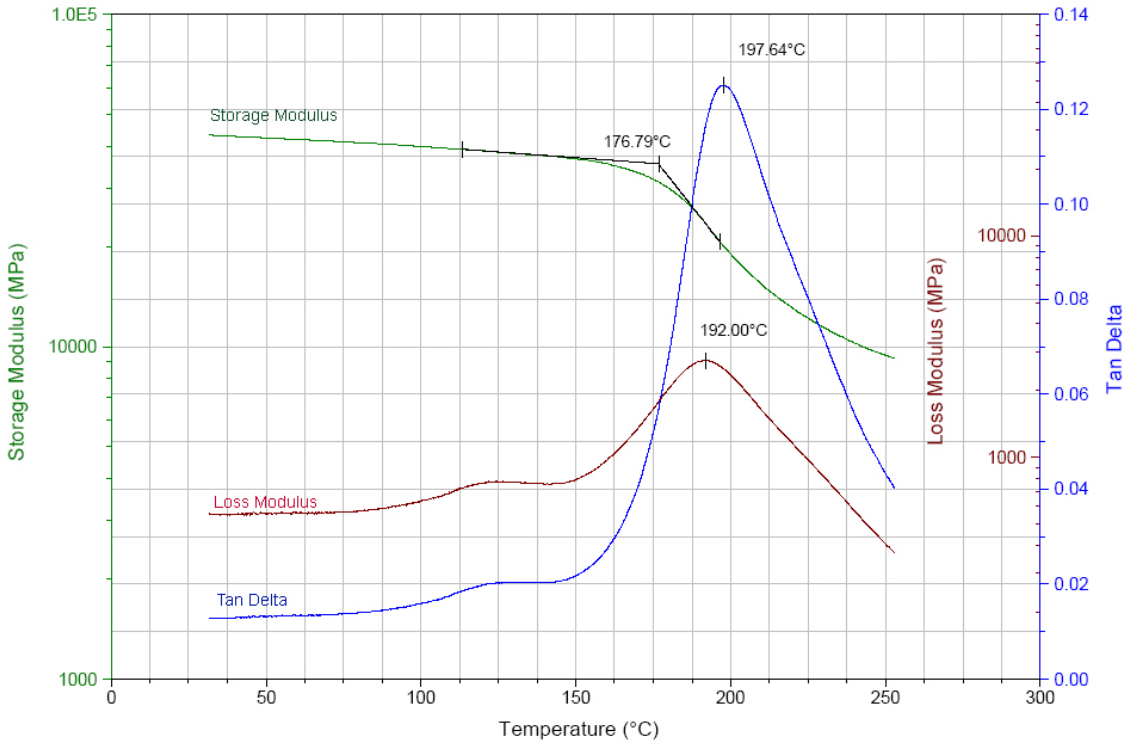

Figure 49. The DMA Data for As-Extracted Coupon From Upper Skin Rib 7 (ASTM Standard)

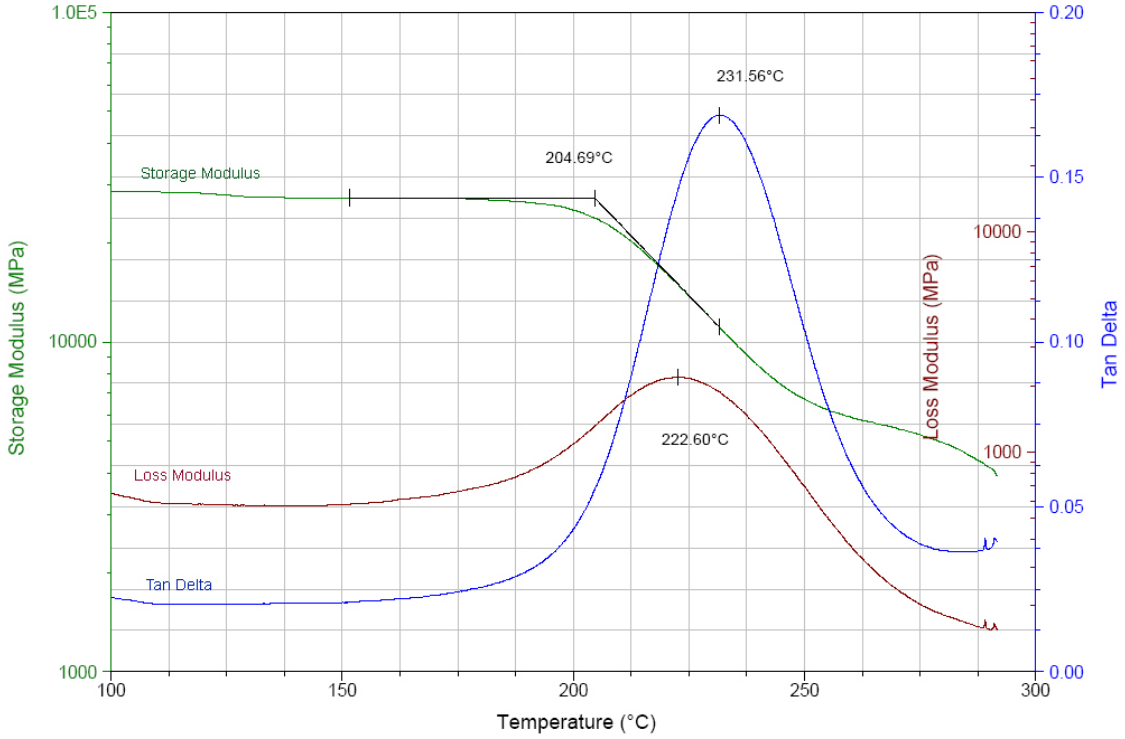

Figure 50. The DMA Data for Dried Coupon From Upper Skin Rib 2 Stringer 4 (ASTM Standard)

Figures 51 and 52 summarize DMA data obtained for the stabilizer lower skin following the Boeing method and the ASTM standard, respectively. The DMA lower skin coupons tested according to the ASTM standard yielded average T_g values of 170.2°C (338.4°F) (onset of storage modulus) and 198.38°C (389.1°F) (peak of tan delta), respectively. The DMA coupons tested according to the Boeing method yielded average T_g values of 196.9°C (386.4°F) and 230.9°C (447.6°F), respectively. The detailed test data are summarized in tables 9 and 10, respectively.

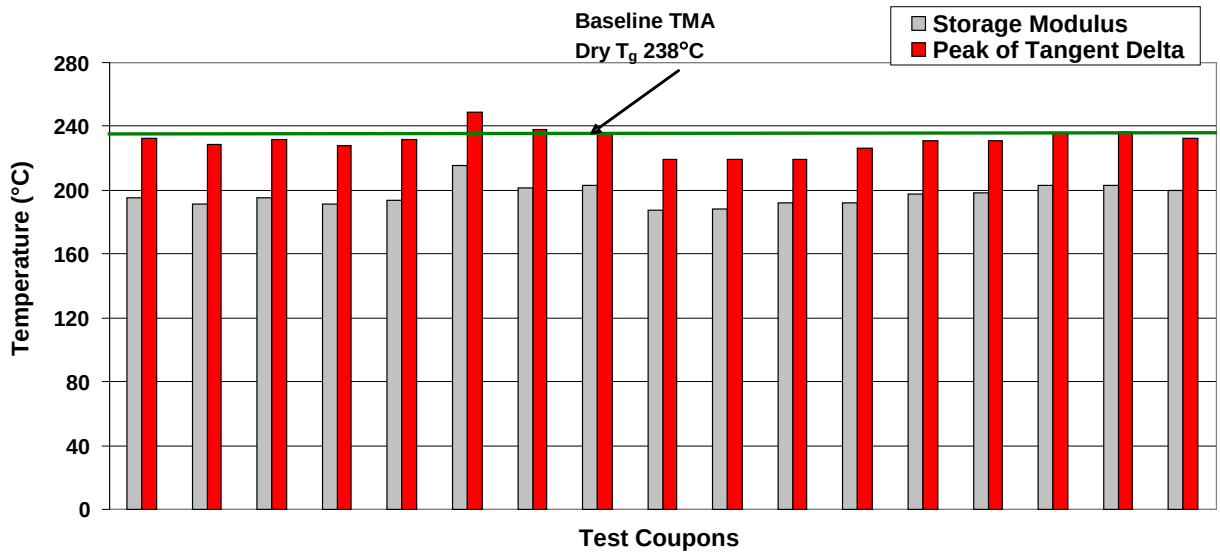

Figure 51. The DMA Results for As-Extracted Coupons From the Lower Skin of B-737 Horizontal Stabilizer (Boeing Method)

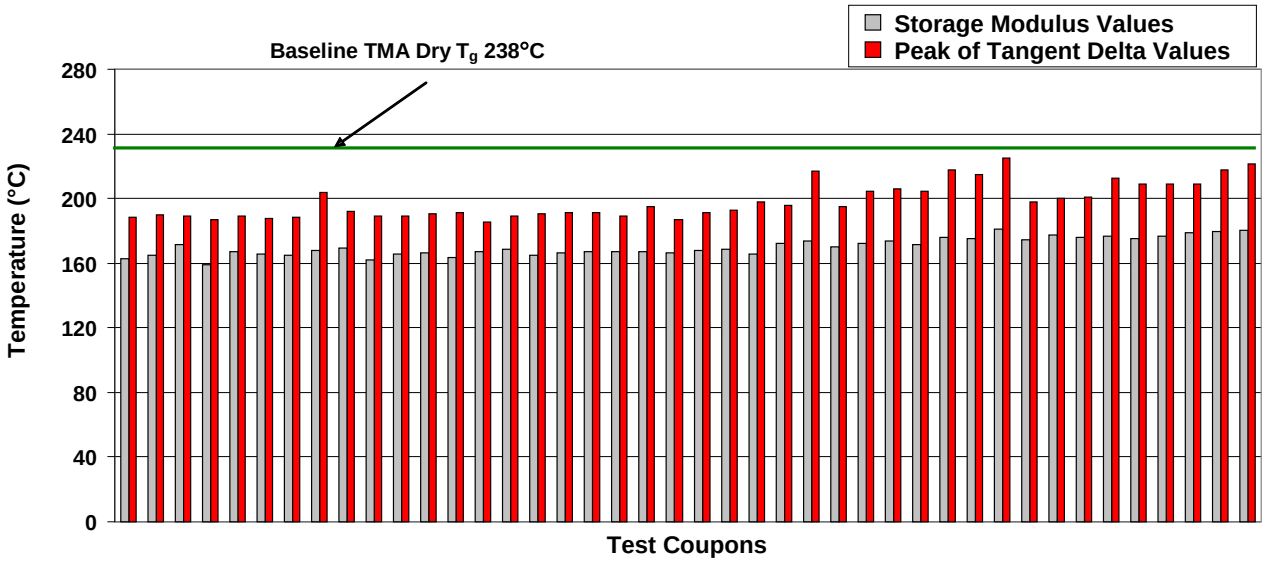

Figure 52. The DMA Results for As-Extracted Coupons From the Lower Skin of B-737 Horizontal Stabilizer (ASTM Standard)

Table 9. The DMA Test Data for Lower Skin Coupons (As-Extracted) Using Boeing Parameters

Coupon ID	Storage Modulus (ºC)	Loss Modulus (ºC)	Tan Delta (ºC)
LS_R2_STR4_5_T1	195.36	216.26	232.48
LS_R2_STR4_5_T2	191.24	210.62	228.88
LS_R4_STR3_4_T1	195.40	217.68	231.62
LS_R4_STR4_5_T1	191.06	215.21	228.06
LS_R4_STR4_5_T2	193.50	216.61	231.55
LS_R6_STR0_1_T1	215.29	240.47	249.13
LS_R6_STR0_1_T2	201.45	225.48	237.72
LS_R6_STR1_2_T2	203.18	224.34	235.35
LS_R2_STR4_5_C1	187.63	208.12	219.18
LS_R2_STR4_5_C2	188.40	207.28	219.59
LS_R2_STR4_5_C3	192.22	208.19	219.15
LS_R4_STR2_3_C1	192.25	212.93	226.11
LS_R4_STR2_3_C2	197.39	218.51	231.17
LS_R4_STR2_3_C3	198.15	219.39	231.11
LS_R6_STR0_1_C1	202.88	224.37	235.69
LS_R6_STR0_1_C2	202.81	225.54	236.48
LS_R6_STR0_1_C3	199.75	219.36	232.86
Average (ºC)	196.9	218.3	230.9
Standard deviation (ºC)	6.9	8.3	7.5

Table 10. The DMA Test Data for Lower Skin Coupons (As-Extracted) Using ASTM Test Parameters

Coupon ID	Storage Modulus (ºC)	Loss Modulus (ºC)	Tan Delta (ºC)
Rib1 Str4-1	162.96	177.52	188.33
Rib1 Str4-2	164.89	181.33	189.90
Rib1 Str10-1	171.25	182.27	189.06
Rib1 Str10-2	159.08	178.30	186.86
Rib2 Str6-1	166.98	182.64	189.32
Rib2 Str6-2	165.70	178.58	187.54
Rib2 Str11-1	164.99	178.06	188.63
Rib2 Str11-2	168.03	187.16	203.89
Rib3 Str4-1	169.64	186.02	191.72
Rib3 Str4-2	162.10	179.70	188.98
Rib3 Str9-1	165.69	178.55	189.09
Rib3 Str9-2	166.66	181.02	190.51
Rib4 Str6-1	163.09	182.59	191.63
Rib4 Str6-2	166.88	171.59	185.34

Table 10. The DMA Test Data for Lower Skin Coupons (As-Extracted) Using ASTM Test Parameters (Continued)

Coupon ID	Storage Modulus (ºC)	Loss Modulus (ºC)	Tan Delta (ºC)
Rib4 Str8-1	168.54	179.17	188.97
Rib4 Str8-2	165.16	181.98	190.93
Rib5 Str6-1	166.22	182.33	191.14
Rib5 Str6-2	167.28	182.26	191.33
Rib6 Str4-1	166.78	179.12	189.17
Rib6 Str4-2	166.81	185.48	194.91
Rib6 Str7-1	166.26	177.11	186.69
Rib7 Str6-1	168.20	183.81	191.41
Rib7 Str6-2	168.84	184.00	192.93
Rib8 Str5-2	165.80	185.56	197.60
LS_R2_STR4_5_T1	172.60	188.48	195.41
LS_R2_STR4_5_T2	173.91	193.31	216.82
LS_R2_STR5_6_T1	169.73	187.90	194.83
LS_R4_STR3_4_T1	172.60	193.83	204.60
LS_R4_STR4_5_T1	173.62	193.66	206.07
LS_R4_STR4_5_T2	171.54	192.09	204.50
LS_R6_STR0_1_T1	176.21	197.92	217.60
LS_R6_STR0_1_T2	175.52	196.90	215.08
LS_R6_STR1_2_T2	180.85	198.89	224.97
LS_R2_STR4_5_C1	174.29	190.96	198.01
LS_R2_STR4_5_C2	177.67	191.83	199.80
LS_R2_STR4_5_C3	175.71	193.13	200.63
LS_R4_STR2_3_C1	176.32	195.78	212.32
LS_R4_STR2_3_C2	175.49	195.45	208.63
LS_R4_STR2_3_C3	176.56	195.81	209.10
LS_R6_STR0_1_C1	178.89	196.61	208.60
LS_R6_STR0_1_C2	179.56	201.80	217.92
LS_R6_STR0_1_C3	180.33	195.82	221.18
Average (ºC)	170.22	186.82	198.38
Standard deviation (ºC)	5.49	7.54	11.10

Similar to the upper skin results, the lower skin DMA results obtained using the Boeing method were consistently higher than the DMA results generated using the ASTM standard. To investigate the effects of moisture on the T_g, dried coupons were tested. The data is summarized in figure 53 and table 11. Drying the coupons increased the average storage modulus by 30°C and the average tan delta by 23°C. Sample DMA curves for as-extracted and dried coupons are shown in figures 54 and 55, respectively.

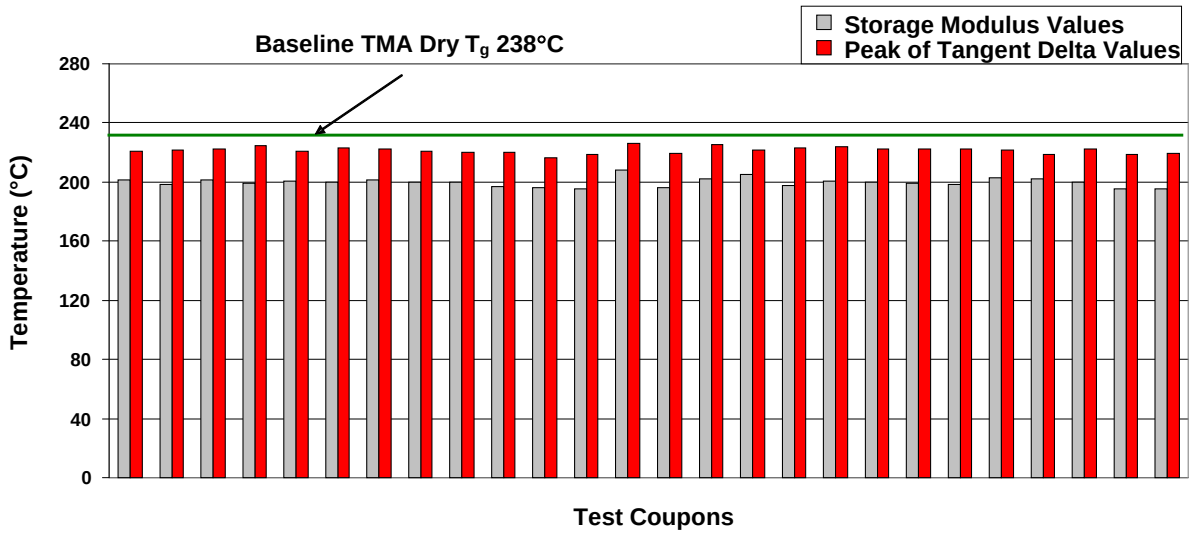

Figure 53. The DMA Results for Dried Coupons From Lower Skin of B-737 Horizontal Stabilizer (ASTM Standard)

Table 11. The DMA Test Data for Lower Skin Coupons (Dried) Using ASTM Test Parameters

Coupon ID	Storage Modulus (ºC)	Loss Modulus (ºC)	Tan Delta (ºC)
Rib1 Str6-1	201.48	208.85	221.03
Rib1 Str7-1	198.44	212.76	221.26
Rib2 Str4-1	201.54	211.36	222.17
Rib2 Str4-2	199.24	215.21	224.27
Rib2 Str5-1	200.32	210.71	220.53
Rib2 Str5-2	199.89	215.01	222.80
Rib3 Str5-1	201.45	213.11	222.18
Rib3 Str5-2	199.80	211.15	220.89
Rib3 Str6-1	199.82	210.93	220.02
Rib3 Str6-2	197.22	210.16	219.98
Rib4 Str1-1	196.42	204.59	216.43
Rib4 Str1-2	195.05	209.05	218.42
Rib4 Str5-1	207.81	223.97	226.22
Rib4 Str5-2	196.10	210.23	219.00
Rib5 Str4-1	202.16	217.68	225.20
Rib5 Str4-2	205.33	213.85	221.70
Rib5 Str5-1	197.94	213.74	222.75
Rib5 Str5-2	200.57	217.57	224.00
Rib6 Str5-1	199.84	214.80	222.56
Rib6 Str5-2	199.25	214.18	222.17
Rib6 Str6-1	198.36	216.19	222.64
Rib6 Str6-2	202.64	215.13	221.66

Table 11. The DMA Test Data for Lower Skin Coupons (Dried) Using ASTM Test Parameters (Continued)

Coupon ID	Storage Modulus (ºC)	Loss Modulus (ºC)	Tan Delta (ºC)
Rib7 Str1-1	202.06	211.36	218.45
Rib7 Str1-2	200.20	214.47	222.00
Rib7 Str4-1	195.39	209.98	218.77
Rib7 Str4-2	195.28	209.29	219.13
Average (ºC)	199.75	212.90	221.39
Standard deviation (ºC)	3.00	3.77	2.25

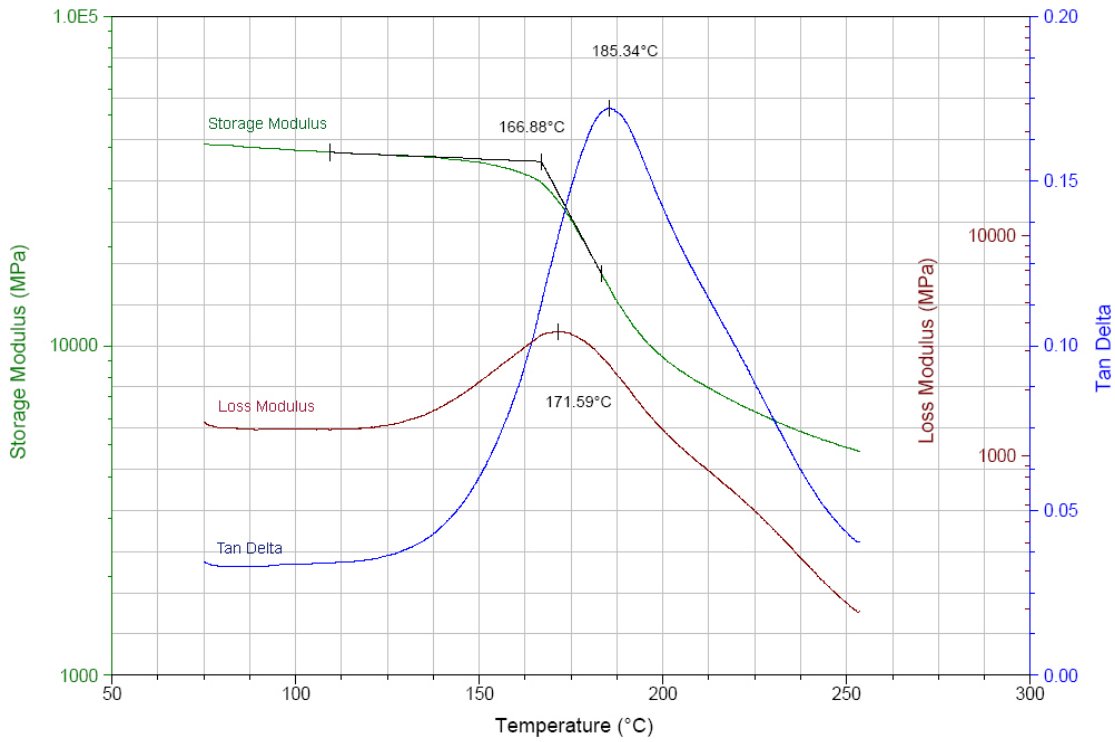

Figure 54. The DMA Data for As-Extracted Coupon From Lower Skin Rib 4 Stringer 6 (ASTM Standard)

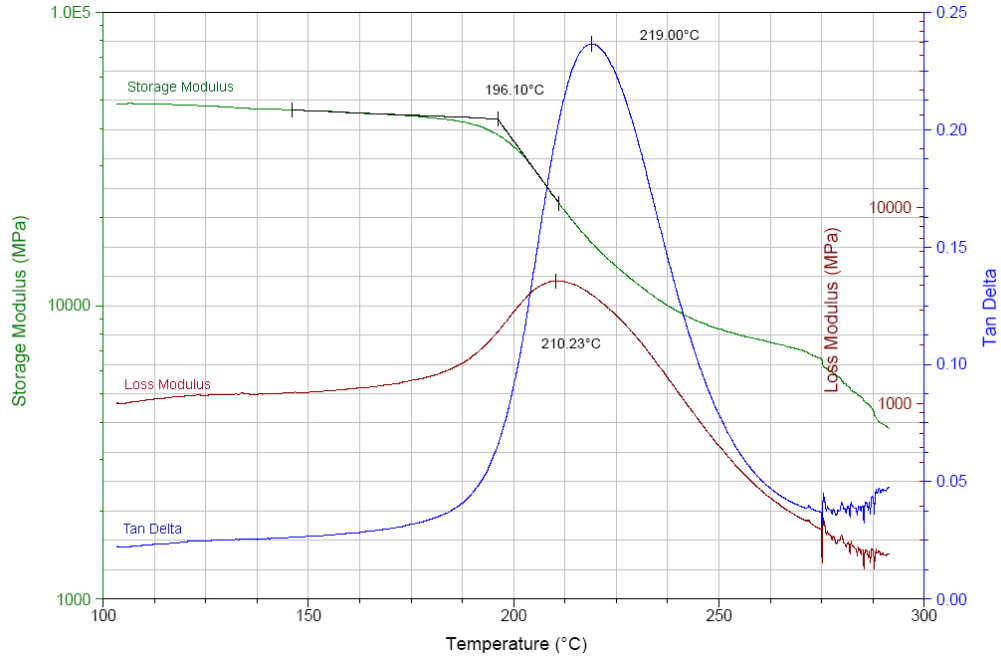

Figure 55. The DMA Data for Dried Coupon From Lower Skin Rib 4 Stringer 5 (ASTM Standard)

Comparing the average DMA results of the upper and lower skins, it is clear that the average T_g values on the upper skin were consistently higher than the average values obtained for the lower skin (4° to 6°C difference). This could be due to ultraviolet exposure that could have contributed to additional curing of the upper skin and thus a higher T_g.

Tables 12 a nd 13 summarize DMA data obtained for the stabilizer front and rear spars, respectively. The DMA front spar coupons yielded an average T_g value of 208.9°C (408.02°F) (onset of storage modulus) and 229.6°C (445.3°F) (peak of tan delta), respectively. The DMA rear spar coupons yielded an average T_g value of 202.3°C (396.1°F) (onset of storage modulus) and 223.08°C (433.5°F) (peak of tan delta), respectively.

Table 12. The DMA Test Data for Front Spar Coupons

Coupon ID	Storage Modulus (ºC)	Loss Modulus (ºC)	Tan Delta (ºC)
FS 111_1	219.79	223.69	239.63
FS 111_2	175.15	196.08	231.09
FS 166_1	221.84	217.00	228.24
FS 166_2	220.40	207.76	224.12
FS 221_1	221.99	218.95	230.20
FS 221_2	182.56	197.63	221.91
FS 256	221.22	220.95	232.11
Average (ºC)	208.99	211.72	229.61
Standard deviation (ºC)	20.71	11.31	5.78

Table 13. The DMA Test Data for Rear Spar Coupons

Coupon ID	Storage Modulus (ºC)	Loss Modulus (ºC)	Tan Delta (ºC)
RS 111_1	180.46	196.12	229.89
RS 111_2	178.87	196.32	205.53
RS 166.3_1	224.87	214.55	233.85
RS 166.3_2	195.58	204.86	220.97
RS 221.5_1	228.04	221.00	233.43
RS 221.5_2	228.71	225.51	234.97
RS 256.47	179.34	198.46	202.91
Average (ºC)	202.27	208.12	223.08
Standard deviation (ºC)	24.04	12.23	13.72

When comparing the T_g values obtained for the front and rear spars to the upper skin T_g, the average T_g obtained from coupons extracted from the spars was at least 21°C higher than the upper skin T_g values summarized in tables 12 and 13. The increased T_g is most probably due to the additional curing that occurred during the secondary bonding of the spars. The skins were only subjected to a single cure, whereas the spars were initially cured as separate C-channels and secondarily bonded using film adhesive.

Similarly, when comparing T_g values obtained for the front and rear spars to the T_g for the lower skin, the average T_g obtained from coupons from the spars was at least 24.7°C higher than the lower skin T_g values, which is consistent with the results obtained for the upper skin.

Throughout the teardown investigation, baseline material capability was not available for all tests and configurations considered. To establish baseline material data for all tests and laminate configurations, current Narmco (now Cytec T300/5208 material) was acquired. Laminates of different configurations were manufactured and tested. The intent was to investigate the thermal, physical, and mechanical properties of the new system and possibly establish baseline capability when the information was not available.

DMA tests were conducted on the new material system and, as show in table 14, yielded an average T_g of 193°C (onset of storage modulus) and 225°C (peak of tan delta), respectively. The new material T_g correlated very well with the average dry skin T_g. The average upper skin dry T_g was 205°C (onset of storage modulus) and 224°C (peak of tan delta), respectively. The average lower skin dry T_g was 199°C (onset of storage modulus) and 221°C (peak of tan delta) for the lower skin.

Table 14. The DMA Test Data for Cytec T300/5208 Material (previously Narmco 5208)

Coupon ID	Storage Modulus (ºC)	Loss Modulus (ºC)	Tan Delta (ºC)
SAMPLE-01	192.14	218.44	224.44
SAMPLE-02	191.45	224.10	229.82
SAMPLE-03	193.36	217.66	222.15
SAMPLE-04	193.42	216.02	220.77
SAMPLE-05	192.75	220.09	225.30
SAMPLE-06	193.68	219.52	225.99
SAMPLE-07	192.72	220.38	225.33
SAMPLE-08	194.46	220.26	225.50
Average (ºC)	193.00	219.56	224.91
Standard deviation (ºC)	0.94	2.37	2.70

DSC tests, per ASTM D 3418-03, were also conducted on coupons extracted from both skins and spars to evaluate the degree of cure of the material. In a DSC test, coupons are heated at a constant heating rate, and the difference in heat input between the test coupon and a reference material due to energy changes is monitored. Transitions due to changes in morphological or chemical reactions in a polymer can be detected as the coupon is heated up, and the corresponding changes in heat flow and specific heat capacity are calculated. Sample DSC curves are shown in figures 56 to 59. Each figure shows three curves: a reversing heat-flow curve, a nonreversing heat-flow curve, and a total heat-flow curve. The nonreversing signal is an indication of the presence of nonreversible processes such as chemical reactions. The reversing signal is typically used to detect reversing reactions such as T_g.

To evaluate the degree of cure of the aged structure, a DSC test was conducted on a Cytec T300/5208 prepreg coupon to determine the heat of reaction required to fully cure the coupon yielding 206.6 J/g. All the heat of reaction values obtained from subsequent tests were normalized with respect to this value to obtain a cure conversion percentage indicative of the degree of cure of the part.

DSC tests were conducted on coupons manufactured from the Cytec T300/5208 material to determine the degree of cure achieved on the newly fabricated coupons. DSC test data for the cured coupons are summarized in table 15. The tests yielded an average heat of reaction of 10.36 J/g, an average exotherm onset temperature of 211.19°C, and an average exotherm peak of 248.76°C. This is equivalent to a 95% cure conversion percentage (i.e., the cured coupons from the new material achieved a degree of cure that averaged, at most, 95%).

Table 15. The DSC Test Data for Cytec T300/5208 Material (previously Narmco 5208)

Coupon ID	Exotherm Onset (ºC)	Exotherm Peak (ºC)	Heat of Reaction of Exotherm (J/g)	Cure Conversion (%)
AS-01	208.27	246.87	12.99	93.71
AS-02	214.20	249.59	9.74	95.29
AS-03	206.67	246.27	9.82	95.25
AS-04	205.63	245.44	9.38	95.46
AS-05	212.30	249.26	10.46	94.94
AS-06	215.37	250.20	9.85	95.23
AS-07	212.55	249.71	9.94	95.19
AS-08	214.52	252.72	10.67	94.84
Average (ºC)	211.19	248.76	10.36	94.99
Standard deviation (ºC)	3.79	2.40	1.14	0.55

The upper skin DSC test data are shown in figure 56 and summarized in tables 16 and 17. DSC tests conducted on the as-extracted coupons yielded an average heat of reaction of 5J/g, an average exotherm onset temperature of 202°C, and an average exotherm peak of 225°C. DSC tests conducted on dried coupons yielded an average heat of reaction of 4.4J/g, an average exotherm onset temperature of 214°C, and an average exotherm peak of 233°C. For both as-extracted and dried coupons, the heat of reaction values were smaller than those obtained with the new material, thus indicative of the degree of cure higher than 95%.

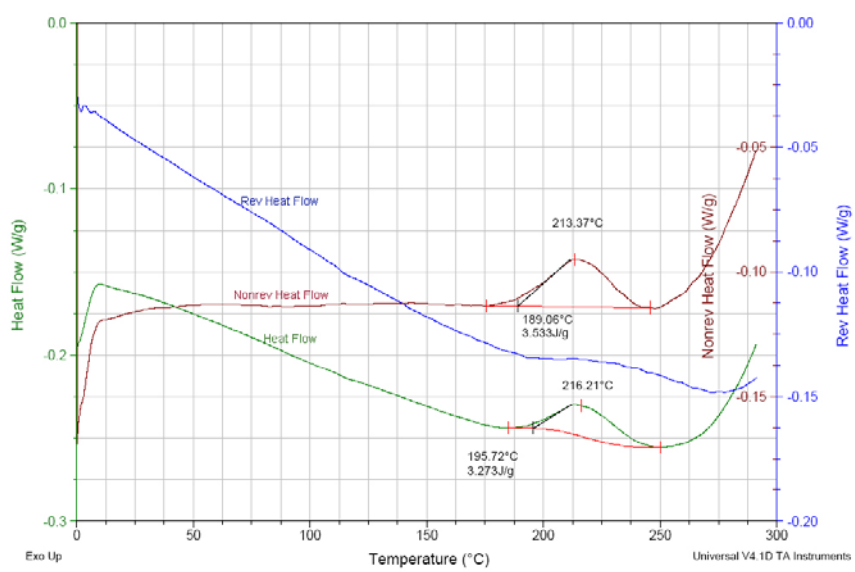

Figure 56. The DSC Data for As-Extracted Coupon From Upper Skin Rib 5 Stringer 8

Table 16. The DSC Test Data for As-Extracted Coupons From Upper Skin

Coupon ID	Exotherm Onset (ºC)	Exotherm Peak (ºC)	Heat of Reaction of Exotherm (J/g)
Rib2 Str1	209.1	234.3	12.2
Rib2 Str11	205.6	225.6	2.8
Rib3 Str1	194.3	226.2	8.7
Rib3 Str4	207.2	225.2	3.0
Rib4 Str1	203.6	227.5	5.0
Rib4 Str6	202.1	220.1	2.6
Rib5 Str1	202.7	229.6	7.5
Rib5 Str5	210.7	228.9	4.9
Rib6 Str1	198.5	226.4	5.5
Rib8 Str2	200.9	223.3	3.0
Rib8 Str4	207.3	224.5	2.3
Rib1 Str4	199.1	228.4	8.5
Rib2 Str1	194.6	221.7	4.5
Rib3 Str10	202.7	226.9	4.1
Rib4 Str6	201.3	229.0	7.2
Rib5 Str8	195.7	216.2	3.3
Rib6	196.2	218.3	2.5
Rib7	201.0	225.5	2.0
Average (ºC)	201.8	225.4	5.0
Standard deviation (ºC)	4.9	4.3	2.8

Table 17. The DSC Test Data for Dried Coupons From Upper Skin

Coupon ID	Exotherm Onset (ºC)	Exotherm Peak (ºC)	Heat of Reaction of Exotherm (J/g)
Rib1 Str7	222.7	238.8	2.8
Rib1 Str8-1	208.7	231.4	5.9
Rib1 Str11-1	210.7	250.1	8.8
Rib2 Str5-1	209.2	228.2	3.4
Rib2 Str11	221.9	235.4	2.4
Rib3 Str6	209.5	229.2	4.9
Rib3 Str7-1	212.6	230.4	3.5
Rib3 Str8-1	210.4	227.1	2.0
Rib4 Str4	220.5	239.2	3.6
Rib4 Str7-1	213.4	232.3	3.8
Rib4 Str8-1	208.0	228.8	4.3
Rib5 Str4-1	213.4	230.4	3.7
Rib5 Str6-1	214.3	235.1	9.0

Table 17. The DSC Test Data for Dried Coupons From Upper Skin (Continued)

Coupon ID	Exotherm Onset (ºC)	Exotherm Peak (ºC)	Heat of Reaction of Exotherm (J/g)
Rib5 Str7	226.3	238.0	2.8
Rib6 Str4-1	213.4	231.1	2.2
Rib6 Str5-1	211.0	230.4	4.7
Rib6 Str6	213.0	232.4	5.8
Rib7 Str1-1	210.5	231.4	5.9
Rib7 Str5	221.3	238.3	3.3
Rib7 Str6-1	212.3	231.3	5.3
Average (ºC)	214.2	233.5	4.4
Standard deviation (ºC)	5.3	5.3	2.0

The lower skin DSC test data are shown in figure 57 and summarized in tables 18 and 19. DSC tests conducted on as-extracted coupons yielded an average heat of reaction of 8 J/g, an average exotherm onset temperature of 203°C, and an average exotherm peak of 230°C. DSC tests conducted on dried coupons yielded an average heat of reaction of 10J/g, an average exotherm onset temperature of 213°C, and an average exotherm peak of 235°C. For both as-extracted and dried coupons, the heat of reaction values were much less or equal to the values obtained for the new material, thus indicative of a degree of cure of at least 95%.

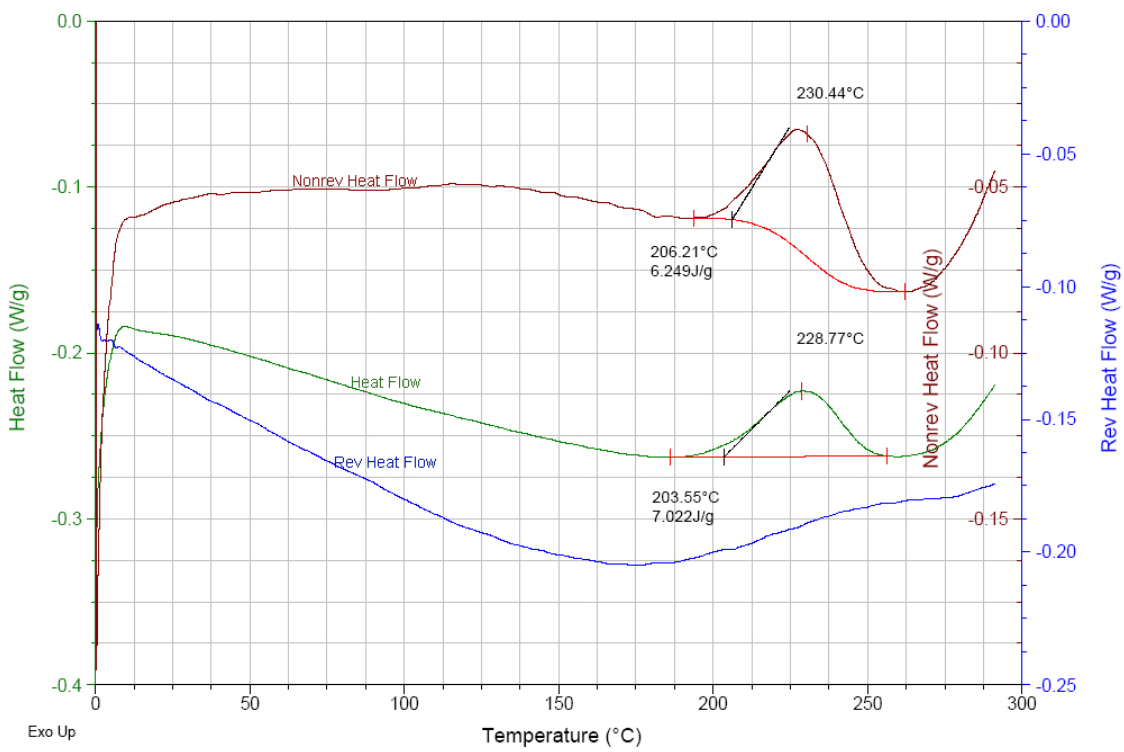

Figure 57. The DSC Data for As-Extracted Coupon From Lower Skin Rib 1 Stringer 4

Table 18. The DSC Test Data for As-Extracted Coupons From Lower Skin

Coupon ID	Exotherm Onset (ºC)	Exotherm Peak (ºC)	Heat of Reaction of Exotherm (J/g)
Rib1 Str4-1	203.55	228.77	7.022
Rib1 Str10-1	200.65	228.02	7.276
Rib3 Str4-1	205.79	233.47	8.592
Rib3 Str9-1	203.67	229.11	7.512
Rib4 Str6-1	208.73	233.00	5.888
Rib4 Str8-1	201.58	228.71	9.756
Rib5 Str6-1	202.30	230.93	11.590
Rib6 Str4-1	203.84	230.89	10.700
Rib6 Str7-1	195.15	225.75	7.309
Rib7 Str6-1	203.30	230.38	7.840
Average (ºC)	202.9	229.9	8.3
Standard deviation (ºC)	3.5	2.3	1.8

Table 19. The DSC Test Data for Dried Coupons From Lower Skin

Coupon ID	Exotherm Onset (ºC)	Exotherm Peak (ºC)	Heat of Reaction of Exotherm (J/g)
Rib1 Str6-1	214.50	237.52	9.89
Rib1 Str7-1	211.67	233.74	7.88
Rib2 Str4-1	214.06	236.24	9.09
Rib2 Str5-1	215.08	224.23	6.04
Rib3 Str5-1	208.91	229.87	7.18
Rib3 Str6-1	213.22	234.32	8.51
Rib4 Str1-1	206.47	235.90	22.26
Rib4 Str5-1	209.97	235.82	12.48
Rib5 Str4-1	213.35	235.19	9.84
Rib5 Str5-1	215.06	236.69	8.86
Rib6 Str5-1	217.30	237.64	7.96
Rib6 Str6-1	216.64	237.84	10.05
Rib7 Str1-1	216.51	236.12	9.24
Rib7 Str4-1	210.89	235.34	8.30
Average (ºC)	213.1	234.7	9.8
Standard deviation (ºC)	3.2	3.6	3.9

The front spar DSC test data are shown in figure 58 and summarized in table 20, and the rear spar DSC test data are shown in figure 59 and summarized in table 21. DSC tests conducted on as-extracted front spar coupons yielded an average heat of reaction of 1.83 J/g, an average exotherm onset temperature of 200°C, and an average exotherm peak of 228°C. DSC tests

conducted on as-extracted rear spar coupons yielded an average heat of reaction of 1.56 J/g, an average exotherm onset temperature of 198°C, and an average exotherm peak of 228°C. The heat of reaction values obtained for both spars were lower than those obtained for the skins, indicating a higher degree of cure for the spars compared to the skins. Unlike the skins, which were subjected to only one cure cycle, the spars were subjected to two cure cycles—the initial cycle to manufacture the channels and the second cycle to bond the channels together.

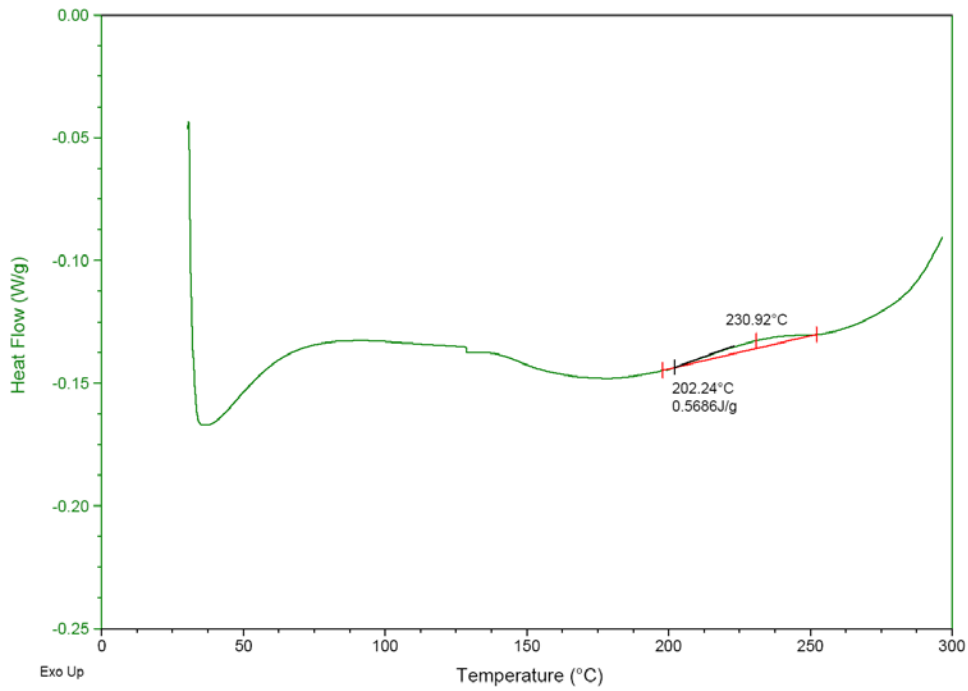

Figure 58. The DSC Data for As-Extracted Coupon From Front Spar at Stabilizer Station 111

Table 20. The DSC Test Data for As-Extracted Coupons From Front Spar

Coupon ID	Exotherm Onset (ºC)	Exotherm Peak (ºC)	Heat of Reaction of Exotherm (J/g)
FS 111_1	202.24	230.92	0.569
FS 111_2	233.03	243.82	0.782
FS 166_1	182.71	213.21	3.018
FS 166_2	195.67	228.64	2.316
FS 221_1	198.08	222.96	0.688
FS 221_2	189.82	225.71	4.684
FS 256	204.68	230.79	0.787
Average (ºC)	200.89	228.01	1.83
Standard deviation (ºC)	16.01	9.28	1.57

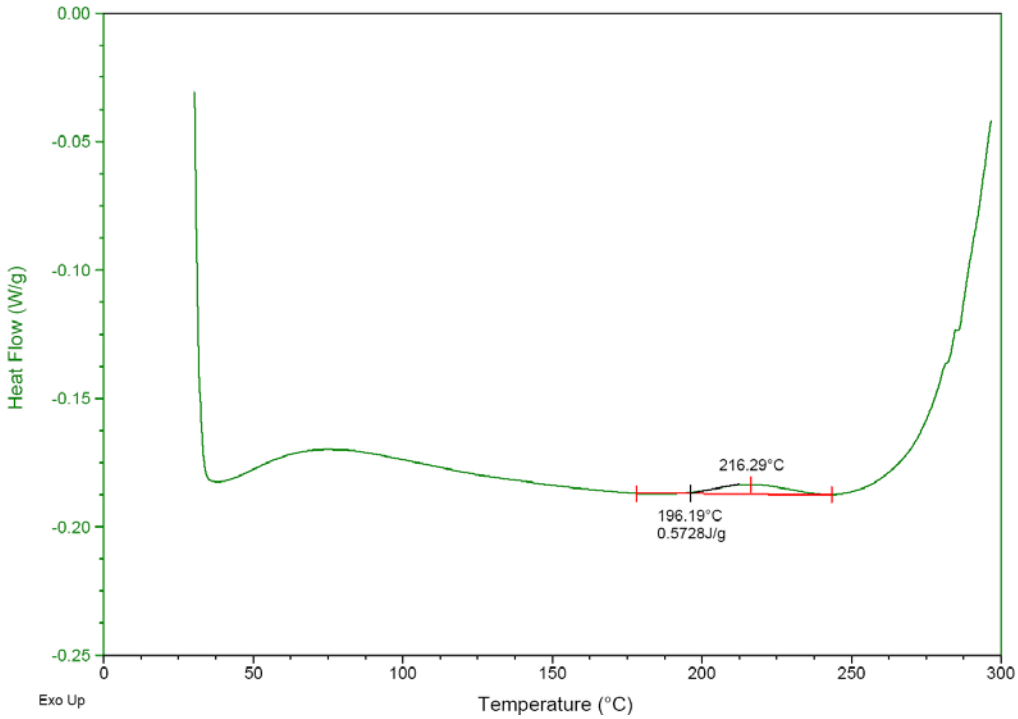

Figure 59. The DSC Data for As-Extracted Coupon From Rear Spar at Stabilizer Station 111

Table 21. The DSC Test Data for As-Extracted Coupons From Rear Spar

Coupon ID	Exotherm Onset (ºC)	Exotherm Peak (ºC)	Heat of Reaction of Exotherm (J/g)
RS 111_1	196.70	224.73	1.579
RS 111_2	196.19	216.29	0.573
RS 166.3_1	195.37	220.08	1.023
RS 166.3_2	201.99	234.99	0.810
RS 221.5_1	203.46	222.44	0.279
RS 221.5_2	183.52	198.12	0.739
RS 256.47	207.14	235.81	5.922
Average (ºC)	197.77	221.78	1.56
Standard deviation (ºC)	7.64	12.74	1.96

The generated DSC data showed that spars almost reached a fully cured status (99% cured), as additional postcuring occurred during the secondary bonding process (4% cure conversion increase with respect to the new material). The upper skin coupons showed a slightly lower degree of cure, because they were only subjected to one cure cycle. The average heat of reaction values obtained from the skin tests showed that the upper skin was 97% cured, whereas the lower skin was 95% cured. All coupons extracted from the aged structure showed an overall higher degree of cure than the new material, since additional curing/aging occurred during the lifespan of the structure.

3.7 MOISTURE CONTENT EVALUATION.

Moisture content in the aged structure was quantified according to ASTM D 5229 using coupons extracted from both skins and both spars. Figure 60 summarizes the moisture loss as a function of time for selected lower skin coupons. Figure 61 s hows the overall lower skin moisture distribution using data obtained from all coupons extracted from the skin. As shown in the figure, lower skin coupons yielded an average moisture content of 0.77%, with a minimum of 0.69% and a maximum of 0.92%. The moisture levels were below the design moisture level of 1.1%.

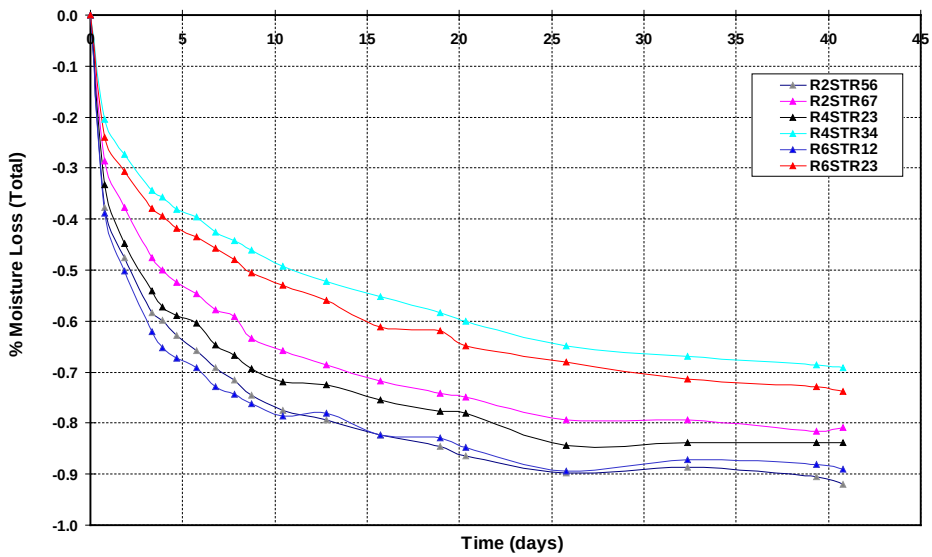

Figure 60. Moisture Loss as a Function of Time for Coupons Extracted From Lower Skin

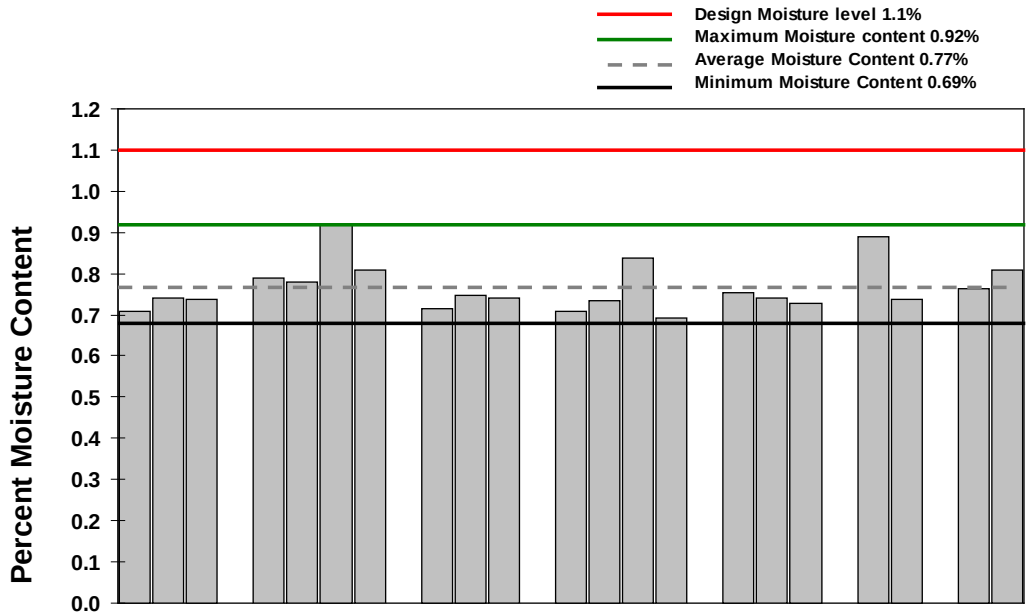

Figure 61. Moisture Distribution in Lower Skin

Figure 62 summarizes the moisture loss as a function of time for selected upper skin coupons. Figure 63 shows the overall upper skin moisture distribution using data obtained from all coupons extracted from the skin. As shown in the figure, lower skin coupons yielded an average moisture content of 0.83%, with a minimum of 0.74% and a maximum of 0.913%. The moisture levels were below the design moisture level of 1.1%.

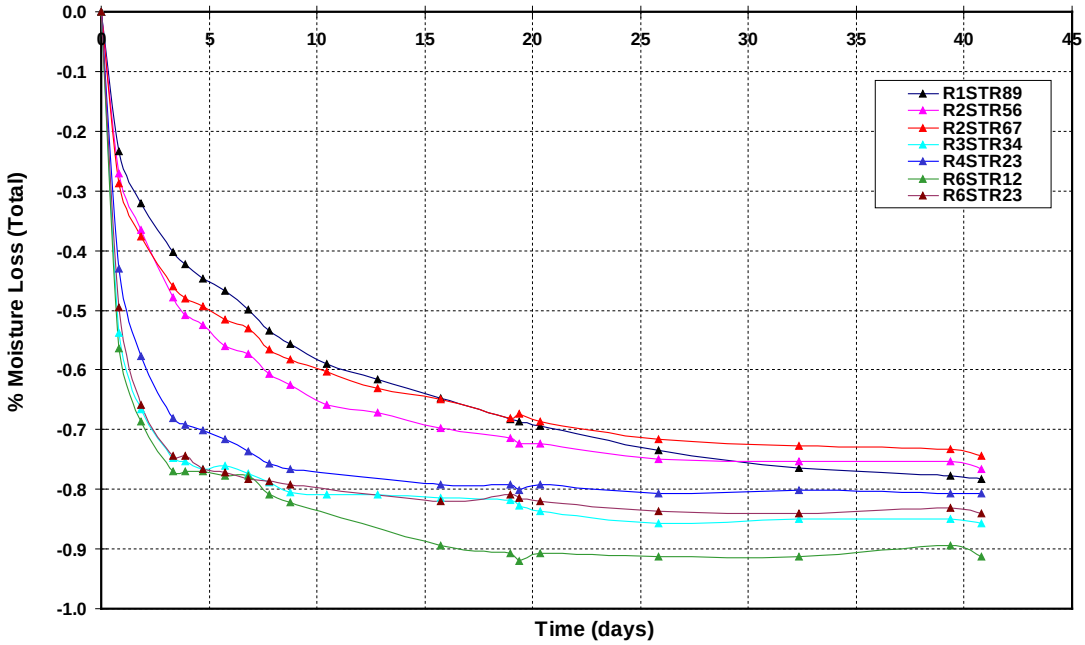

Figure 62. Moisture Loss as a Function of Time for Coupons Extracted From Upper Skin

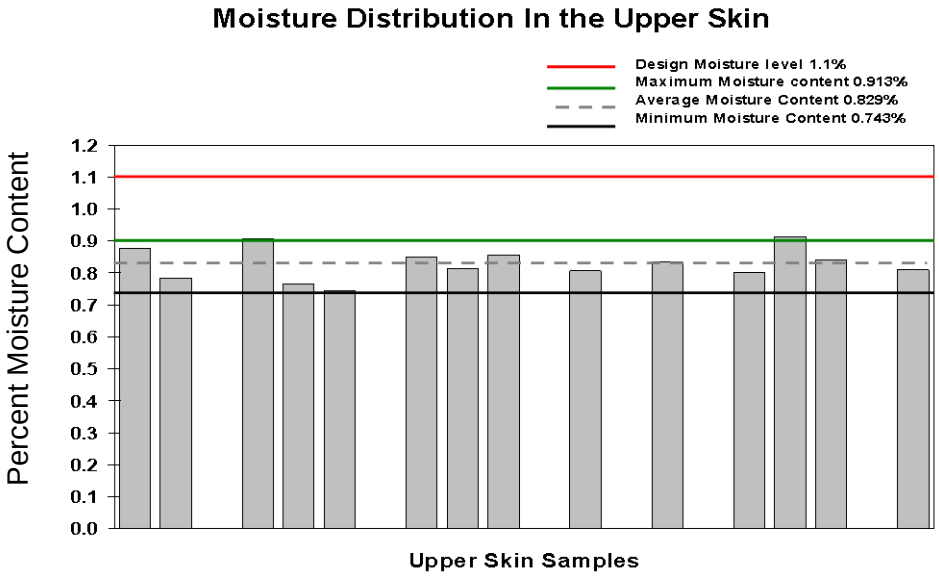

Figure 63. Moisture Distribution in Upper Skin

Figures 64 and 65 summarize the moisture loss as a function of time for front and rear spar coupons, respectively. Figure 66 shows the overall spar moisture distribution using data obtained from all coupons extracted from the spars. As shown in figure 66, front and rear spar coupons yielded an average moisture content of 1.04%, with a minimum of 0.924% and a maximum of 1.194%. The moisture levels exceeded the design moisture level of 1.1% for several coupons. The spars had higher moisture content because they were dried for over 100 days, whereas the skins were dried for only 40-60 days because they were thinner. Figure 60 indicates that the moisture may not have been completely eliminated.

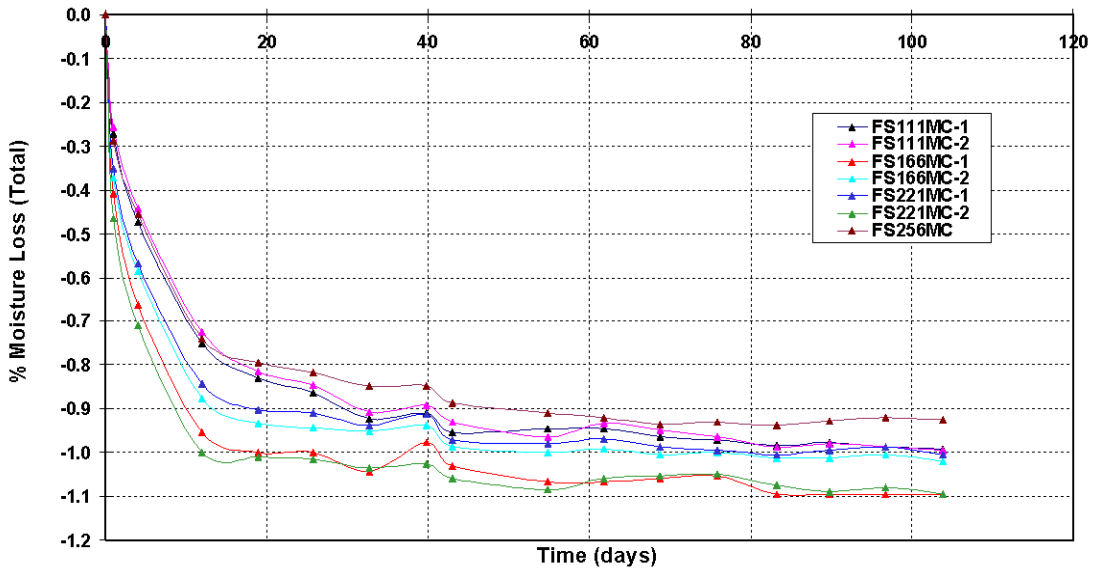

Figure 64. Moisture Loss as a Function of Time for Coupons Extracted From Front Spar

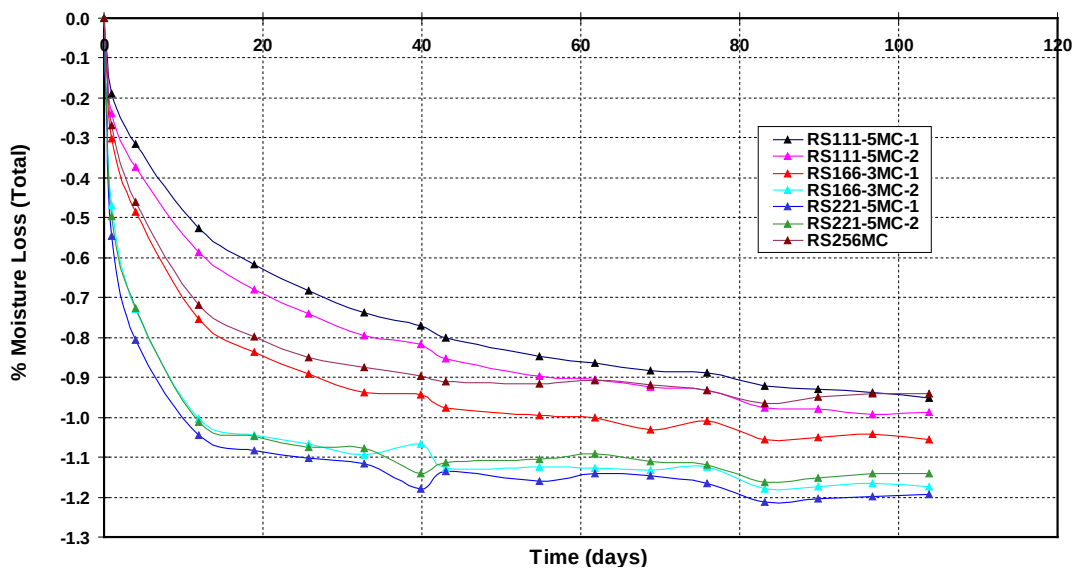

Figure 65. Moisture Loss as a Function of Time for Coupons Extracted From Rear Spar

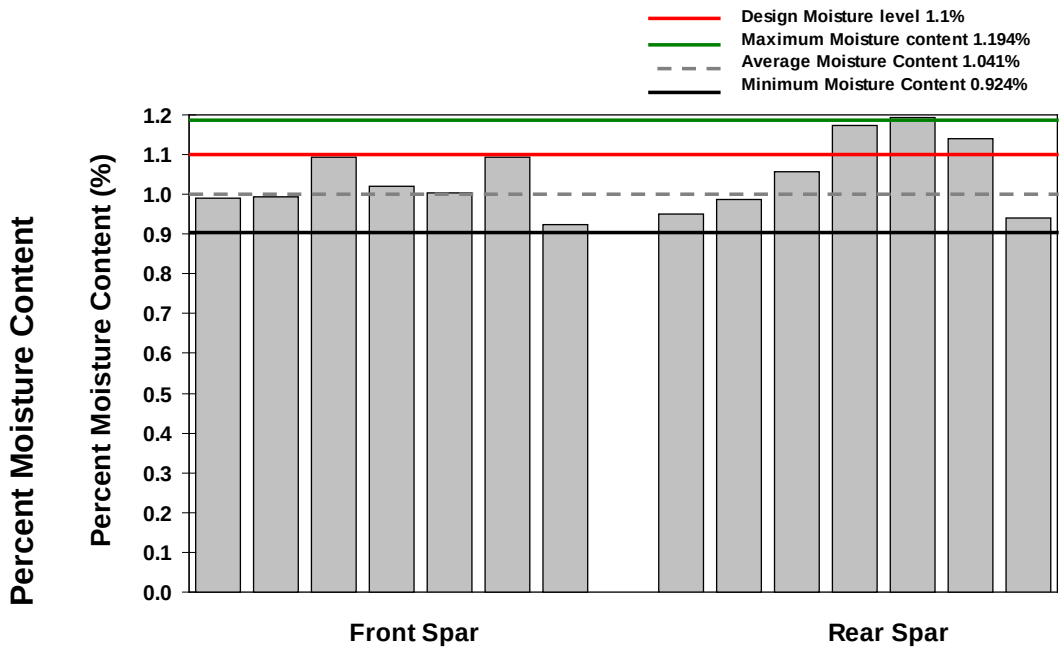

Figure 66. Moisture Distribution in Spars

3.8 VOID CONTENT EVALUATION.

Physical tests were conducted per ASTM D 3171 and D 2734 to determine the resin and fiber volume fractions in the structure and to quantify the different levels of porosity in the structure. As shown in figure 67, the maximum void content in the upper skin was on the order of 7.14%, whereas the maximum void content found in the lower skin was on the order of 3%.

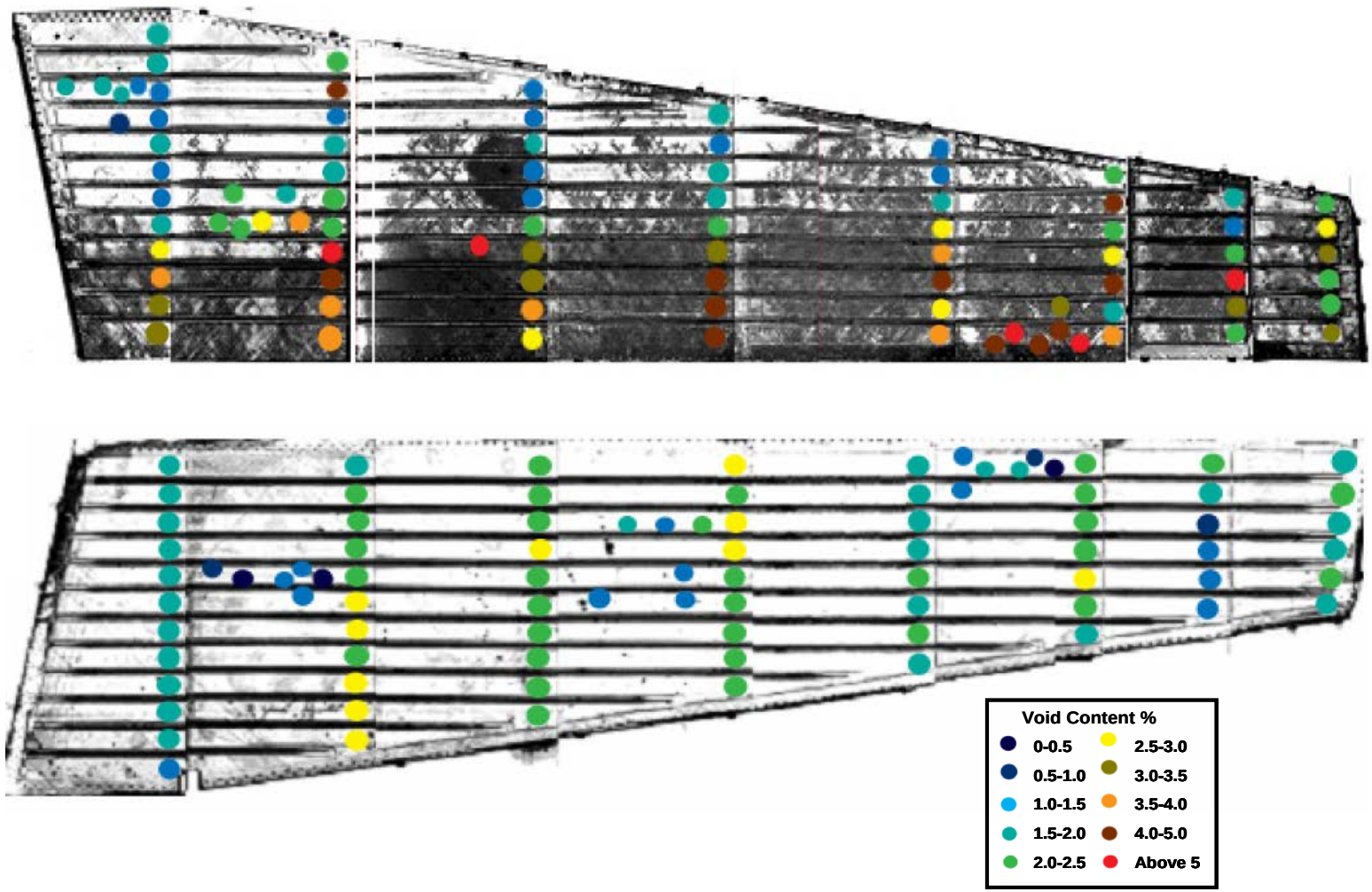

Figure 67. Void Content Summary

3.9 MICROSCOPIC IMAGE ANALYSIS.

Image analysis was conducted on coupons extracted from both the upper and lower skins to microscopically inspect the structure for voids, microcracks, or any evidence of aging or material degradation. The extracted coupons were potted, polished, and viewed under the microscope to detect possible evidence of material aging. Various images showed porosity, voids, microcracks, macrocracks, small cracks emanating from voids, as well as sound porosity-free structure. Figure 68 shows porosity, microcracks, and cracks emanating from the voids and porous areas. Figure 69 shows porosity in a stringer web section. Examples of macrocracks are illustrated in figure 70, and examples of a sound structure are shown in figure 71.

Porosity, present throughout the structure, was caused by a combination of the resin system (low flow), the material form, (fabric inherently entraps more air than tape), and the fabrication technique (co-curing a stiffened cover panel produces a large, complicated part with a substantial amount of tooling for stringer mandrels and caul sheets). Microcracks could have been caused by resin shrinkage following cure, in-service degradation, or machining the section used to produce the image. Macrocracks were most likely caused by an impact event, but the timing is unknown. The impact could have occurred before, during, or following revenue service as a result of the teardown itself. Particularly on the upper surface, removing the blind fasteners required a fair amount of force.

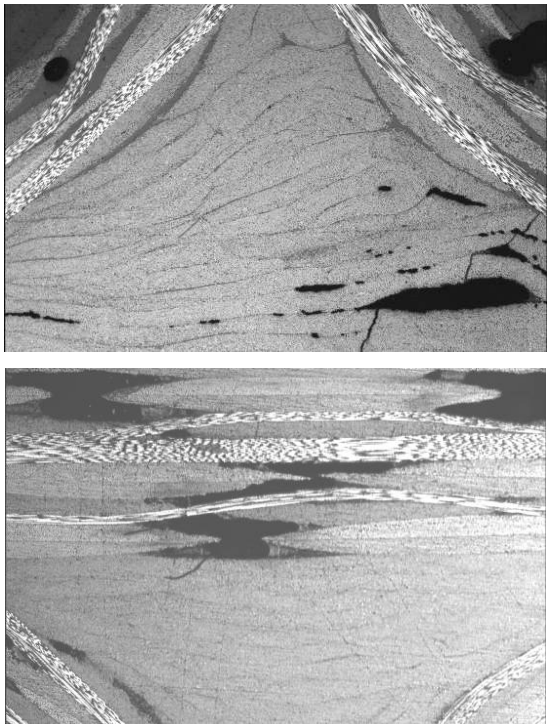

Figure 68. Cross Section of Stringer Web and Flange Intersection for Stringer 2 (top) and Stringer 3 (bottom) at Rib Station 2 (Upper Skin) Showing Porosity at Magnification 50X, Microcracks, and Cracks Emanating From the Voids and Porous Areas

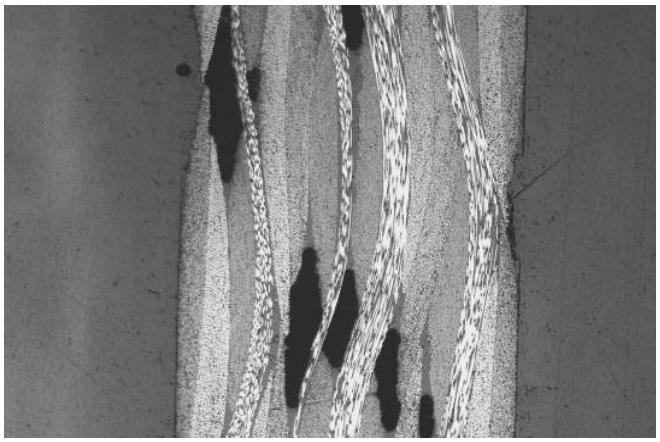

Figure 69. Cross Section of Upper Skin Stringer 2 at Rib Station 2 Web Showing Porosity at Magnification 50X

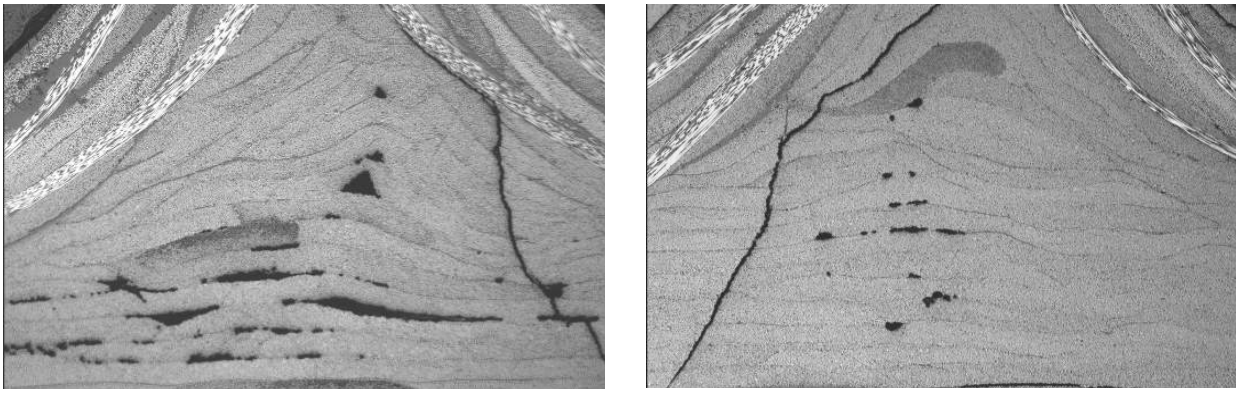

Figure 70. Cross Section of Stringer Web and Flange Intersection for Upper Skin Stringer 2 at Rib Station 1 (left) and Lower Skin Stringer 2 at Rib Station 3 (right) Showing Macrocracks at Magnification 50X

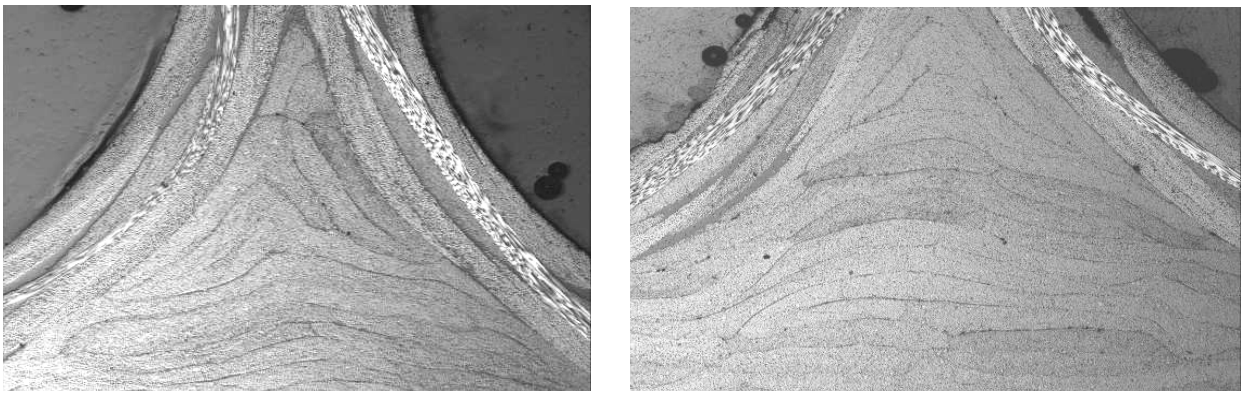

Figure 71. Cross Section of Stringer Web and Flange Intersection for Stringer 3 (left) at Rib Station 7 and Stringer 1 (right) at Rib Station 5 (Lower Skin) Showing a Sound Structure at Magnification 50X

3.10 MECHANICAL TESTS.

Mechanical tests were conducted using 1980s' coupon configurations and standards whenever possible. This was done to provide the most direct measure of property changes that may have taken place during the 18 years of revenue service. Because of lay-up schedule variations between the different rib stations, thickness variation due to porosity and ply drop-offs, and curvature in the structure, mechanical test coupons were carefully extracted and individually tabbed when applicable, then machined and tested. Baseline strength and strain data were not available for all laminate configurations in the structure; thus, the data points corresponding to an existing baseline [1] are clearly marked in the strength and strain graphs presented in this section.

All mechanical tests were conducted using either a 22- or 55-kip MTS servohydraulic load frame. The MTS test equipment was calibrated and verified according to the ASTM E 4 standard to ensure the accuracy of load and displacement readings. The coupons were loaded at a rate of 0.05 in/min. The actuator was controlled with the MTS Flextest™ GT system, and MTS Testworks® software was used to program the parameters for controlling the test and acquiring data.

As shown in figure 72, the compression coupons were 1 inch wide by 5.5 inches long. The same rectangular geometry was used during the design phase to generate compression allowables for the stabilizer structure. The fixture used for testing consisted of two anti-buckling plates supporting the entire length of the coupon with a 0.2-inch opening to allow coupon deformation during loading. The compressive loads were transferred to the coupons primarily through end loading. Two edge extensometers were used to measure displacements and calculate stiffness and strain values for the different configurations tested.

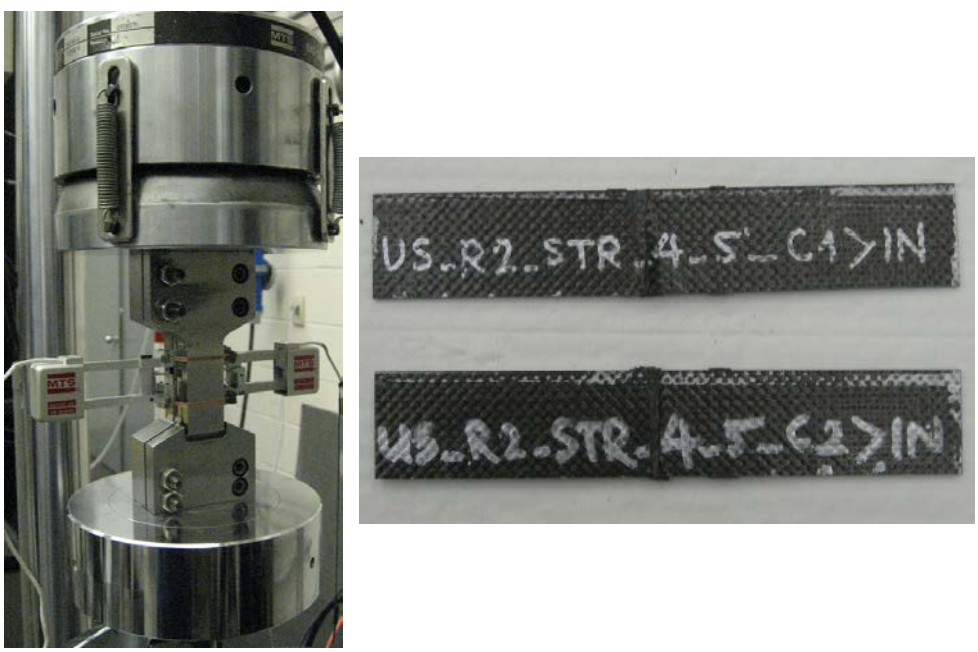

Figure 72. Compression Test Fixture and Test Specimens

Figures 73 through 76 summarize typical compression results obtained for as-extracted coupons that were taken from the upper and lower skins. These figures show measured and normalized room temperature ambient (RTA) compression strength and calculated ultimate strain values for coupons extracted from different locations on the upper and lower skins. It should be noted that the baseline strength values presented [1] are calculated based on nominal thickness values (0.053″ for 7-ply skin). It should also be noted that the compression strain to failure are calculated values. For 102-1 and 102-2 compression baselines, the average ultimate compression strength is 49.35 ksi, and the corresponding average compression strain to failure is 9250 με.

The measured compression strength was derived using the measured thickness, whereas the normalized strength was obtained using the laminate nominal thickness corresponding to the location from where the coupons were extracted. It should also be noted that only coupons extracted from the region around upper skin rib 1 had the same stacking sequence as baseline coupons 102-1 and 102-2. Similarly, lower skin coupons extracted around rib 4 had the same stacking sequence as baseline coupons 102-1 and 102-2. As illustrated in the figures, normalized compression strength and failure strain values for the stabilizer upper and lower skin coupons, with the same stacking sequence as the baseline coupons, correlated very well with the baseline strength and ultimate strain values. The RTA compression data did not show any evidence of material degradation that could be attributed to the aging of the stabilizer.

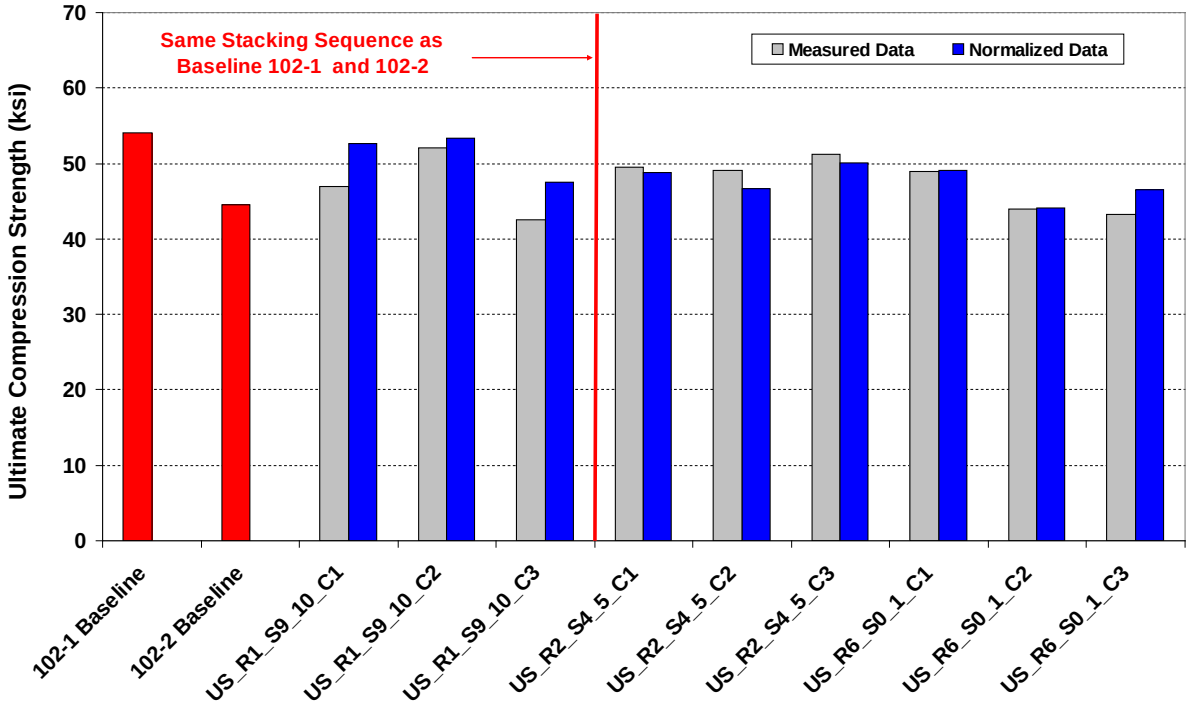

Figure 73. Upper Skin Compression Strength Test Data of As-Extracted Coupons

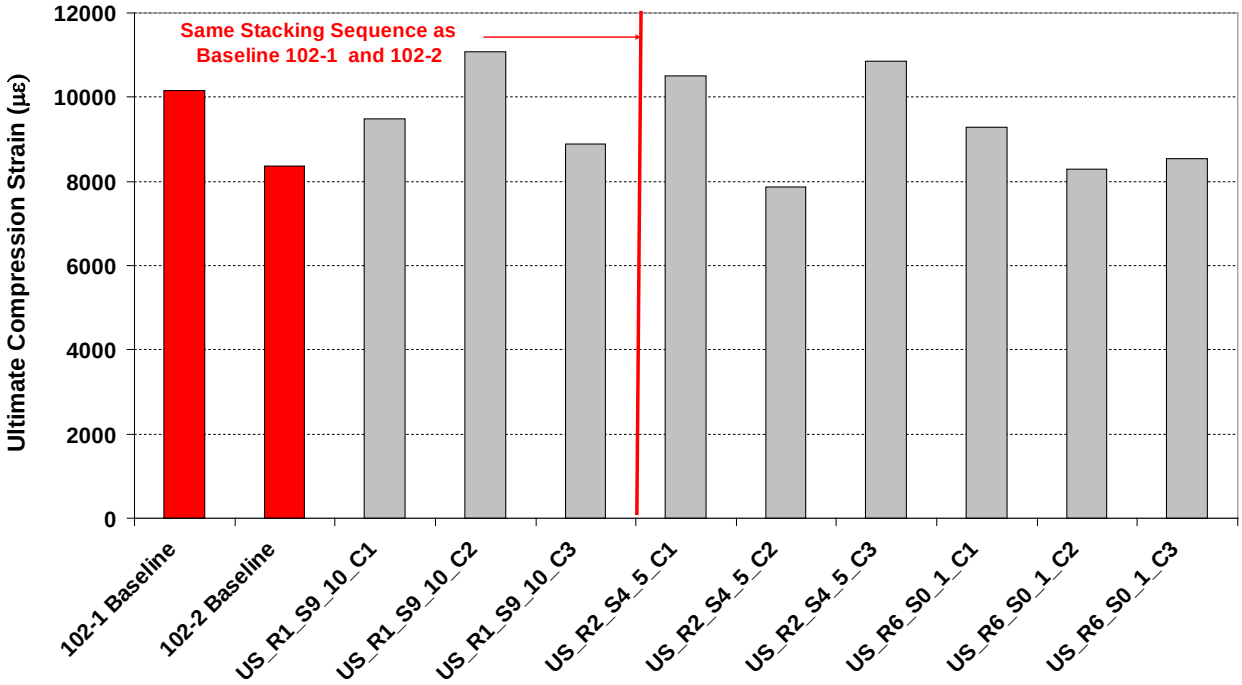

Figure 74. Upper Skin Compression Ultimate Strain Test Data (Calculated) of As-Extracted Coupons

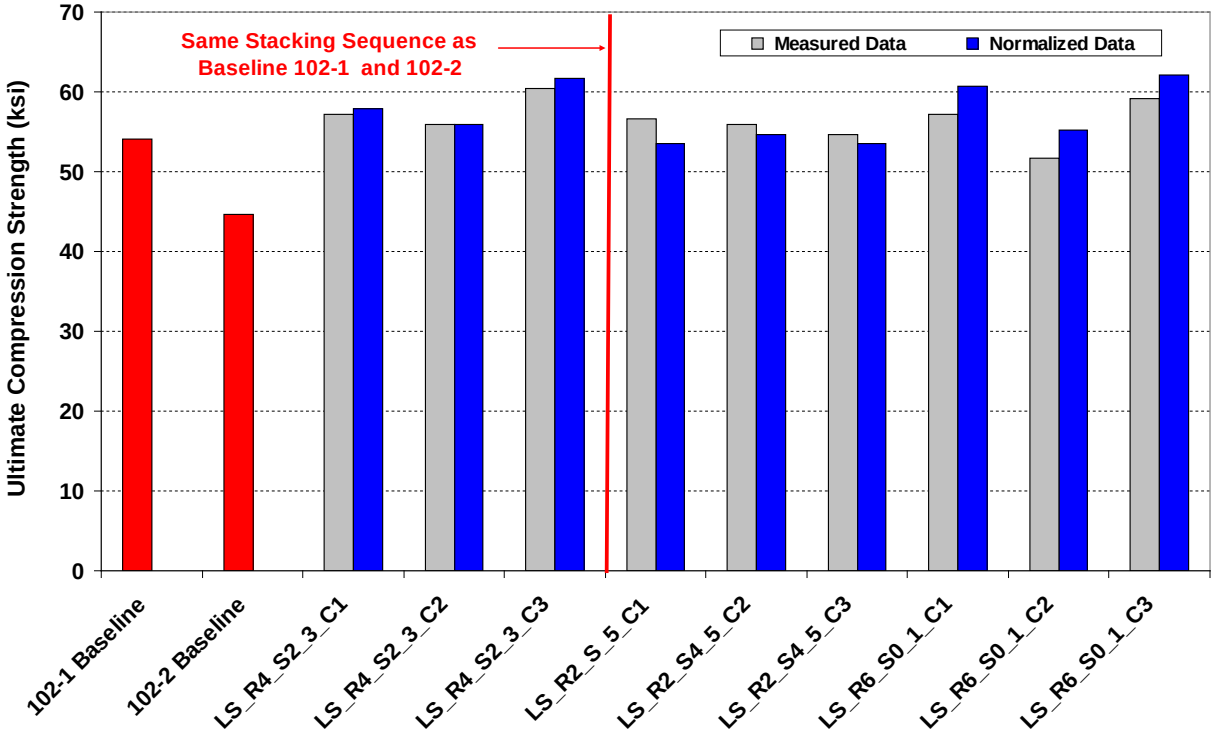

Figure 75. Lower Skin Compression Strength Test Data of As-Extracted Coupons

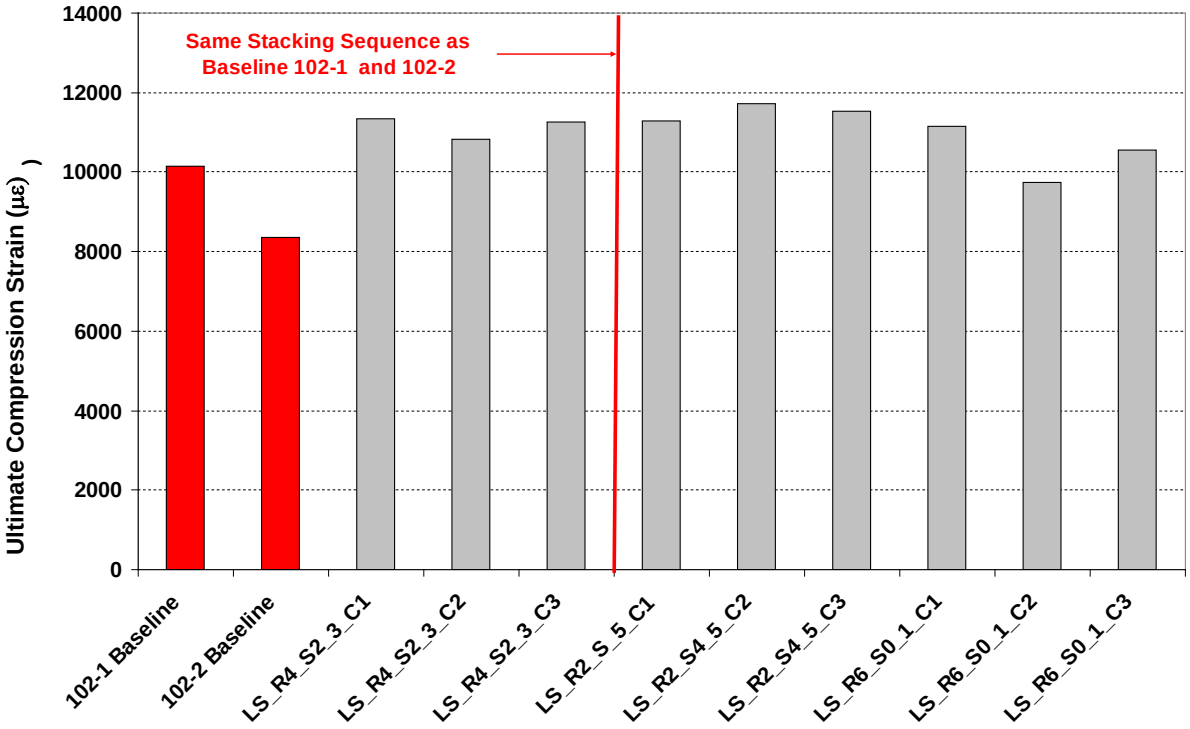

Figure 76. Lower Skin Compression Ultimate Strain Test Data (Calculated) of As-Extracted Coupons

Tension tests of extracted coupons from the aging stabilizer were also conducted according to the 1980s' requirements and specifications. All tension coupons were individually tabbed, as shown in figure 77. The tension coupon has a tapered cross section with a 1-inch width at the gage section and a 1.5-inch width at the ends, as shown in figure 78. This same coupon geometry was used during the design phase to generate tension allowables for the stabilizer structure. Biaxial strain gages were used to measure strains for the different configurations tested.

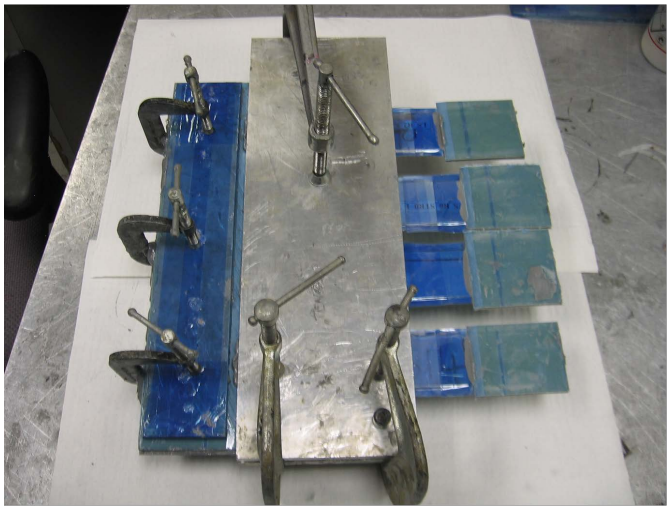

Figure 77. Tabbing Fixture for Tension Coupons

Figure 78. Tension Test Setup and Coupon Configuration

Figures 79 through 82 summarize typical tension results obtained for as-extracted coupons that were taken from the upper skin and lower skins. These figures show measured and normalized RTA tension strength and measured ultimate strain values for coupons extracted from different locations on the upper and lower skins. It should be noted that the baseline strength values presented [1] are calculated based on nominal thickness values (0.053″ for 7-ply skin). It should also be noted that the tension strain to failure are measured values. For 101-1 and 101-2 tension baselines, the average ultimate tensile strength is 50.025 ksi, and the corresponding average tensile strain to failure is 9400 με.

The measured tensile strength was derived using the measured thickness, whereas the normalized strength was obtained using the laminate nominal thickness corresponding to the location from where the coupons were extracted. It should also be noted that only coupons extracted from the region around upper skin ribs 1 and 3 had the same stacking sequence as baseline coupons 101-1 and 101-2. Similarly, lower skin coupons extracted around rib 4 had the same stacking sequence as baseline coupons 101-1 and 101-2. As illustrated in the figures, normalized compression strength and failure strain values for the stabilizer upper and lower skin coupons, with the same stacking sequence as the baseline coupons, correlated very well with the baseline strength and ultimate strain values. The RTA tension data did not show any evidence of material degradation that could be attributed to the aging of the stabilizer.

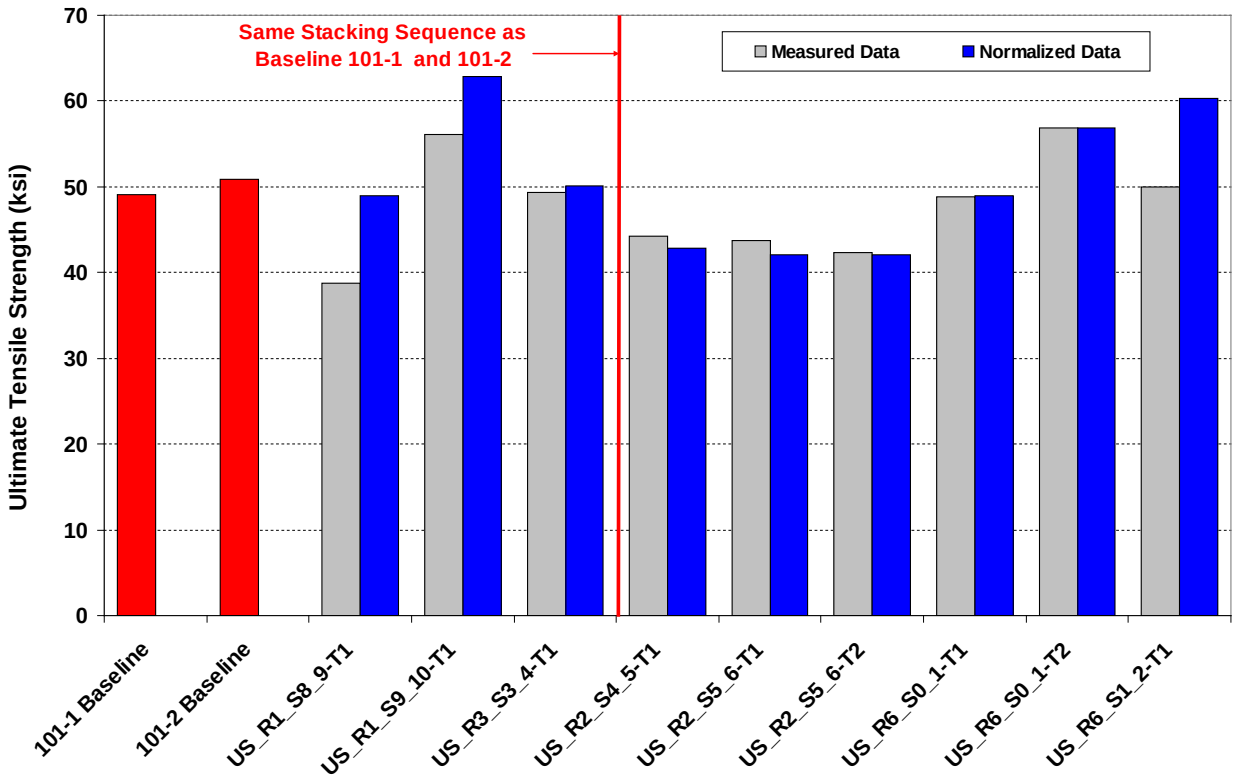

Figure 79. Upper Skin Tension Strength Data of As-Extracted Coupons

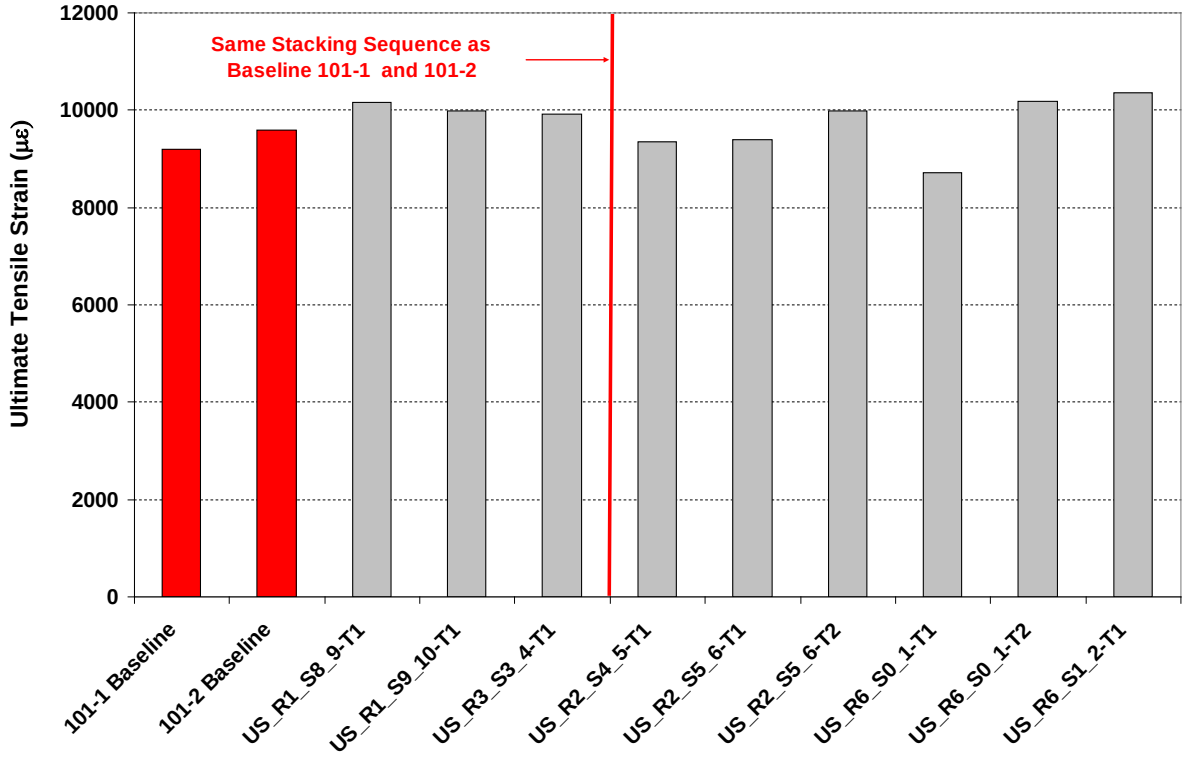

Figure 80. Upper Skin Tension Ultimate Strain Test Data (Measured) of As-Extracted Coupons

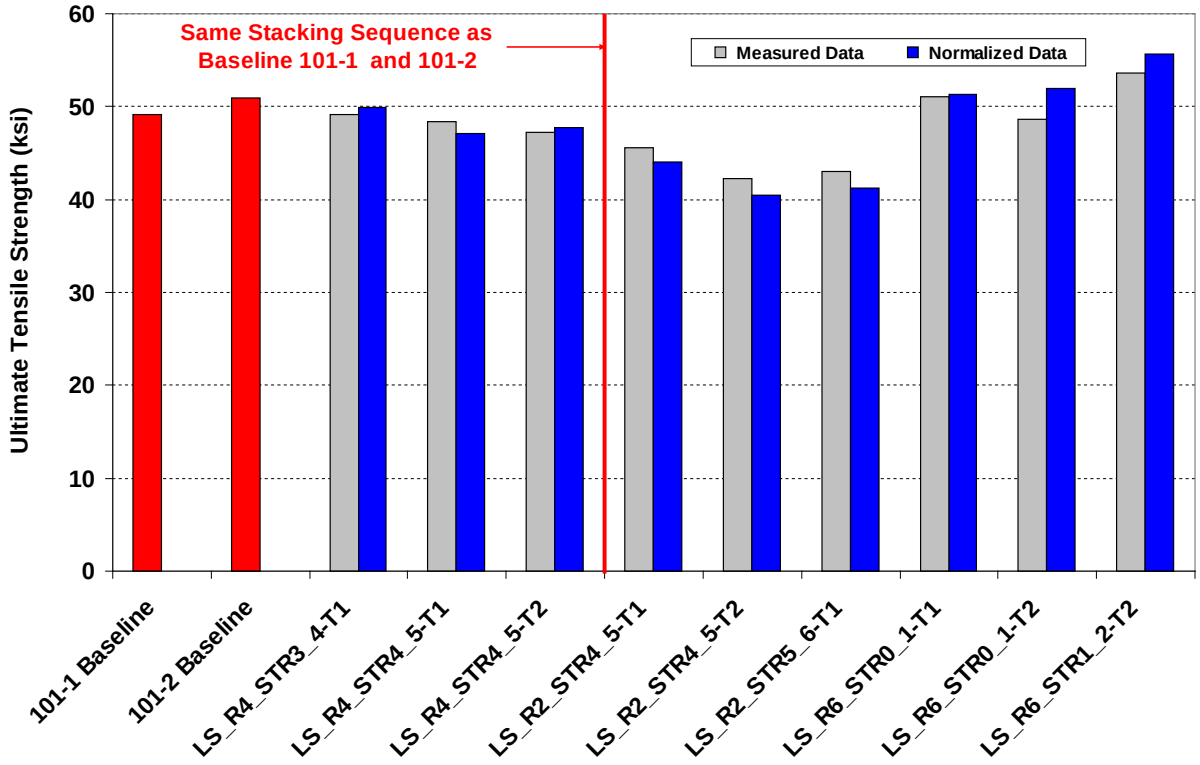

Figure 81. Lower Skin Tension Strength Data of As-Extracted Coupons

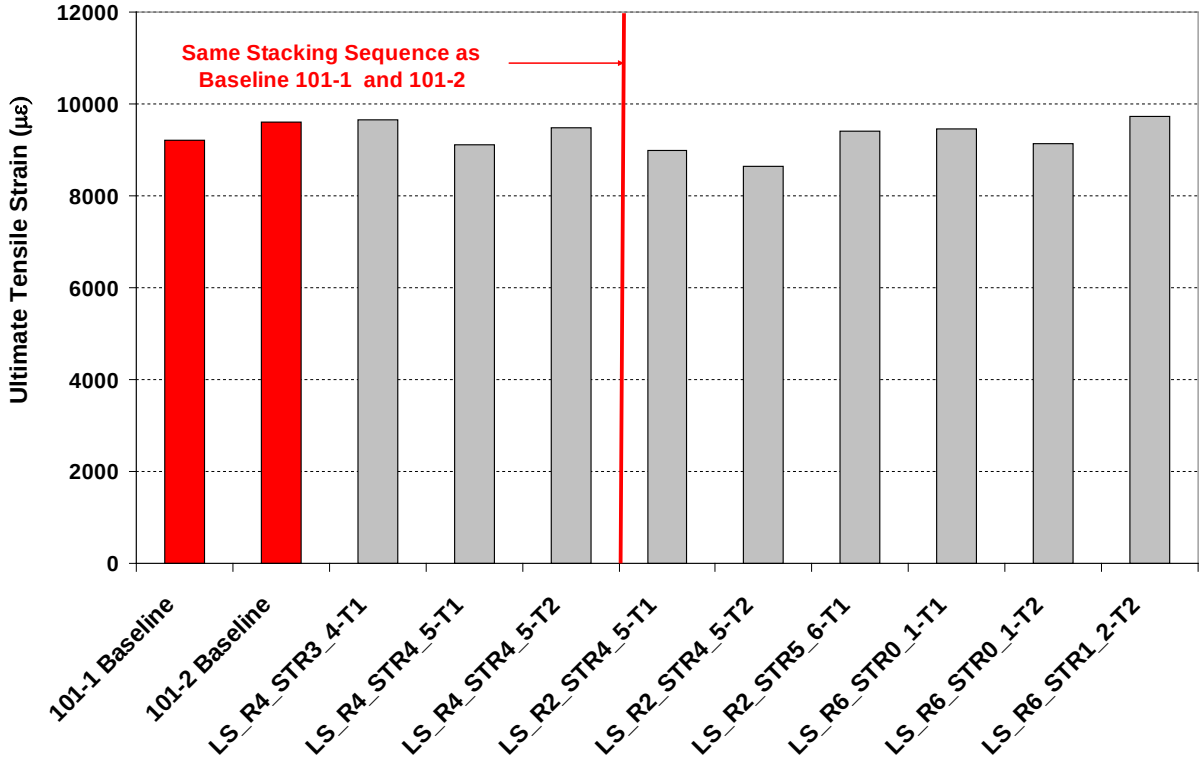

Figure 82. Lower Skin Tension Ultimate Strain Test Data (Measured) of As-Extracted Coupons

Crippling tests on a three-stringer panel were conducted on a few elements extracted from the upper and lower skins. The test setup is shown in figure 83.

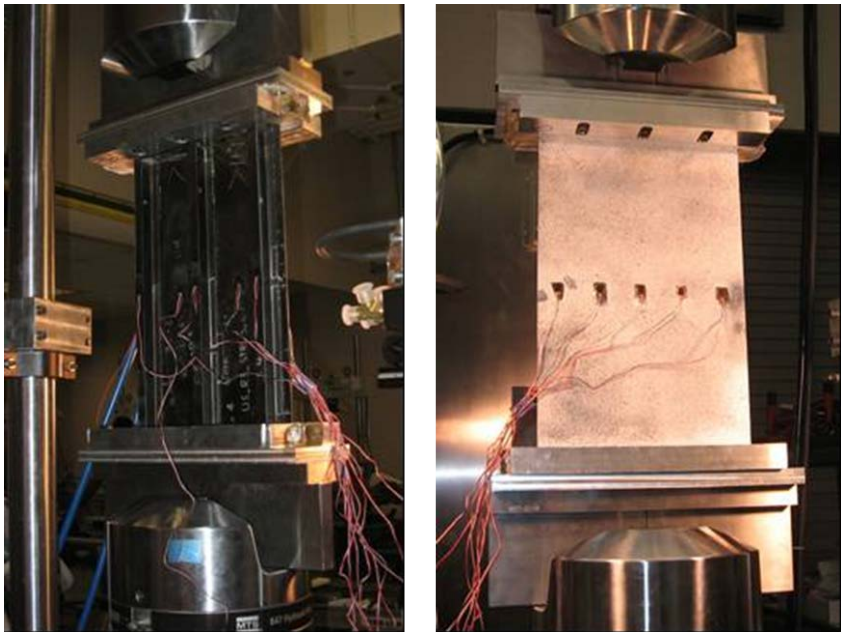

Figure 83. Crippling Test Setup for Three-Stringer Element

A three-stringer crippling element is shown in figure 84. Failure load of the stiffened skin panel, though slightly lower, correlated very well with the failure load of the equivalent panel tested during the design and certification phase. Load versus strain data is shown in figure 85. It should be noted that all coupons and elements tested during the design phase were flat, whereas all coupons extracted from the aged stabilizer had the slight curvature characteristic of the structure. The failure strain achieved, 5200 microstrains, correlated very well with the strains to failure of the equivalent panel tested during certification.

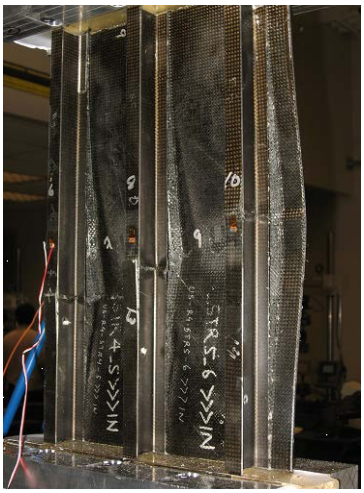

Figure 84. Post-test Three-Stringer Element

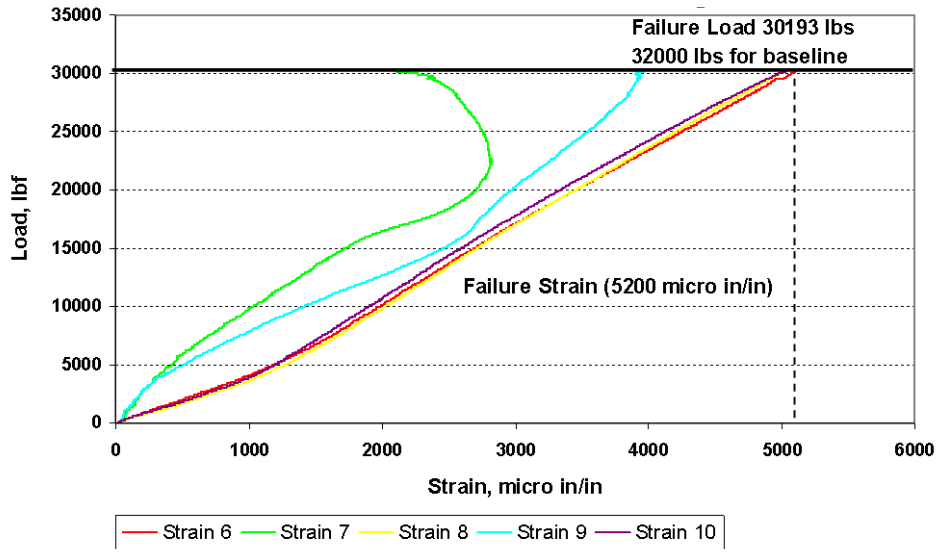

Figure 85. Crippling Element Load vs. Strain Data

4. CONCLUSIONS.

The teardown of the Boeing 737-200 right-hand (RH) stabilizer revealed a composite structure that held up extremely well after 18 years of service, with no obvious signs of aging to the naked eye, such as pitting and corrosion, as a metal structure with a similar service history would exhibit.

The teardown of shipset 5 demonstrated good agreement between the results obtained from the RH and left-hand (LH) stabilizers. Partial LH test results, conducted by the original equipment manufacturer, were presented in a previous conference paper.

Physical test results showed moisture levels in the structure after 18 years of service as predicted during the design phase. Thermal analysis results were very consistent with those obtained for the LH stabilizer and with the baseline data provided by the supplier.

Thermal analysis showed that the degree of cure of the spars is close to 100% and that additional curing may have occurred during the secondary bonding of the spars. Furthermore, additional curing may have occurred in the upper skin due to environmental exposure (overall at least 95% cure was achieved in the structure).

For mechanical tests where baseline data was available (1970s certification and test data), the residual strengths met or exceeded the baseline values. No significant degradation was noted in any of the tests.

The teardown also showed that significant improvements in composite manufacturing processes and non-destructive inspection methods have been made in the last 30 years. Void contents observed in these parts are not allowed according to today's standards.

Furthermore, the new T300/5208 material appeared to have comparable thermal properties to the 1970s material, i.e., comparable resin system but significantly higher tensile and compressive properties indicative of improvement in fiber processing in the last 30 years.

The teardown provides closure to a very successful National Aeronautics and Space Administration program and affirms the viability of composite materials for use in structural components. From all data generated, the margins were sufficient to warrant a "no significant degradation" conclusion.

5. REFERENCES.

1. Aniversario, R.B., Harvery, S.T., McCarty, J.E., Parsons, J.T., Peterson, D.C., Pritchett, L.D., Wilson, D.R., and Wogulis, E.R., "Design, Ancillary Testing, Analysis, and Fabrication Data for the Advanced Composite Stabilizer for Boeing 737 Aircraft," Volume II NASA CR 166011, Final report, December 1982.

2. Leonard, R.W. and Wagner, R.D., "Airframe Technology for Energy Efficient Transport Aircraft," SAE 760929, November-December 1976.

3. Maddalon D.V. and Wagner, R., "Energy and Economic Trade Offs for Advanced Technology Subsonic Aircraft," NASA TM X-72833, Langley Research Center, Hampton, Virginia, April 1, 1976.

4. Kraus, E. and Van Abkoude, J., "Cost/Benefit Trade Offs for Reducing the Energy Consumption of the Commercial Air Transportation System," Volume I, Technical Analysis, NASA CR-137923; Volume II, Market and Economic Analysis, NASA CR-137924; Volume III, Summary Report, NASA CR-137925, October 1976.

5. Hopkins, J., "Cost/Benefit Trade Offs for Reducing the Energy Consumption of the Commercial Air Transportation System," Final report, NASA CR-137926, Summary, NASA CR-137927, October 1976.

6. Ethell, J.L., "Fuel Economy in Aviation," NASA-SP-462, 1983.

7. Povinelli, F.P., Klineberg, J.M., and Kramer, J.J., "Improving Aircraft Energy Efficiency," *Astronautics and Aeronautics*, Vol. 14, No. 2, February 1976, pp. 18-31.

8. Braslow, A.L. and Alford, W.J., "Advanced Subsonic Transport Technology," *Astronautics and Aeronautics*, Vol. 10, No. 8, August 1972, pp. 26-55.

9. Shevell, R.S., "Technology, Efficiency and Future Transport Aircraft," *Astronautics and Aeronautics*, Vol. 13, September 1975, pp. 36-42.

10. Steiner, J., "Airline Airplanes for the Eighties—A Response," *Astronautics and Aeronautics*, Vol. 12, March 1974, pp. 42-51.

11. Maddalon, D.V., "Rating Aircraft on Energy," *Astronautics and Aeronautics*, December 1974, pp. 26-43.

12. Braslow, A.L. and Whitehead, A.H., "Aeronautical Fuel Conservation Possibilities for Advanced Subsonic Transports," NASA-TN-X-71927, December 20, 1973.

13. Nagel, A.L., Alford W.J., and Dugan, J.F., "Future Long-Range Transports—Prospects for Fuel Efficiency," NASA-TM-X-72659, February 1975.

14. Ardema, M.D., Harper, M., Smith, C.L., Waters, M.H., and Williams L.J., "Conceptual Design of Reduced Energy Transports," *Journal of Aircraft*, Vol. 13, No. 8, August 1976.

15. Dow, M.B., "The ACEE Program and Basic Composites Research at Langley Research Center (1975 to 1986)."

16. Harris, L.A., "Advanced Composites, an Assessment for the Future," *Astronautics and Aeronautics*, March 1976.

17. Goodmanson, L.T. and Gratzer, L.B., "Recent Advances in Aerodynamics for Transport Aircraft, Part I," *Astronautics and Aeronautics*, December 1973.

18. Goodmanson, L.T. and Gratzer, L.B., "Recent Advances in Aerodynamics for Transport Aircraft, Part II," *Astronautics and Aeronautics*, January 1974.

19. Cone, C.D., Jr., "The Theory of Induced Lift and Minimum Induced Drag of Non-Planar Lifting Systems," NASA TR R-139, 1962.

20. Dogett, R.V., Abel, I., and Ruhlin C.L., "Some Experiences Using Wind Tunnel Models in Active Control Studies," presented at the *Symposium on Advanced Control Technology and its Potential for Future Transport Aircraft*, Los Angeles, California, July 1974.

21. Sandford, M.C., Abel, I., and Gray, D.L., "Development and Demonstration of a Flutter Suppression System Using Active Controls," NASA TR R-450, December 1975.

22. Redd, L.T., Gilman, J., Cooley, D.E., and Sevart, F., "A Wind Tunnel Investigation of a B-52 Model Flutter Suppression System," AIAA Paper, April 1974, pp. 74-401.

23. White, R.C., Sudderth, R.W., and Wheldan, W.G., "Laminar Flow Control on the X-21," *Astronautics and Aeronautics* (AIAA), Vol. 4, No. 7, July 1966.

24. Davis, J.G., "Composites for Advanced Space Transportation Systems (CASTS) Technical Report for Period July 1, 1975-April 1, 1978," NASA Technical Memorandum 80038, March 1979.

25. Griffin, C.F. and Dunning, E.G., "Development of an Advanced Composite Aileron for the L-1011 Transport Aircraft," NAS1-15069, 1982.

26. Hart-Smith, L.J., "Lessons Learned From the DC-10 Carbon-Epoxy Rudder Program," *SAE Aerospace Technology Conference and Exposition*, Long Beach California, October 1986.

27. Chovil, D.V. et al., "Advanced Composite Elevator for Boeing 727 Aircraft, Volume 1," technical summary, NASA CR-3290, November 1981.

28. Jackson, A.C., "Advanced Composite Vertical Fin for L-1011 Aircraft Design, Manufacture, and Test," NASA CR 3816, 1984.

29. Palmer, J.M., Stephens, C.O., and Sutton, J.O., "Damage Tolerance and Fail-Safe Testing of the DC-10 Composite Vertical Stabilizer," NASA-CR-172359, ACEE Composite Structures Technology, McDonnell Douglas Corporation, August 1984.

30. Stephens, C.O. et al. "Advanced Composite Vertical Stabilizer for DC-10 Transport Aircraft," Quarterly Technical Progress Report, NASA CR-172780, 1978.

31. McCarty, J.E., "737 Graphite Epoxy Horizontal Stabilizer Certification," Boeing Commercial Airplane Company, Seattle, Washington, May 1982.

32. U.S. Federal Register, Title 14 C ode of Federal Regulations Part 25, " Airworthiness Standards: Transport Category Airplanes."

33. Aniversario, R.B. et al., "Full-Scale Testing, Production and Cost Analysis for the Advanced Composite Stabilizer for Boeing 737 Aircraft," Volume II—Final Report, NASA CR 166012, December 1982.

34. Quinlivan, J.T., Kent, J.A., and Wilson, D.R., "NASA-ACEE/BOEING 737 Graphite-Epoxy Horizontal Stabilizer Service," *9th DoD/NASA Conference on Fibrous Composite in Structural Design*, NASA document 95N28489, 1991.

35. Federal Aviation Administration, "Composite Aircraft & Structure," Advisory Circular (AC) 20-107A, Apri 25, 1984.

36. Ekvall, J.C. and Griffin, C.F., "Design Allowables for T300/5208 Graphite-Epoxy Composite Materials," American Institute of Aeronautics and Astron., January 1981.

37. Aniversario, R.B. et al., "Full-Scale Testing, Production and Cost Analysis for the Advanced Composite Stabilizer for Boeing 737 A ircraft," Volume I—Technical Summary, NASA CR 3649-1983, April 1983

38. Tomblin, J., Salah, L., Davies, C., Miller, M., Hoffman, D., and Kollgaard, J., "Aging Effects Evaluation of a Decommissioned Boeing CFRP 737-200 Horizontal Stabilizer," *8th Joint FAA/DoD/NASA Aging Aircraft Conference*, January 31-February 3, 2005.